QATAR UNIVERSITY

COLLEGE OF ENGINEERING

DISCRETE ELEMENT MODELING OF RAILROAD BALLAST UNDER

SIMULATED TRAIN LOADING

BY

YAHIA ABDULNASER ALABBASI

A Thesis Submitted to

the Faculty of the College of Engineering

in Partial Fulfillment of the Requirements for the Degree of

Masters of Science in Civil Engineering

June 2019

COMMITTEE PAGE

The members of the Committee approve the Thesis of
Yahia Abdulnaser Alabbasi defended on 17/04/2019.

_____
Dr. Mohammed Farouk Mohammed Hussein
Thesis/Dissertation Supervisor

_____
Dr. Mohammed Zein Elabidin Babiker Elshafie
Committee Member

_____
Prof. Omar Laghrouche
Committee Member

_____
Dr. Wael Alnahhal
Committee Member

Approved:

_____
Abdel Magid Hamouda , Dean, College of Engineering

ABSTRACT

ALABBASI,YAHIA,A.,Masters

June : 2019, Masters of Science in Civil Engineering

Title: Discrete Element Modeling of Railroad Ballast Under Simulated Train Loading

Supervisor of Thesis: Dr. Mohammed, F, Hussein .

Ballasted tracks have been widely used in many countries around the world. Ballast layer is the main element in ballasted track. After service, ballast aggregates degrade and deform. Periodical maintenance for ballast layer is required; which is a cost and time expensive activity. Researchers used numerical approaches to understand the behavior of railroad ballast that leads to efficient design and maintenance. The Discrete Element Method (DEM) has been used increasingly to understand the mechanical behavior of railroad ballast, more frequently through box test. Most researches in the literature simulate the train loading as a pure continuous sinusoid based on train speed and axle spacing; unlike the actual loading induced by trains. This study aims to show the influence of simulated train loadings on ballast mechanical behavior using DEM via box test. The study utilizes the theory of Beam on Elastic Foundation to simulate a more realistic train load. The results from the more realistic simulated train load are compared with those from a sinusoidal load. The compared results highlight the influence of the simulated train load on the mechanical behavior of railroad ballast.

DEDICATION

To my grandparents, parents, family, wife and son.

ACKNOWLEDGMENTS

First, I would like to sincerely thank almighty Allah for giving me the countless blessings, strength, endurance and knowledge to complete this study.

I am grateful to my research supervisor Dr. Mohammed Hussein for his endless support during my undergraduate and graduate studies at Qatar University. I would like to thank him from my heart for his motivation, enthusiasm, patience and support in securing the funding during my study. I thank him for his endless contributions to enrich my level of knowledge during my study. I would like to show my deepest gratitude to him for being as a great brother before being my supervisor.

Finally, I would like to express my grateful thanks to my family who acted as a motivation to me to complete my study. I thank them for their continues support and great efforts to complete this study.

TABLE OF CONTENTS

LIST OF TABLES

LIST OF FIGURES

CHAPTER 1: RESEARCH INTRODUCTION

1.1 Introduction

In many countries around the world, railways play a vital role as a mean of transportation. Railways have many advantages with relative to other means of transportation. Railways cover long distances in high speed. It is cheap, safe, efficient and environmentally friendly mean of transportation [1-3]. Moreover, railways are considered as a public welfare for many countries around the world [4].

A railway track is considered as the basic element of railway infrastructure as shown in Figure 1 . A railway track is the supporting platform that transforms the trains' loads from track superstructure to track substructure. Trains run on different railway track systems; ballasted and ballast less (e.g. slab and embedded track) systems [5]. The ballasted tracks have the majority usage in the world as they were introduced with the invention of railways [6] and their low construction cost [7] compared to new ballast less tracks. Ballasted tracks have lower construction cost and higher maintenance cost compared to ballast less tracks.
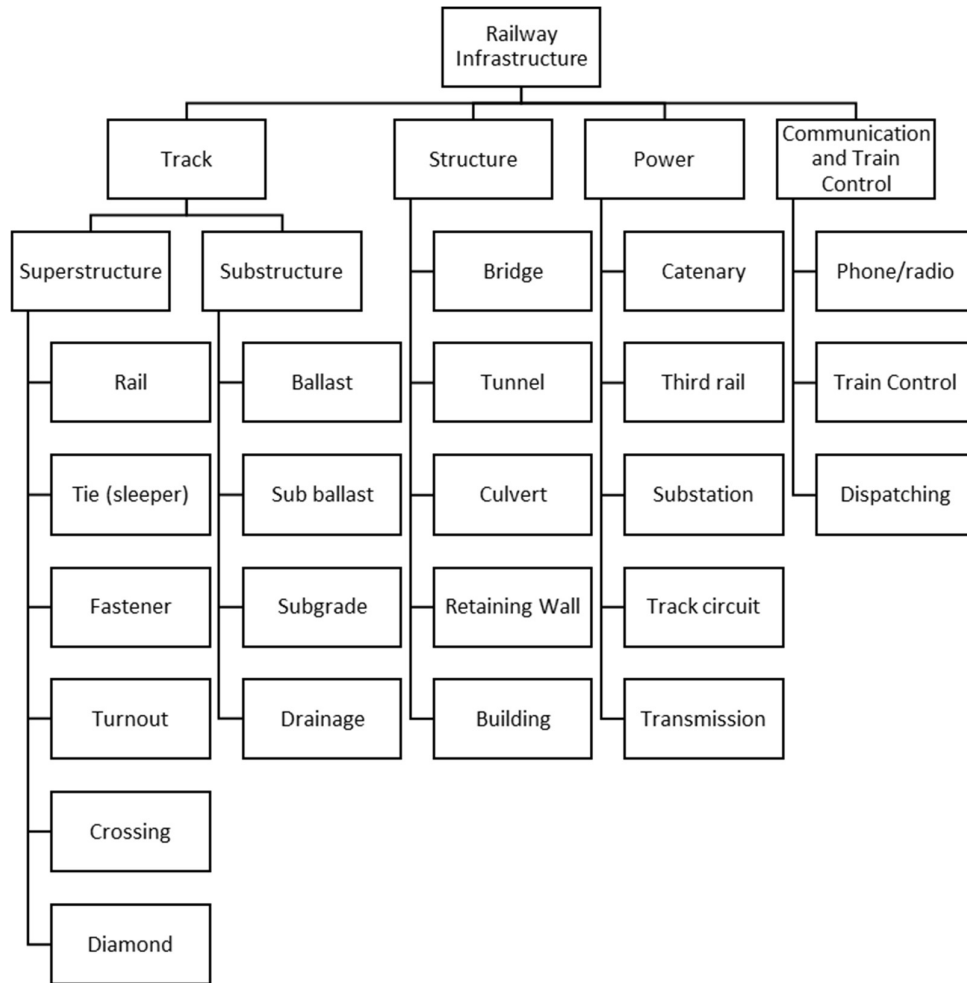
Figure 1: Railway Infrastructure's components reproduced from [8].

A ballasted track consists of two main structures: superstructure and substructure [9]. Figure 2 and Figure 3 show the main elements of typical ballasted track. In general, good knowledge of track superstructure is gained through research and experience throughout the years. However, substructure mechanical behavior still not fully understood with relative to superstructure components. The importance of ballast element in ballasted track beside the needs of costly maintenance [10, 11] raise the interests to increase the research work on understanding and estimating the

mechanical behavior of railroad ballast. This leads to better ballast design and efficient

maintenance.
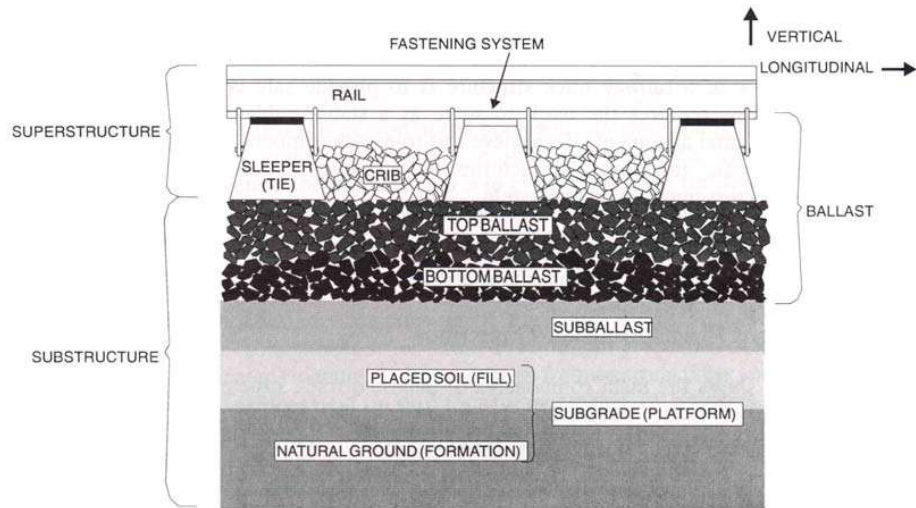
Figure 2: Side view of typical ballast track [9].
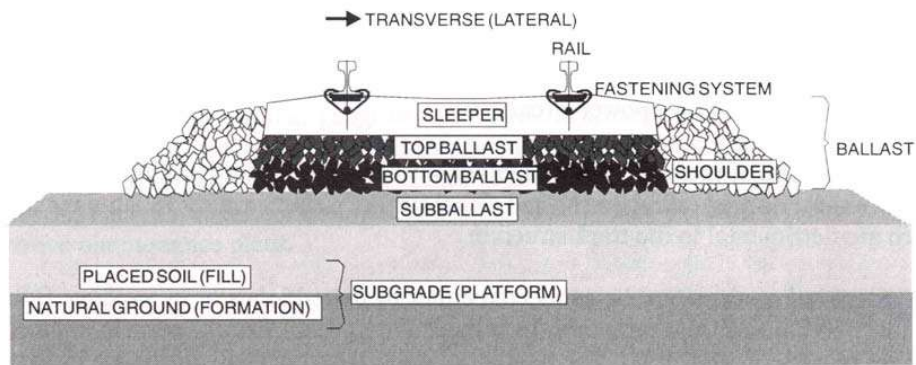
Figure 3: Cross section view of typical ballast track [9].

1.2 Research Motivation

Ballasted tracks were introduced with the invention of railways. There is a huge number of ballasted tracks around the world. The main advantage of ballasted track is the low construction cost. However, the maintenance cost is quite high. This is considered as the main reason of the introduction of a new ballast less track systems (e.g. slab tracks) recently, despite the associated high construction cost.

Nevertheless, improving the understanding of the mechanical behavior of railroad ballast has a positive impact on ballast material from environmental and financial perspectives. This is considered as one of the main motivation of this study, to develop a good understanding of ballast mechanical behavior which leads to a better alternative of substructure material for railway tracks to be used considering the financial and environmental aspects.

Other motivation of this research is the potential demand in the Gulf region to have railway lines connecting the Gulf Cooperation Council (GCC) countries. The initial phase of railway project between the GCC countries determines the need of five lines for passenger and freight. The final phase of the project is in 2030. Moreover, the availability of national resources for railroad ballast material (e.g. Qatar's Rock) inside Qatar (Figure 4) and GCC countries supports the demand of this project; and raises the research interests and awareness about ballast behavior in the region.

In a brief, sorting out the main challenges, issues and concerns related to ballast material increase the attraction and potential towards the use of an economic and environment-friendly track material. This can be done by the good development of knowledge and understanding about ballast mechanical behavior; which leads to better ballast design and efficient maintenance.
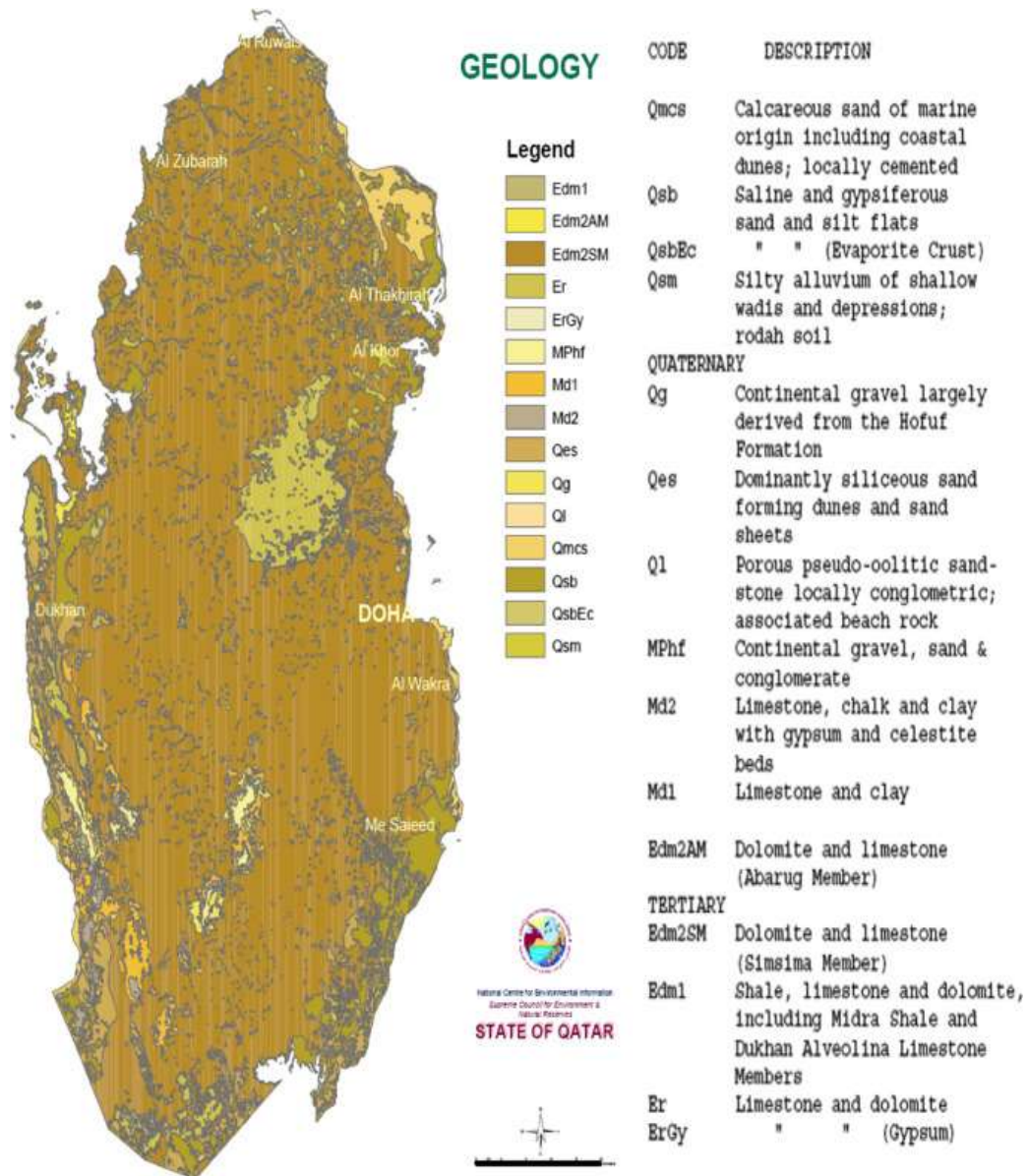
Figure 4: Geological map of Qatar [12].

1.3 Problem Statement

It is vital to understand the mechanical behavior of railroad ballast which leads to better ballast design and efficient maintenance. To understand the mechanical behavior of railroad ballast using either numerical or experimental work, it is essential to apply a proper and more realistic train loading on ballast layer. This represent the

5

scenario in the field. Train loading has different shapes based on various parameters like train weight, train velocity, car length, axle number and axle spacing.

1.4 Aims and Objectives

This study aims to develop a better understanding of the mechanical behavior of railroad ballast under simulated train loading cases; to investigate the influence of different simulated train loading cases on the mechanical behavior of railroad ballast.

To achieve the aim of this study, DEM is used to understand the mechanical behavior of railroad ballast under simulated train loading cases. EDEM [13] software by DEM Solutions is used for DEM analysis of railroad ballast material. Microsoft Visual Studio [14] software is used as a language platform to develop the force control mode via C++ language. MATLAB [15] software is used for loading cases analysis.

1.5 Thesis Outline

This section provides a brief outline of the thesis. This thesis consists of six chapters.

Chapter 1, provides brief introduction of the research done in this thesis including research motivation, problem statement, aims and objectives.

Chapter 2, provides an intensive background related to ballast material. It highlights the key characteristics of railroad ballast that influence its mechanical behavior. Furthermore, it provides a general background about the different approaches used in the literature to understand the mechanical behavior of railroad ballast material.

Chapter 3, reviews the literature about understanding the mechanical behavior of railroad ballast using Discrete Element Method through box test. The chapter reviews the different perspectives of ballast modeling using DEM through different sections.

Chapter 4, explains the modeling methods and procedures used to model the behavior of railroad ballast under different simulated train loading cases.

Chapter 5, consists of two main sections; analysis and results and discussion. In the analysis section, some perspectives related to this study and described in Chapter4 are analyzed. Those perspectives produce results that require analysis. The second section (results and discussion) highlights and discusses the main results of this study form macroscopic and microscopic scales.

Chapter 6, provides a brief conclusion of this thesis and recommendations for future research work.

CHAPTER 2: RESEARCH BACKGROUND

2.1 Introduction

Railroad ballast is the basic material of railway track. Railroad Ballast layer is a granular material that consists of ballast aggregates. Ballast aggregates are a result of crushed rocks. Those crushed rocks are identified as parent rocks. The characteristics of railroad ballast is based on the characteristics of parent rocks. Railroad ballast has special characteristics that contribute to its functionality.

It is essential to know and understand the material characteristics that influence the mechanical behavior of railroad ballast; to select the proper railroad ballast material and develop better understanding of ballast mechanical behavior. Ballast material selection depends on material characteristics. The proper material selection helps ballast to function properly and be maintained efficiently.

It is important before presenting a review of the literature to introduce some background and information about the recommended characteristics that influence the mechanical behavior of railroad ballast; and the different approaches used in the literature to understand the mechanical behavior of railroad ballast material. This will help with the presentation of literature review as well as the discussion in the following chapters.

2.2 Characteristics of Railroad Ballast Material

Railroad ballast material has specific characteristics that help ballast layer to function and maintain its functionality under train loading properly. This section begins with a brief information from the literature about the key functions of railroad ballast. It presents the main and recommended characteristics that influence the mechanical behavior of railroad ballast.

2.2.1 Ballast Functions

Many researchers [8, 9, 16, 17] emphasized on the significance of ballast layer and summarized its main roles as discussed in the following sentences. It transmits the loads from the superstructure to the ground and act as a bearing platform. It enhances the track stability as it provides the sufficient vertical, lateral and longitudinal resistance. Furthermore, ballast layer reduces the resulted noise and vibration due to dynamic forces from wheels and rails by providing resilience and damping. Moreover, the ballast layer provides the track with many voids to pass dirt and a good have draining property. Besides, ballast resists the frost action and reduces vegetation. Ballast can be divided into four zones as shown in Figure 5. Each zone in the ballast layer has certain contribution to ballast functionality as described by Sadeghi et al. [18] in Figure 6.
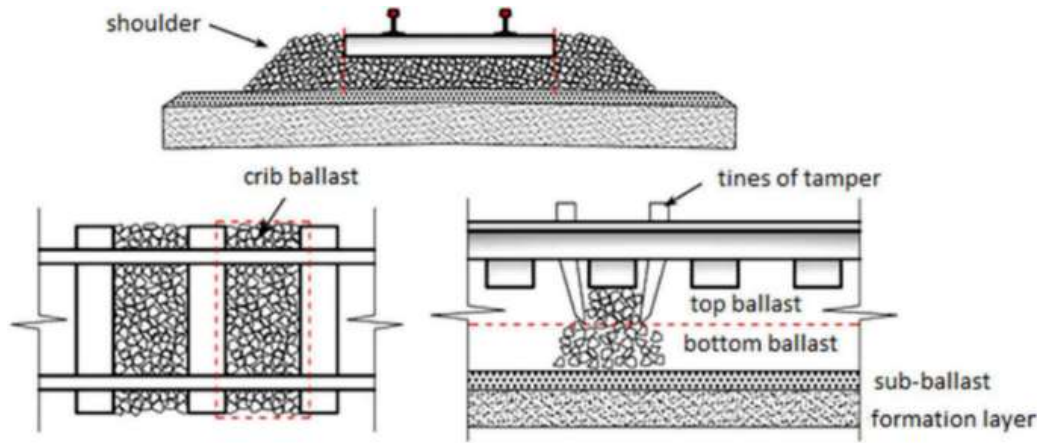
Figure 5: Ballast portions described by [18].

Ballast Duties	Crib Ballast	Shoulder Ballast	Bottom Ballast	Top Ballast
Vertical strength			■	■
Lateral strength	■	■		■
Longitudinal strength	■			■
Resiliency			■	■
Adjusting and track leveling	■		■	■
Drainage	■	■	■	■
Load distribution and dispersing			■	■
Prevent growth of plant	■		■	■
Shock absorption and noise attenuation	■	■	■	■
Electrical resistivity	■			■
Subgrade protection layer	■	■	■	■

Figure 6: Contribution of each ballast zone to the ballast layer functionalities [18].

2.2.2 Ballast Parent Rock

Ballast aggregates are a result of crushed rocks. It is important to know the type of the ballast parent rocks as it affects ballast strength related properties like particle size, shape, cleavage fracture, porosity and angularity [18]. Moreover, ballast parent rock characteristics influence the mechanical behavior of railroad ballast under real traffic loadings [19, 20].

Ballast parent rock can be estimated by petrographic analysis. Petrographic analysis is an evaluation of the source, composition and nature of the hand-sample material under microscopic vision of thin sections of the specimen by an expert petrographer. Raymond [21] considered petrographic analysis as an important test in selecting ballast material and he concluded that petrographic analysis can be a valuable estimation to the shape and porousness of railroad ballast.

Sadeghi et al. [18] classified the parent rock of ballast aggregates into four classifications as shown in Figure 7. Extrusive igneous rocks (rheolite, andesite and basalt) are the most sufficient parent rocks for railroad ballast. Followed by metamorphic then sedimentary rocks and finally slag as the weakest rock to be chosen for railroad ballast. Indraratna [22] stated that the main parent rocks that are used to derive railroad ballast are igneous or metamorphic rocks and this is why ballast morphology usually consists of rheolite, dolomite, basalt, gneiss, quartzite and granite minerals.
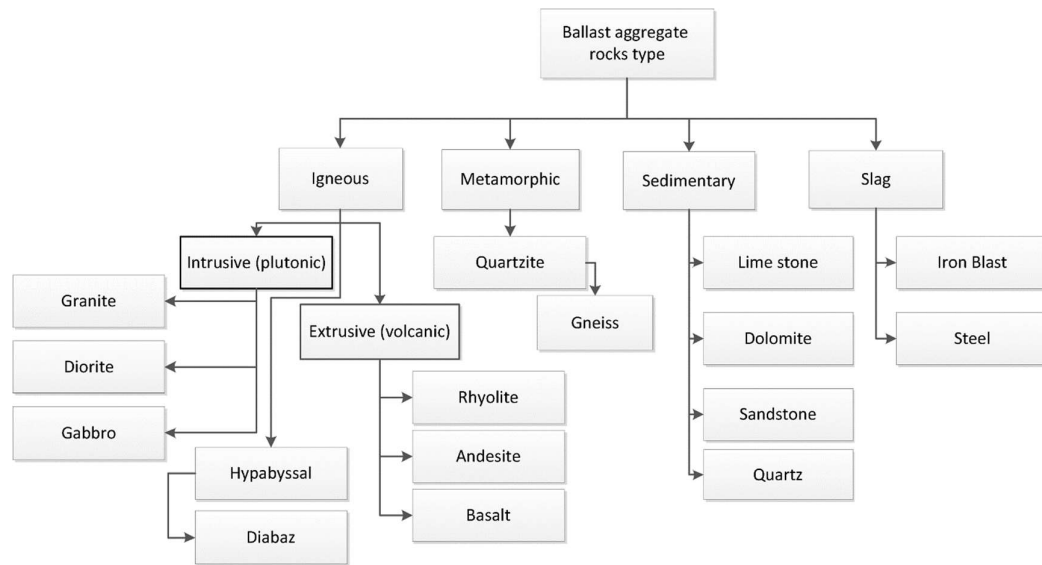
Figure 7: Railroad ballast parent rock classification by [18].

2.2.3 Particle Size Distribution

Ballast aggregates are narrow graded, large, angular, free of dust and dirt, not disposed to cementing action and derived from crushed hard rock material [23]. The Particle Size Distribution (PSD) of railroad ballast has a significant influence on ballast performance under real track conditions. Ballast strength, deformation resistance and drainage properties are dependent on ballast PSD. Ballast aggregate size gradations are commonly narrow not broad. Broad graded ballast aggregates layer provides strength and resistance to deformation with relative to narrow graded ballast aggregates layer; because of the low void ratio and the dense arrangement of particles [24, 25]. Broad gradation provides low capacity for fouling material to be stored and low drainage features to the track as well as challenges in material handling and delivering due to the high chance of segregation during construction. But narrow graded ballast aggregates layer provides good void capacity for fouling storage, good drainage capability of the track and easy handling during construction as it is not exposed to segregation. Selig

[26] suggested that the perfect ballast particle sizes are in the range of 10-50 mm with some aggregates outside this range. However, there is no specific ballast gradation to be used everywhere, as each railway association has its own ballast gradation specification. However, the most general used and recommended PSD of railroad ballast is narrow gradation with a particle size range almost of 10-60 mm.

2.2.4 Particle shape, angularity and texture

Ballast aggregates' shape, angularity and texture have the main contributions to the ballast slipping resistance and particle breakage. Ballast aggregate significantly influences the material strength [27]. Angularity and texture of ballast particles are the major influences of material slipping resistance. Surface texture is considered as the main factor of surface friction. Rough surface particles have more friction than smooth surface particles.

The recommended ballast particle's shape that mostly contribute to ballast strength is well-proportioned particles that are almost cubical not elongated, flaky or rounded shapes [9, 21, 28]. Elongated and flaky particles have certain dimensions larger than others; this leads to certain weak plane that could break quickly under loading and may be a reason of slip failure. Rounded particles are stronger under loading than flaky and elongated, but they have very low slipping resistance due to high rolling properties derived from their shape. Number of researchers [10, 24, 29, 30] observed that the more the ballast is angular the more the interlocking between internal particles occurs, which raises shear strength and slipping resistance; unlike sub rounded and rounded particles. Selig and Waters [9, 24] discussed that ballast angularity and roughness have positive and negative impacts on ballast performance. They noted that ballast aggregates with high angularity and roughness properties have higher chance of particle wearing and/or breakage due to the small contact surface areas that causes high internal stress. Even

though, they recommended to select rough and angular aggregate for railroad ballast material as the advantage of high bulk shear strength dominates the disadvantage of high probability of particle wearing and/or breakage.

2.2.5 Abrasion and Crushing Resistance

Loadings from the frequent passage of trains cause stress on the ballast layer, especially at the top part of ballast where the stress is maximum [31, 32]. This stress could cause particle breakage. There are two types of ballast breakage. The first is corner breakage by which the sharp corners of the particles break. The second is particle splitting breakage by which weak aggregate breaks into smaller fragments. Corner breakage occurs mostly under low confining pressures while splitting breakage occurs mostly under high confining pressures [33]. Ballast particle breakage is the main cause of the track permanent differential settlement [34]. Ballast layer has the main contribution to track settlement; 50–70% of the total vertical deformation is from the ballast layer [9].

There are two conventional tests used to identify the ability of ballast under abrasion and crushing. The Los Angles abrasion test (LA) and Mill Abrasion test (MA). LA measures the crushing resistance of ballast to estimate the strength of ballast particle against brakeage under the tie. For railroad ballast low values of both LA and MA are preferred.

2.2.6 Ballast Fouling Degree

The voids in the ballast layer provide drainage and storage of fouling material for the track. Ballast fouling over time may be one of the key reasons of the track deterioration, alignment and poor drainage. Over time of service, the large voids will be filled of fouling materials, which reduce the permeability and increase the presence of water in ballast layer. Ballast fouling prevents ballast layer from functioning as a

drainage layer for the track. Ballast fouling has a significant influence on the mechanical behavior of railroad ballast.

Selig [26] considered the significant influence of fouling on ballast layer when 10% or more of ballast aggregates are fine size aggregates. Lim [35] found experimentally that fouling material influences the mechanical behavior of ballast layer positively or negatively based on different factors such as fouling material, degree of fouling and the water content. Han and Selig [36] found that as the fouling degree increased the settlement of ballast layer increased for all fouling materials through experimental tests. They found that water content of ballast influenced ballast behavior for different fouling degrees and fouling. Furthermore, they concluded that the increase of water content with the increase of fouling degree for ballast layer caused a dramatic increase in the layer settlement due to the extra lubrication of wet fouling materials between ballast particles. Lubrication affects the shear strength of ballast layer as it rises the pore water pressure. As pore water pressure increases, effective stress decreases and this leads to lower shear strength. Therefore, ballast settlement and plastic deformation are mostly observed in the pore drained ballast layer due to the high fouling degree.

Selig and Waters [9] found that the fouling material sources for railroad ballast layer are different as shown in Figure 8, where the main sources of fouling materials are: particle breakage of ballast (76%), infiltration from sub-base (13%), infiltration from ballast surface (7%), infiltration from sub-grade (3%) and sleeper wear (1%). Where ballast breakage is due to; handling, thermal stress, chemical weathering, tamping damage and/or traffic loading. The track surface infiltration source is from; ballast, train, windblown, water borne and/or wet spots. The underlying granular layer infiltration is due to; old track bed breakdown or/and sub ballast particle migration from

poor gradation. Selig and Waters [9] concluded that breakdown of ballast has the highest contribution to ballast fouling in North America. However, in British railways the biggest source to ballast fouling is external wagon spillage and airborne dirt [9]. In Qatar and GCC countries, it is crucial to consider the presences of sand fine particles (from sand storms) in ballast layer and the different maintenance methods to be used for sand extraction.
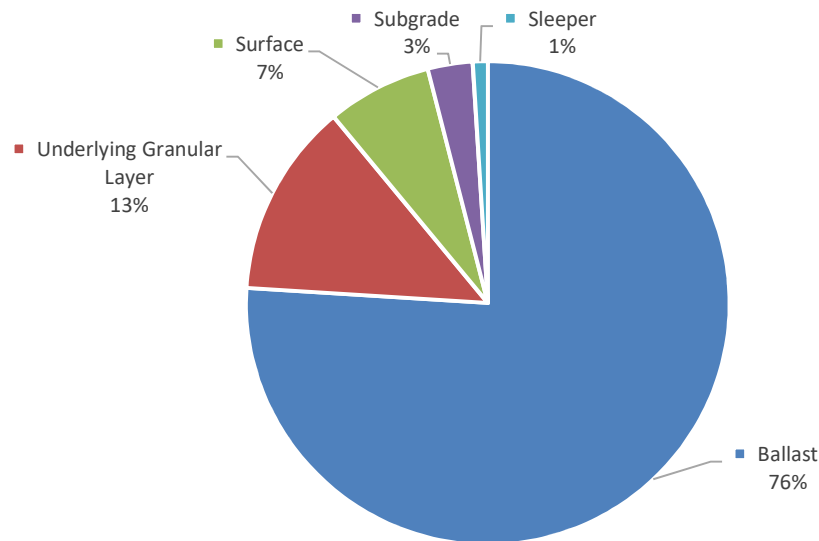
Figure 8: Sources of fouling material reproduced from [9].

Ballast fouling degree can be measured by fouling index as well as it can be classified based on the fouling index. There are various fouling indices used in the literature. Selig and Waters [9] defined the fouling index (FI) as the summation of the percentage of weight of fouled material that passes through a 4.75 mm and 0.075 mm sieves. Ionescu [37] modified Selig and Waters' fouling index to outfit used ballast

material in Australia as Selig and Waters defined their fouling index based on their study in North America. The previous indices are based only on the weight of fouling material. However, Feldman and Nissen [38] introduced the Percentage Void Contamination (PVC) ratio which include the variations of fouling material's specific gravity. PVC is the ratio of bulk fouling material volume to the clean ballast voids volume. But they did not consider the effect of particle size distribution of fouling material in their ratio. Indraratna et al. [39] introduced the Void Contaminant Index (VCI) which include the influence of many parameters like void ratio, specific gravity and particle size distribution of both fouling material and ballast.

2.3 Ballast Material Selection Standards

Ballast material selection should be based on the recommended characteristics of railroad ballast as discussed in the previous chapter. There are different standards and specifications for railroad ballast material selection by different railway transportation agencies worldwide. Each standard has different specifications to determine the properties of railroad ballast discussed above. Some of the used standards for railroad ballast material selection and their agencies are shown in Table 1. The most common standards used around the world for ballasted tracks are from American Railway Engineering and Maintenance of Way Association and British Standards Institutions.

Table 1: Railroad Ballast Standards Used in Ballast Material Selection

Standard	Agency
Manual of Railway Engineering-Section 1, Roadway and Ballast.	American Railway Engineering and Maintenance of Way Association (AREMA)
Aggregates for Railway Ballast - BS EN 13450:2013	British Standards Institution
Aggregates and rock for engineering purposes Railway ballast - AS 2758.7:2015	Standards Australia
Railway - Ballast - Requirements and Test Methods - NBR 5564:2011	Brazilian Standards

2.4 Loading Exerted on the Ballast Layer

The main role of the ballasted track substructure is to distribute and transmit the traffic loads from the superstructure to the ground. The substructure of the railway track is exposed to different types of loads. Selig and Waters [9] classified the loads exposed to ballast layer into two main types; vertical and sqeezing loads. Additionally, the other minor loads like lateral and longitudinal forces which are difficult to be estimated. It is essential to understand and know the different types of loading exerted on the track foundation, so a proper railway tack design and maintenance can be achieved [40].

2.4.1 Vertical Loading

The train vertical loads depend on train weight, train size, train speed and track irregularities. There different types of vertical loads exerted on ballast layer based on the rate of load application; static, quasi-static and dynamic train loads.

2.4.1.1 Static & Quasi-Static Loading

Static loads are dead and live loads. Dead load is the weight of railway track and live load is the weight of a non-moving train. Static loads are unchanged loads for a long time period and applied on the ballast layer [40] as shown in Figure 9. The response behavior of the ballast layer to the static load is governed by its stiffness. In static load condition, inertial forces of the track are equal to zero due to a zero-loading rate for long-time period, so masses in the track system have zero acceleration.
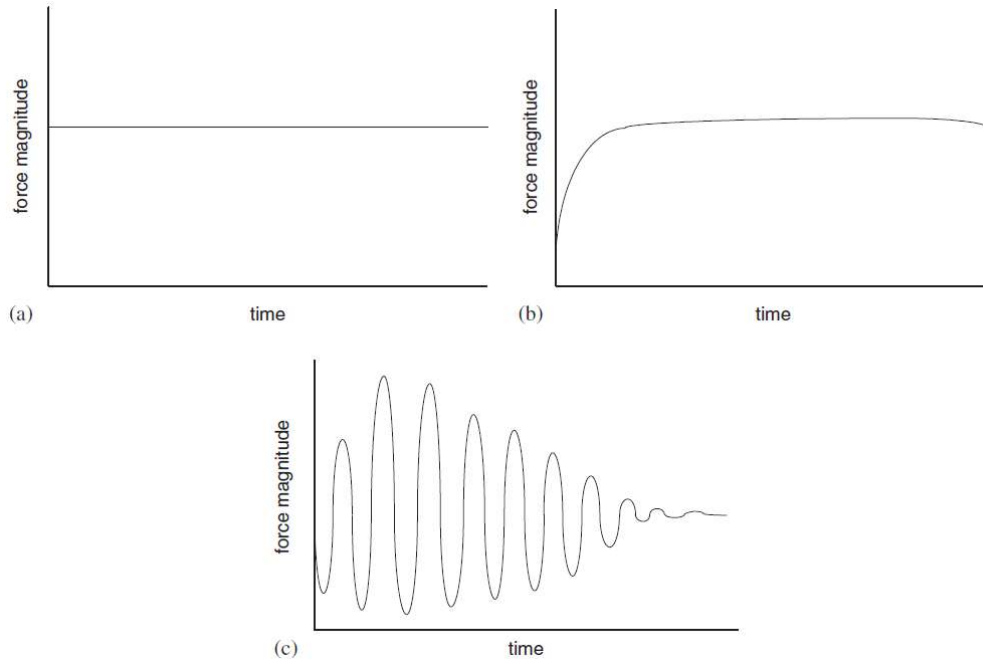
Figure 9: Loading time histories for (a) static (b) quasi-static (c) dynamic load conditions [40].

Static live load from train weight is more considerable than static dead load. Dead load is considerable in analyzing and designing certain topics like slope stability of track built on high embankment and subgrade issues at a large ballast layer [8]. In shallower ballast layer depth (< 1.3 m), live load is larger than dead load [8].

Typical axle load for high-speed passenger trains are presented in Table 2. Fryba [41] presented statistical measurements of train operations in Czech Republic. He summarized that there are three major live load ranges; 180 – 200 kN for fully loaded freight cars and locomotives, about 100 kN for the passenger cars and partially loaded freight cars and about 50 kN for empty freight cars.

Table 2: Typical Axle Loads of Trains in Different Countries Reproduced From [8]

Country	Vehicle	Axle Load (tonne)
Japan	0, 100 series	16.1
	300 series	11.3
	500, 700 series	11.1
China	Passenger car running on dedicated high-speed line	17
Germany	ICE 1, ICE 2, Passenger car on shared line	19
	ICE 3, ICEM 4	16
England	Eurostar	17.3
France	TGV-R	17
United States	Acela power car	22.7
	Acela coach car	16.4

Li et al. [8] described the typical static dead load ranges for each track component; rails weighted from about 45 kg/m to 75 kg/m, timber tie weighted about 110 kg and concrete tie weighted 360 kg. They described the typical track substructure density for ballast (1760 kg/m^3), sub ballast (1920 kg/m^3) and subgrade (2240 kg/m^3).

Remennikov and Kaewunruen [40] defined the quasi-static loading as an applied vertical loading with slow application rate as shown in Figure 9. The magnitude of a quasi-static loading slightly changes in the long time period with a frequency range of 0-20 Hz [42, 43]. Inertial forces are introduced but they can be neglected as they are small due to the slow rate of load application. The quasi-static loads typically are around

1.4–1.6 times the static wheel load without the effects of unbalanced super elevation [44]. The quasi-static loads usually introduced to the railway track from loads that slightly change in the long time period like centrifugal force, gross tare and cross winds [7].

2.4.1.2 Dynamic Loading

A ballasted railway track is also exposed to dynamic loading due to the train repetitive passages. A train consists of a number of train cars. Each train car has typically four axles with different spacings. Each axle exerts a load on ballast layer. For one train passage, the train applies a number of vertical loadings on the ballast layer. This generates a number of loading pulses. Dynamic loading is the application of loading pulses on railroad ballast within a short period of time.

Remennikov and Kaewunruen [40] defined the dynamic loading as a time dependent loading; where the application rate of the dynamic load and between consecutive pulses is very small as well as the load magnitude changes rapidly in a short period as shown in Figure 9. Lee [45] pointed out that dynamic loading exerted on railway tracks are applied within very short periods of 2–10 micro seconds. Track and vehicle irregularities can introduce dynamic loads to the track. For example, irregular track stiffness, rail corrugations, rail discontinuities (welds, joints and switches), wheel burns and wheel flats [7]. Remennikov and Kaewunruen [40] estimated the dynamic loading due to the generated high frequencies from the irregulated wheel/rail interaction to be about 1.5 times the static wheel load.

Under dynamic loading the track response is governed by both stiffness and inertial forces. Stiffness forces are based on the track material properties. Inertial forces are based on the mass and acceleration of track elements under loading. Under dynamic loading, forces are applied in a short period of time. The track responses are governed

by both stiffness and inertial forces. Inertial forces are considered as additional forces applied on the track and may cause serious failure to the railway track [44]. However, under static and quasi-static conditions, the system is governed by stiffness forces only. The inertial forces are marginal and can be neglected, where the track acceleration is close to zero.

2.4.2 Squeezing Loading

Tamping is a maintenance process by which track alignment is reestablished. Kumara and Hayano [46] recommended that ballast tamping should take place when FI_p of the fouled ballast exceeds 30%. Selig and Waters [9] concluded that the squeezing forces from track tamping machines during the tamping process cause considerable damage to railroad ballast. However, Wright [47], Aursudkij [48] and Nålsund [49] found that the high impact force due to the injection of the tamping tines into the ballast cause more damage to ballast than squeezing. Wang et al. [50] used the discrete element modeling method to study the effect of tamping and tamping frequency on the degradation and deformation of railroad ballast.

2.5 Ballast Deformation Mechanisms

Ballast behaves under cyclic loading as an elastoplastic material [35]. Both non-linear resilient (elastic behavior) and permanent (plastic behavior) deformations may occur in one cycle as shown in Figure 10. The permanent deformation is maximum at the first cycles of cyclic loading. At the final cycles, permanent deformation is minimum, and ballast almost starts to behave as an elastic material. Lekarp et al. [51, 52] presented reviews on the state of the art of the resilient and permanent deformations of granular material.
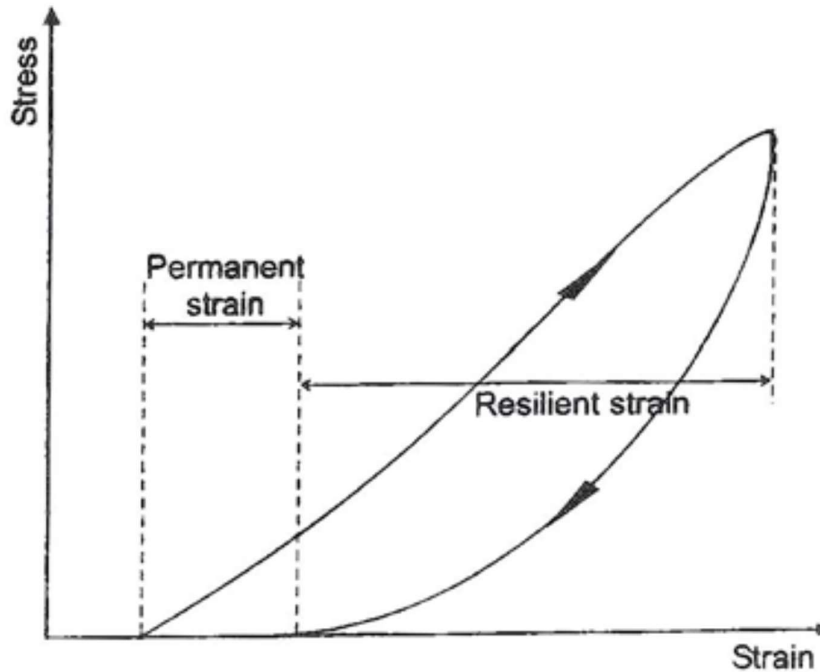
Figure 10: Permanent and resilient deformation within one cycle [51].

Mainly, there are two shapes of permanent ballast deformation [9]; frictional slip and particle breakage. Due to train running on the rails, either of these shapes may occur to ballast layer. Liao et al. [53] defined the frictional slip as the relative particle motion in contact under the loads. Katzenbach and Festag [54] defined the particle breakage as the division of grains into portions under loading due to the slipping and rolling movements of angular/sub angular aggregates. McDowell et al. [55] found that particle breakage is proportionally related to the applied load and particle size, while it is inversely related to the coordination number, i.e. number of contacted particles.

Chan [56] assumed that the deformation mechanisms of unbounded granular material undergoes three main mechanisms; consolidation, distortion and attrition. However, as pointed out by some researchers e.g. [51, 57], the true deformation mechanism of granular material is still not fully understood.

2.6 Understanding Ballast Behavior

From the literature, experimental and modeling approaches are used to estimate and understand the mechanical behavior of railroad ballast.

2.6.1 Experimental Testing

There are number of traditional experimental tests used to identify the mechanical and physical characteristics of granular material like conventional triaxial test, conventional direct shear test, petrographic analysis, crushing test and Los Angles abrasion. Indraratna et al. [10] recommend avoiding the use of conventional tests for understanding the mechanical behavior of granular material as they rottenly produce confusing results due to the large granular particles size relative to test sample size.

Large scale box test has been used intensively in the literature to understand the mechanical behavior of railroad ballast under traffic loading. Box test is introduced in the early 1980s by [58, 59]. Box test is an experimental approach used to represent the real field ballast behavior and performance under traffic loading; where a small box portion of real track is represented by box test [35].

2.6.2 Numerical Modeling

Modeling of railroad ballast is used extensively in the literature to understand its mechanical behavior. The main significant advantages of modeling are the conservation of cost relativly to experimental approach. Field and large-scale experimental tests are used to evaluate and understand the real mechanical behavior of railroad ballast. Nevertheless, testing ballast behavior either in the field or in the lab is an expensive exercise. Alternatively, modeling the mechanical behavior based on theoretical models that reflect the real mechanical behavior is introduced. Modeling of railroad ballast has the ability to increase the knowledge of understanding the behavior of railroad ballast under different loading conditions and material properties.

Furthermore, modeling of railroad ballast develops the knowledge and tools needed for predictions. Such tools have the potential to make huge financial savings within the design constrains.

There are two different types of modeling methods used to model the mechanical behavior of railroad ballast based on the problem-solving type; analytical and numerical. There are two main numerical methods used to model ballast layer based on material characteristics, continuum and discrete. The continuum-based numerical method is the Finite Element Method. The discrete-based numerical method is the Discrete Element Method. This section describes and highlights the main key advantages and disadvantages of the different modeling approaches used in the literature to understand the mechanical behavior of railroad ballast.

In this study, the analytical modeling using Beam on Elastic Foundation theory is utilized to simulate train loading. The simulated train loading is used as an input in the Discrete Element Model of box test. The numerical Discrete Element Method is used to model the behavior of railroad ballast under different train simulated loading cases using box test.

2.6.2.1 Key Concerns and Limitations

There are various modeling methods used in the literature to model the behavior of railroad ballast as discussed previously. Each method has certain advantages and disadvantages. This section highlights the key concerns and limitations of each modeling method in modeling the mechanical behavior of railroad ballast.

2.6.2.1.1 Analytical Modeling

Analytical models describe the mechanical behavior of each track element based on its characteristics using mathematical models. The ballasted track elements have been analytically modeled using different structural elements based on their

characteristics. Rails are modeled as beams. Sleepers are modeled as rigid masses. Other track elements such as rail pads and ballast layer are modeled as mass-spring systems. Track subgrade is modeled either as a rigid foundation or a half space.

Analytical models of ballasted tracks have been used enormously in the literature to study the ballasted track dynamic behavior. Nevertheless, they have a number of drawbacks in modeling the mechanical behavior of the ballast layer. While analytical modeling being useful for scoping and investigating the short-term mechanical behavior, they lack many characteristics to analyze and visualize the complex and long-term mechanical behavior of the ballast layer. Analytical modeling of ballasted tracks is used for static and dynamic analysis. In the static analysis, the ballast layer is mostly modeled as a simple linear elastic spring with a constant stiffness. In the dynamic analysis, other structural elements are used to analytically model the ballast layer like masses and viscous dampers with constant damping coefficient and mass values to count for the damping and dynamic effects of the ballast layer.

The analytical approach of modeling a ballast layer does not represent the real complex behavior of railroad ballast under cyclic loading, where ballast behaves as elasto-plastic material with non-linear load-deformation behavior under cyclic loading. Furthermore, the stiffness and damping properties of a ballast layer is not constant with time due to ballast densification and deterioration under cyclic loading and after long term service. Moreover, analytical models do not have the ability to study the effect of variable parameters on ballast mechanical behavior e.g. particle breakage, particle shape, particle size distribution and fouling.

However, analytical models have been used extensively in the literature to study the dynamic behavior of ballasted tracks due to their simplicity [60] and effectiveness in the track static and dynamic analysis. They can enrich the understanding of the

defined theoretical problems and they can be used as validation tools to numerical models.

2.6.2.1.2 Numerical Finite Element Method

Finite Element Method (FEM) is a continuum numerical method that is widely used in many research applications. It is considered as an essential part of Computer Aided Engineering (CAE). Madenci and Guven [61], Zienkiewicz and Taylor [62] and Moaveni [63] defined the FEM as a powerful computational tool that estimates the solutions of different real problems that have sophisticated domains with boundary conditions. It is introduced to solve complicated civil engineering problems related to structural and elasticity analyses. The first numerical models used to understand the mechanical behavior of ballasted tracks were in the period of 1970s-1980s. Modeling the mechanical behavior of railroad ballast using FEM has increased throughout the years as shown in Figure 11.
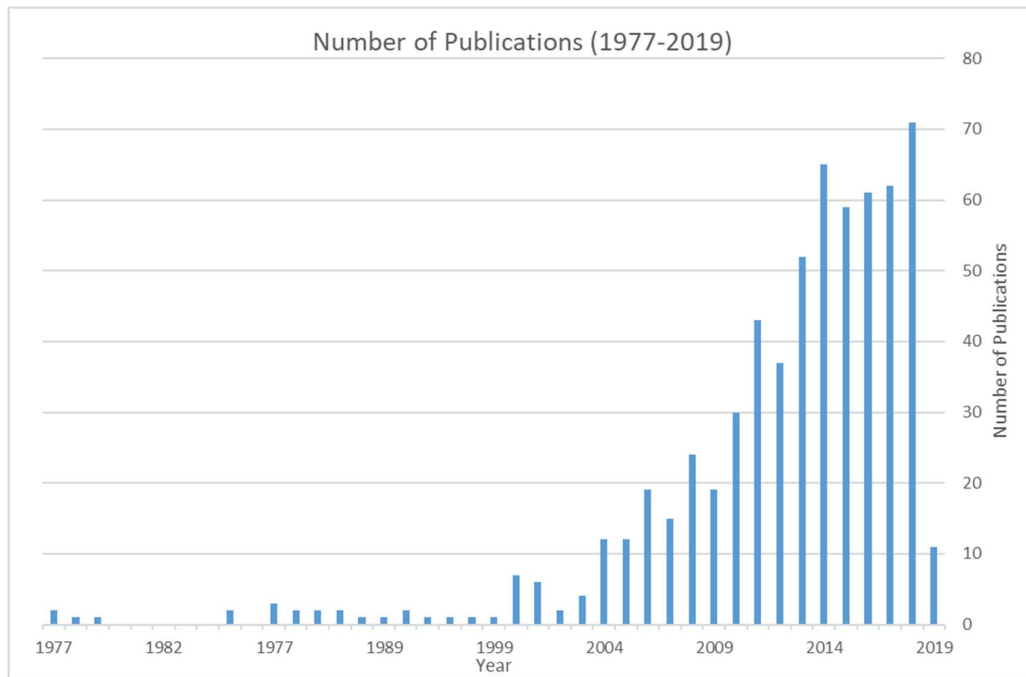
Figure 11: Number of publications from 1977 to 2019 related to modeling railroad ballast using the Finite Element Method. Obtained from the Scopus using the following keywords: Railroad Ballast OR Ballast Track OR Ballasted Track AND Finite Element Method OR Finite Element Model OR FEM.

FEM is a useful tool in modeling the long-term overall ballasted track behavior under different loading conditions and large number of cycles. It provides the macroscopic behavior of railroad ballast layer. Few FEM models are used to validate experimental test results like box test [64-67] and direct shear test [68] unlike DEM where most of the models are done to validate and calibrate experimental results as discussed below.

The most significant limitation of FEM in modeling the mechanical behavior of railroad ballast is the application of the material model that reflects the realistic discontinuous and elasto-plastic properties of railroad ballast. Although the continuum

assumption works in most cases, the insight visualization of stresses and displacement cannot be correctly evaluated using FEM because the ballast layer is modeled as a continuum material. For instance, it is difficult to model ballast layer initial settlement, volumetric change, particle breakage, force chain distribution, particle displacement, particle shape, particle size distribution and fouling using FEM.

2.6.2.1.3 Numerical Discrete Element Method

Many Researchers have used the Discrete Element Method (DEM) to model the mechanical behavior of railway ballast. DEM considers the discontinuous properties of railroad the ballast layer. Ballast aggregates are modeled as distinct particles using DEM. The number of publications related to modeling railroad ballast using DEM has significantly increased as shown in Figure 12.
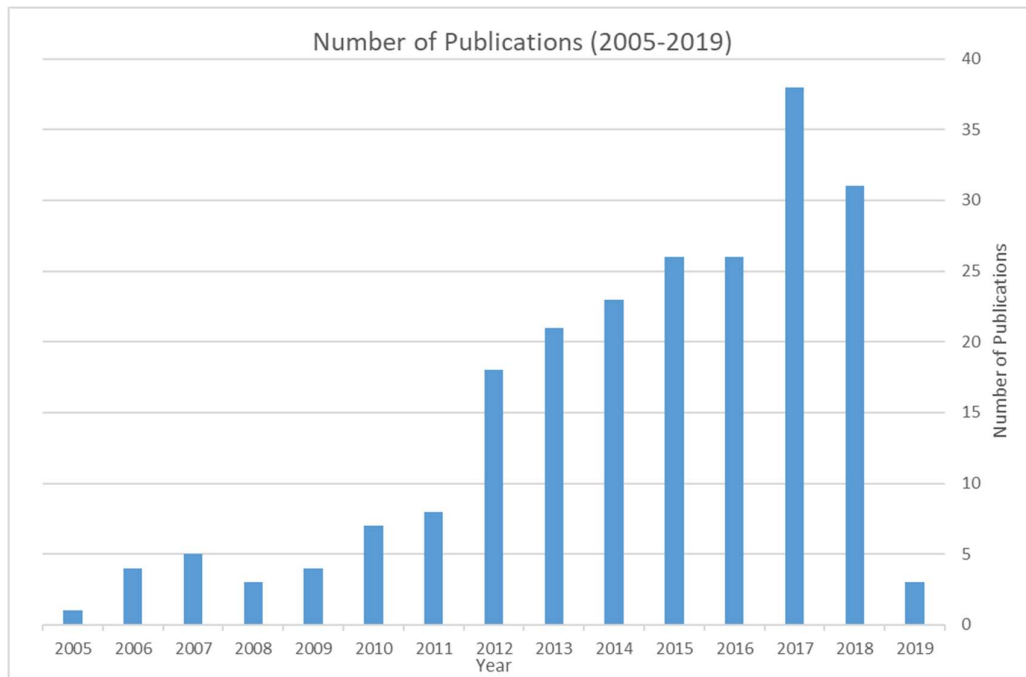
Figure 12: Number of publications from 2005 to 2019 related to modeling railroad ballast using the Discrete Element Method. Obtained from the Scopus using the following keywords: Railroad Ballast OR Ballast Track OR Ballasted Track AND Discrete Element Method OR Discrete Element Model OR DEM.

DEM accounts for the discontinuity property of railroad ballast. DEM is a powerful modeling tool in understanding and visualizing microscopic and macroscopic behavior of railroad ballast. DEM provides a comprehensive insight to the particle velocity, displacement and contact forces during the simulation unlike FEM and analytical modeling. DEM can study the effect of different parameters of railroad ballast like particle shape, particle size distribution, particle breakage and fouling on the mechanical behavior of railroad ballast.

The main limitation of DEM in modeling the behavior of railroad ballast is the high computational requirements (even with the significant advancement of computational resources) including the need for large computational resources.

Table 3 below, summarizes the differences between analytical methods, DEM and FEM in modeling railroad ballast behavior.

In this study, the analytical modeling using Beam on Elastic Foundation (BOEF) theory is utilized to simulate train loading transferred to the ballast layer. The simulated train loading form BOEF is used as an input to DEM of box test. Discrete Element Method is used to model the behavior of railroad ballast as it well considers the discontinues properties of the material. Numerical Discrete Element Method is used to model the behavior of railroad ballast under different simulated train loading cases using box test; and to study the influence of different simulated train loading cases on the mechanical behavior of railroad ballast.

Table 3: Comparison Between DEM and FEM in Modeling Railroad Ballast Behavior.

	Analytical Methods	FEM	DEM
Origin and History	Very old, introduced in 1867 by [69]	Old, introduced in 1940s	New, introduced in 1979 by [70]
Length Scale	Large	Large	Small
Analysis Scale	Macroscopic	Macroscopic	Microscopic
Material	Continuous/Discrete spring-mass system	Continuous	Discontinuous
Main Principles	Based on mathematical models, the stresses, moments and displacements of the system is found.	Based on material constitutive and discretization of continuum ballast layer, the stresses and strains of the system is found.	Based on individual discrete elements interactions, the whole system behavior is found.
Ballast Behavior	☒	☒	☑
Ballast Particle Breakage	☒	☒	☑
Ballast Particle Displacement	☒	☒	☑
Force Chain Distribution	☒	☒	☑
Ballast Fouling	☒	☒	☑
Ballast Particle Shape	☒	☒	☑
Ballast Size Distribution	☒	☒	☑
Entire Track Behavior	☑	☑	☒
Computational Time	Low	Moderate	High
Memory Usage	Low	Moderate	High

CHAPTER 3: LITERATURE REVIEW

3.1 Introduction

Trains run on different railway track systems; ballasted and ballast less (e.g. slab and embedded track) systems [5]. The ballasted tracks have the majority usage in the world due to their low cost and greater experience that has been gained compared to new ballast less tracks [7]. Ballasted tracks have been used in the beginning of railways and ballast less tracks have been introduced in the 1960s [6]. Kerr [71] provided a detailed discussion of the changes in track structure elements throughout the years.

The basic element of ballasted track is the ballast layer. It has a significant role in maintaining the track alignment and stability. It is the loading platform of the track. It transmits and distributes the train loading from track superstructure to subgrade. It is important to understand the key characteristics that influence the mechanical behavior of railroad ballast. The previous chapter highlights the key characteristics that influence the mechanical behavior of railroad ballast.

After service, ballast material loses its functionality. Ballast deforms and degrades. Ballast maintenance is required which is an expensive activity [10]. The importance of the ballast layer and costly maintenance raise the interest of researches about understanding the mechanical behavior of railroad ballast. Understanding the mechanical behavior of railroad ballast results in a better ballast design and efficient maintenance. The previous chapter discusses the two approaches used in the literature to understand the mechanical behavior of railroad ballast; experimental and modeling.

Experimental Testing for railroad ballast requires large scale instruments. Traditional equipment provides misleading results due to the particle size with respect to sample size. There are various large-scale tests used to understand the behavior of

ballast like uniaxial, triaxial and box test. From the literature, large scale box test is used extensively to understand ballast's behavior. In this study, there is no experimental testing done due to the absence of large-scale instruments in Qatar University's labs. Large scale instruments design and set up require time, technical and financial support. In this study, a modeling approach is used to model the behavior of railroad ballast using box test.

The previous chapter points to the common modeling approaches used in the literature to understand the mechanical behavior of railroad ballast. In this study, the Discrete Element Method is used to model the behavior of railroad ballast using box test. The analytical Beam On Elastic Foundation theory is utilized to simulate a more realistic train loading.

This chapter reviews the literature about understanding the mechanical behavior of railroad ballast using the Discrete Element Method through box test. The chapter reviews the different perspectives of ballast modeling using DEM through different sections. The different perspectives are DEM type, contact detection contact models, particle shape, particle size distribution and DEM software packages. After reviewing the literature for each perspective related to railroad modeling using DEM, the used parameter for each perspective is highlighted at the end of each section. At the end of this chapter the gap of knowledge in this topic is summarized and the novelty of this work is highlighted.

3.2 Discrete Element Method Types

The Discrete Element Method (DEM) is a numerical method used to solve mathematical problems associated to discrete characteristic material like granular material. Each particle has its own properties of displacement, velocity, acceleration and contact forces. The calculation process for each property of each particle in a granular assembly is tremendous and complex. Therefore, discrete characteristics of granular material make the understanding of its mechanical behavior very difficult. DEM is a powerful tool that can analyze the mechanical behavior of granular material both microscopically and macroscopically [70]. There are two approaches used in DEM based on particle contact nature; hard and soft spheres as described below.

Hard sphere and soft sphere and are the two most common types of Discrete Element Methods. The hard sphere method considered the contact between particles to be rigid (stiff). The overlaps and deformations of particles are not simulated using this approach. Forces between particles are impulsive and implicitly considered. Only momentum exchange is considered due to collisions. Particles' velocities are explicitly calculated based on the material properties (coefficient of restitutions). One collision at a time is considered. Never two or three collisions are considered simultaneously. A typical application of hard sphere method is rapid granular flow simulation [72].

The soft sphere method considers the contact between particles to be rigid partially. The soft sphere approach considers the overlaps and deformations of particles during the simulation [73]. Soft sphere method has the ability to a handle number of particle contacts [72]. Soft sphere DEM has been used broadly to study many discrete particles phenomena. O'Sullivan [74] drew a schematic diagram to illustrate and summarize the differences between hard and soft sphere DEM approaches as shown in Figure 13.

Hard Sphere - Event Driven Approaches   Soft Sphere - Molecular Dynamics Approaches

Pre-Contact   Contact duration ≅ 0 No overlap   Post-Contact v'=f(change in momentum, coefficient of normal restitution, coefficient of friction, coefficient of tangential restitution)   Pre-Contact   Contact duration > 0 overlap > 0   Post-Contact v'=f(overlap, contact forces calculated using contact constitutive model, inertia)

(m₁, m₂, particle masses)

Figure 13: Schematic illustration of the differences between hard and soft DEM approaches [74].

Cundall and Hart [75] set the basics of soft sphere DEM. They defined DEM as a calculation tool that recognizes the contacts and allows the rotations and displacements of each discrete element. In 1971, the first computer model that models the progressive failure of a rocky discrete elements was introduced by [76]. His model was based on the friction and normal stiffness for the interaction between discrete blocks. In 1979, the distinct element method which is commonly known now as DEM was introduced to model granular assemblies including particles overlapping by [70]. The purpose was to simulate the particle contact force chain in the assembly. In his computer program "Ball", he utilized the aspects of calculation cycle, law of force displacement, law of motion and damping effects to simulate the contact force distribution. He studied the internal mechanisms of 100 and 1000 discs and their responses to stress. The initial state of 100 discs is shown in Figure 14.

Maximum force:
■■■■ 0.1379E+09

B. STRESS:
(1,1) -1.500E+06
(1,2) 0.000E+00
(2,1) 0.000E+00
(2,2) -1.500E+06

components of applied
stress tensor

boundary particles
identified by dashed line
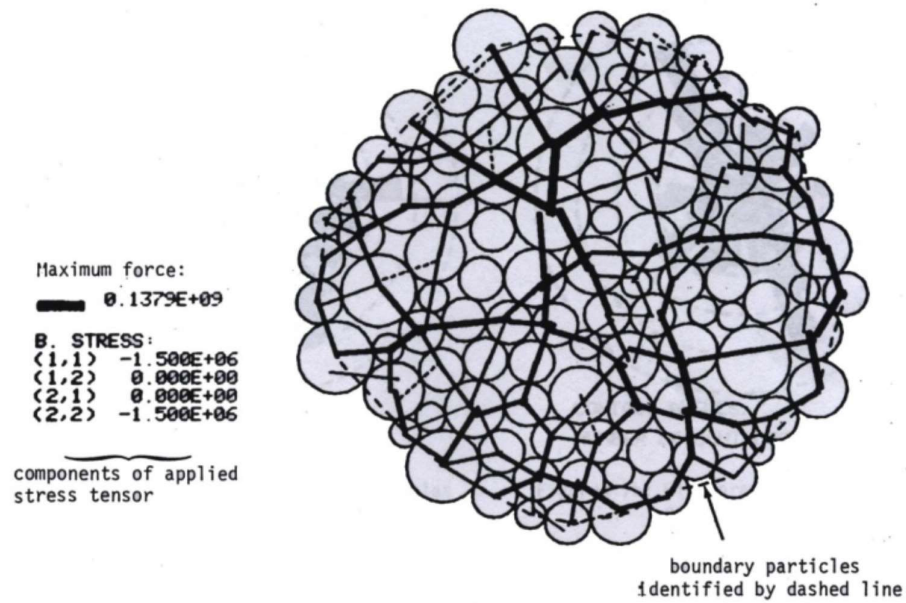
Figure 14: Initial contact force chain in 100 discs by [70].

Soft sphere DEM has been used broadly in many research areas and DEM software packages [77]. From the literature, most of the DEM models for railroad ballast used the soft sphere discrete element method. Few of them used the hard sphere discrete element method like [78, 79]. Lim and McDowell [80] were the first authors who used soft sphere DEM to simulate the mechanical behavior of railroad ballast. In this study, soft sphere DEM is used and supported by the used software EDEM (3.10).

3.3 Main Principles

Cundall and Hart [75] defined the DEM as a numerical modeling method that can automatically detect the contacts between particles in the system to calculate the finite rotations and displacements for each particle. The main outcome of DEM is to update the positions of each distinct element in the simulation based on their interactions during the simulation time.

The main principles of DEM mechanism are illustrated in Figure 15. Contact detection algorithm is firstly applied to a system to detect the contact zones. Then at each contact zone, contact forces are calculated based on defined contact models that are based on material properties like normal and tangential stiffness. After that, using newton second law, particle acceleration is calculated. Then, by numerical integration particle's velocity and position can be found.
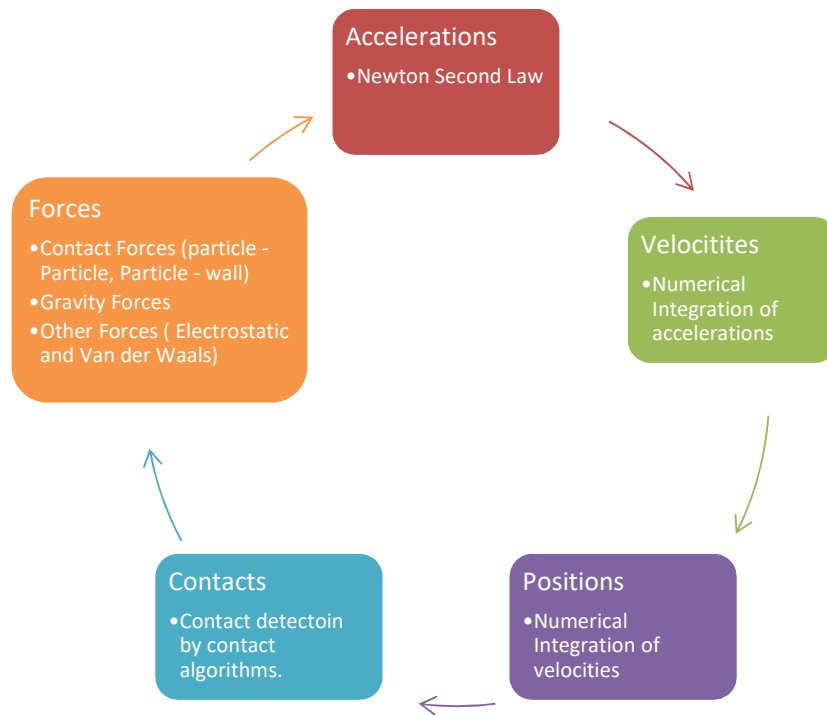
Figure 15: Main concept of calculation cycle of DEM.

The main components of any DEM model are distinct elements (particles) and contact models. There are various geometrical shapes of distinct elements as well as various contact models that have been used in modeling railroad ballast as will be discussed later.

3.4 Calculation Mechanism

During the simulation time distinct particle interacts with other distinct particles or wall that leads the particle to move in two ways of motion; translational and rotational. Each distinct element in DEM model has six degrees of freedom based on two ways of motion. Each motion way has three degrees of freedom as shown in Figure 16. The main objective of DEM is to calculate those finite rotations and displacements of each distinct element during simulation time at each finite time step. Newton's second law is used to calculate particle's motions both rotational and translational after calculating the forces and torques acting on a particle. Then by numerical integration over the time step the particle's velocity and position are found.
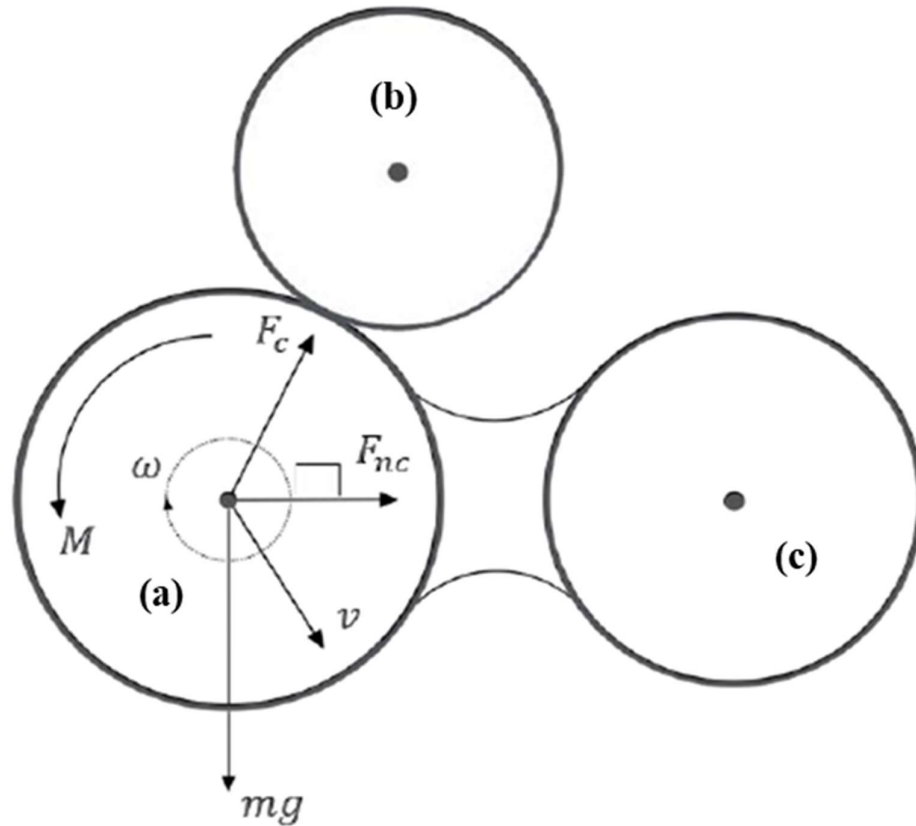
Figure 16: Free body diagram of paarticle 'a'.

It is critical to choose the appropriate time step in DEM simulations [81, 82]. Too large time steps may result in inaccurate results with low computational time [83]. However, too small time steps could provide accurate results but need considerable computational time.

Particle's rotation (rotational motion) is calculated based on equation 3.1 below

$$I\frac{d\omega}{dt} = M \tag{3.1}$$

and particle's displacement (translational motion) is calculated based on equation 3.2 below

$$m\frac{dv}{dt} = Fg + Fc + Fnc \tag{3.2}$$

where, I is the particle's moment of inertia, ω is the particle's angular velocity, M is the resultant contact torque acting on the particle, t is the time, v is the particle's translation velocity, m is the particle's mass, Fg is the gravitational force, Fc is the resultant acting contact force on the particle and Fnc is the acting resultant non-contact force on the particle.

There are two types of contact forces (Fc); (a) Particle to Particle contact force (b) Particle to Wall contact force. The contact forces are calculated based on contact models. There are number of contact models provided in the literature and used in DEM packages as discussed below (3.6). The non-contact force (Fnc) is a force acting on the particle without contact with other particles like electrostatic and Van der Waals. The non-contact force has not been used in discrete element modeling of railroad ballast.

After calculating the acting forces and torques on each distinct particle, angular and linear accelerations can be calculated. Then by numerical integration particle's velocity and displacement (linear and rotational) can be found.

There are different schemes of numerical integration used in DEM: Euler integration (1st order); Leapfrog integration (2nd order); Verlet integration (2nd order); Respa (higher order); Gear integration (higher order); and Taylor expansion (1st, 2nd and higher order). Rougier et al. [84] and Kruggel-Emden et al. [85] compared different explicit numerical schemes used in DEM based on different aspects for each numerical method like stability, accuracy and efficiency. Rougier et al. [84] showed that lower order integration methods are faster than higher order integration schemes for the same accuracy level. Kruggel-Emden et al. [85] found that orders two and three of Taylor expansion integration scheme and improved Verlet scheme are recommended to be

used for large-scale DEM models. Mishra [86] recommended the leapfrog integration scheme due to its performance in terms of accuracy, efficiency and stability.

Nevertheless, Euler integration scheme is widely used in discrete element modeling due to its simplicity and low computational time relative to others [82, 85, 87]. Additionally, It was used and discussed by Cundall and Strack [70] who introduced the DEM theory. Therefore, in this study Euler integration scheme is used.

3.5 Contact Detection

Contact detection is the most time-consuming part in DEM modeling. It takes the most portion of DEM model's computational time and effort [77, 88, 89] as shown in Figure 17. The computational time is dependent on the geometrical shape of distinct elements. For complex particle shape (non-spherical), contact detection may takes 80% of computational time [90]. There are different approaches for contact detection in DEM. However, contact detection in DEM analysis for spherical shapes is usually done in two main steps.
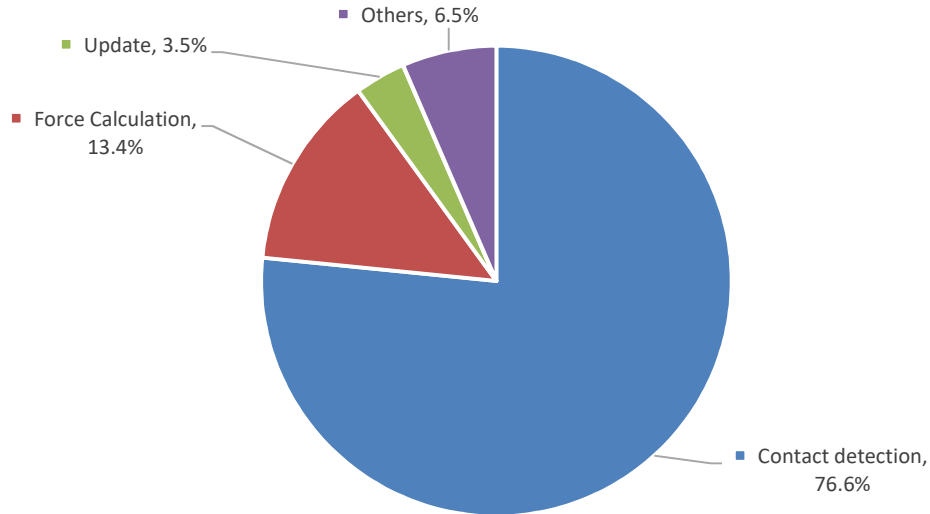
Figure 17: Computational time percentages for each step in DEM analysis [89].

The first step is the contact detection which is also known as neighbour search [91]. It purpose is to know the contacted particles in the model and this is done by different approaches. The nearest neighbour search is done by grid or tree based algorithms. The different grid and tree based neighbour search algorithms are described and compared in details by [88, 92]. Williams and O'Connor [91, 93] reviewed the algorithms used in neighbour search step. Several publications in the literature like [93-98] discussed about optimizing the nearest neighbour searching approach.

The grid based approach [99, 100] is based on dividing the model domain into grid cells (Figure 18 a and b). At each time step the simulator searches the grid cells for possible particle contacts. The size of the grid cell depends on the minimum particle radius (R_{min}). The recommended grid cell size is in the range of 3-6 of R_{min}.
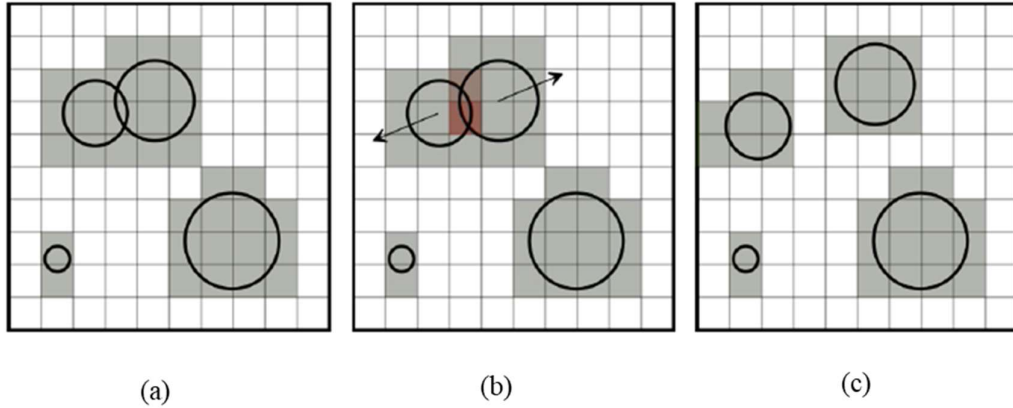
Figure 18: Typical steps of grid based contact detection algorithm for 2D circles. The same approach for 3D spheres is used (a) domain discretization into equal grid size cells and checking the active cells (b) cells with particle contacts are checked and contact forces are calculated (c) updating particles' positions and active cells [77].

The tree based [101, 102] approach is based on dividing the model domain into sub-domains. The simulator starts dividing the domain into two sub-domains based on the cantered particle. Then, two cantered particles in each of the sub domain is used to spilt the sub domain into smaller sub-domains (Figure 19). This process is continuous until the defined number of subdomains is reached. The tree of the subdomains is formed. The neighbours can be determined by following the tree upwardly.
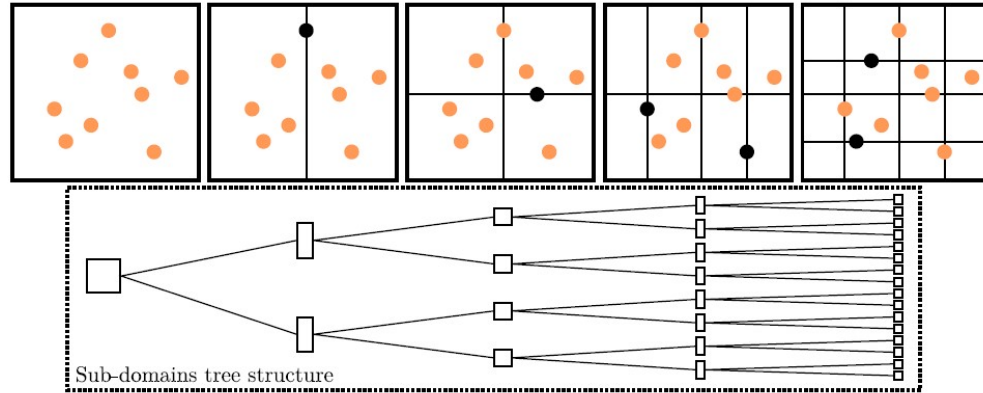
Figure 19: Tree based approach [103].

From the literature, the grid based approach shows better performance and requires lower computational time, especially for large scale models compared to tree based approach [92]. Furthermore, most of DEM software packages use grid based nearest neighbour searching approach like EDEM and PFC [77, 104]. In this study, grid based approach is used as EDEM (used software in this study) uses grid based approach.

The second step is contact or geometric resolution [91]. After detecting the contacted particles, the details of the contact between particles are identified in this step. Then the contact forces are calculated using the contact models and particles positions are updated accordingly (Figure 18 c). This process is repeated to the last time step of DEM simulation.

3.6 Contact Models

In DEM there are two types of interactions between the distinct elements; particle to particle and particle to wall. The main purpose of contact models is to simulate both interactions during the simulation period based on theoretical knowledge of contact mechanics science. Modeling the contact mechanics of granular materials

using DEM has been discussed extensively by geotechnical scientists [105-107]. The contact models used in discrete element modeling of railroad ballast are discussed in this section.

The contact between two particles is not at a single point but on a very small finite area because of the particle's deformation. At the contact area there are normal and tangential contact plans. Therefore, total contact force consists of normal and tangential forces. It is not easy to accurately simulate the contact area between particles due to many factors like geometrical shape and material characteristics [72].

The accuracy of DEM results is dependable on the accuracy of material properties parameters used in the contact model [72, 82]. DEM commonly uses simplified contact models that find the forces and torques acting on a particle due to contact, in the sake of efficient computational time. There are different contact models for different element shapes (i.e. spheres, polyhedrons or others). Most of the contact models are developed for spherical contacts using springs and dashpots [72, 108]. Mishra [86] discussed the different contact models used for spherical shapes.

The most used contact models for railroad ballast modeled as spherical shapes are linear elastic contact model by [70] and non-linear elastic Hertz-Mindlin contact model by [109, 110].

The linear elastic model is simpler and requires less computational time compared to the non-linear elastic Hertz-Mindlin contact model. There arre many comparative studies e.g. [111, 112] between the linear elastic and non-linear elastic Hertz- Mindlin contact models and they found that results using both models are close and in good agreement. However, Di Renzo and Maio [111] recommended the Hertz-Mindlin contact model to be used in modeling granular behavior using spherical shapes that can provide an accurate and deep understanding to granular motion.

Therefore, Hertz-Mindlin contact model is used in this study to model railroad ballast using DEM. Besides, it is the default contact model in EDEM for spherical particles, it produces accurate results.

Non-spherical shapes like polyhedrons have their own complicated and time-consuming contact models that are based on mathematical equations. For polyhedrons, there are few methods to calculate and detect the contacts between them. Cundall et al. [113, 114] introduced the common plane method to detect the contacts between polyhedrons. This method is then improved in terms of faster computational time to detect the contacts between the polyhedrons by [115]. Eliáš [116] introduced a new method to calculate the contacts of polyhedrons based on the intersecting overlapped volume with an application to railroad ballast behavior. The author simulated odometer test for railroad ballast. The results of the DEM model are promising but only 120 particles are used in the model due to high computational time. A new method is introduced by Ahmed et al. [117]. It is called the potential particle shapes that is based on representing the polyhedron particles as modified rounded particles. They simulated the triaxial test of railroad ballast. The results are in very good agreement with the experimental work. However, their method is only able to represent convex particles. Table 4, shows the contact models used in the literature to model railroad ballast.

Table 4: Contact Models Used in the Literature to Model Railroad Ballast using DEM.

Contact models	References
Linear Contact model (spherical shape)	[16, 17, 80, 118-134]
Hertz-Mindlin (spherical shape)	[50, 135-142]
Other contact models based on mathematical equations (non-spherical shape)	[78, 79, 116, 117, 143-151]

3.7 Particle Shapes

There are different particle shapes used in DEM. For realistic results, the modeled distinct element should have almost the same real shape. The complexity of particle shape in DEM has a direct relationship with computational time and result's accuracy. The more the particle shape used in DEM model is complex, the more the computational time is needed to detect the contacts. But DEM results are more realistic. Particle shape should be efficient to accurately describe the real shape and at the same time it should be simple enough to reduce the computational time. Many studies [121, 130, 152, 153] presented the importance of particle shape modeled in DEM simulations and its effect on the accuracy of DEM results.

Spheres in 3D or circles in 2D are the mostly used shapes in DEM applications. As they require low computational time and most of contact modeled are developed for spherical shapes as discussed previously in section 3.6.

Lim and McDowell [80] and Lobo-Guerrero and Vallejo [118] introduced the DEM modeling of railroad ballast using spheres and disks respectively. However, spheres and disks do not reflect the real behavior of railroad ballast due to their easy rotation under loading and they do not provide the interlocking property of railroad ballast [80, 118, 121, 154]. Therefore, three approaches are done in the literature to model railroad ballast with taking into consideration the shape effects.

The first approach is multi-sphere. Its main advantage is that it almost considers the irregularity and angularity of ballast meanwhile it sustains the computational efficiency. It gives a better approximation to the real ballast shape than spheres. It is used in many other studies like geotechnical [155-157] and aerospace [154, 158]. In this approach, the railroad ballast shape is approximated by a number of overlapping or touching spheres to form a clump (Figure 20 b). The bond between the spheres is

normally set to infinity to form a rigid clump. Particle breakage in this case is not allowed. The contact forces calculation is done only between clumps, not spheres in each clump. Some researchers set a finite bond strength between the spheres to model particle breakage and crushing [118, 120, 159]. However, this increases the computational time.
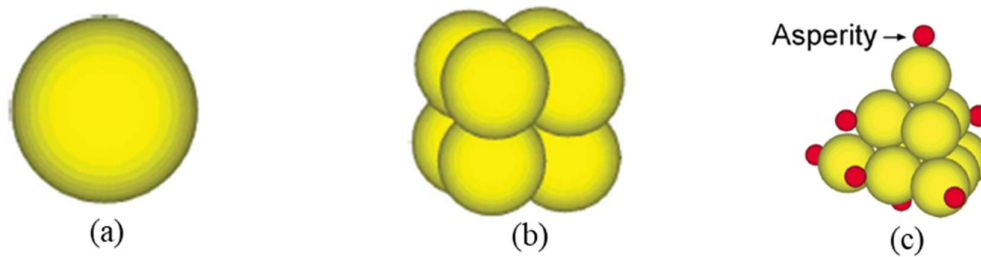
Figure 20: Ballast particles modeled as (a) sphere (b) cubical clump of 8 spheres (c) tetrahedral clump of 10 un-breakable spheres with 8 breakable asperities [122].

Lu and McDowell [121] developed simple steps to generate clumps. Their technique aims to overlap different ball numbers and diameters to form complex clumps. It includes the aspects of ballast angularity, sphericity, and surface roughness. Mahmoud et al. [16] developed novel two multi-circles approaches that capture the angularity of railroad ballast using MATLAB and AutoCAD routines in addition to the typical routine of spherical clumps. MATLAB routine generates hexagonal close-packed assemblies. A closed hexagonal shape is used for each scanned ballast shape and then it is filled by the same sized circular elements. AutoCAD routine represented by filling each scanned ballast with number of tangential different size circles. The two innovative routines allow the modeling of particle breakage. The 2D scanned ballast

images were taken from Aggregate Imaging System (AIMS) of the authors' database. Another new variation of multi-sphere approach is introduced by [119, 122, 126]. They used clumps with bonded asperities to model particle abrasion as shown in Figure 20 c. Chen et al. [160] used simplified clump shape of two overlapped spheres to model large number of particles and load cycles with low computational time. Zhang et al. [128] introduced a new approach to generate multi spheres clusters of bonded spheres using laser scanning technology. First, point cloud data of the ballast surface is taken by laser scanner. Second, based on the point cloud a closed surface is made to model the particle geometry. Then, spheres are generated within the cloud surface. Figure 21, summarizes the flow diagram of their approach. Indraratna et al. [124] recommended the proper number of spheres in a cluster to be 10 to 20 spheres. Many studies [80, 121, 122, 153] showed the realistic deformation behavior of railroad ballast modeled as clumps compared to spheres due to the interlocking property of clumps. The main limitation of this approach is the computational time. The larger number of spheres used in forming the clump, the more particle shape is realistic. However, the more computational time is required.
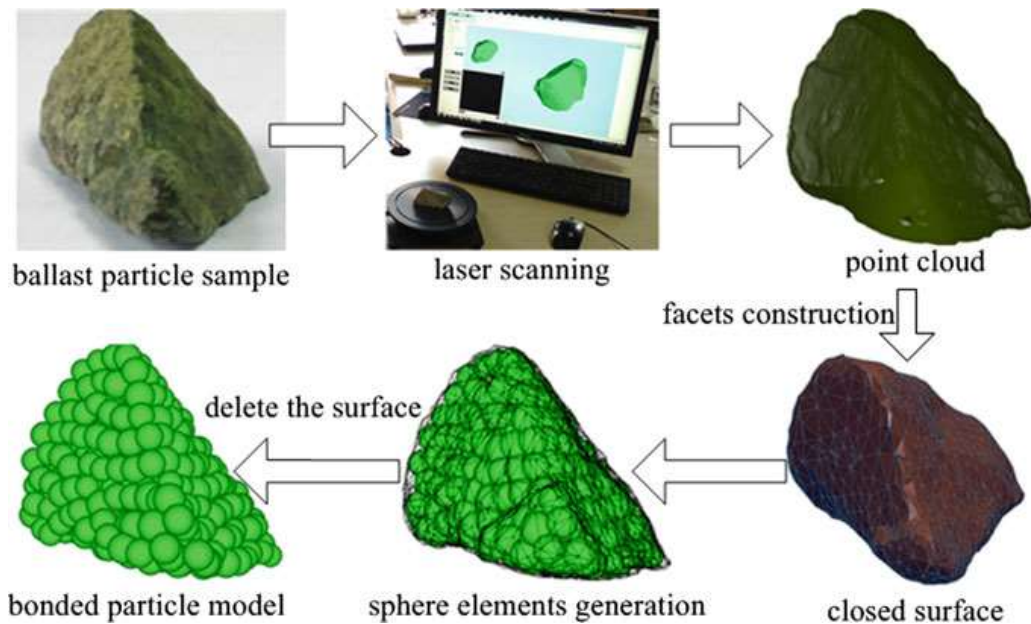
Figure 21: Flow diagram of cluster of bonded spheres generation by Zhang et al. [128].

The second approach is to model the ballast shape as polyhedrons (polygon in 2D). A polyhedron shape is defined by the number of corners, edges and faces (Figure 22). Its main advantage is that it represents the realistic shape of ballast. However, it is very time expensive due to the massive time needed to detect and calculate the contacts of each particle, especially edge contact force [154]. Another disadvantage of using polyhedrons shapes in DEM models is that there are low numbers of descriptive contact models for this shape. Contact detection algorithm and contact force calculations should be designed. Most DEM software use sphere shapes. BLOKS3D allow the usage of polyhedrons and LMGC90 allow the usage of polygons.

Figure 22: Real ballast and corresponding polyhedron simulated ballast [117].

Saussine et al. [143] modeled ballast as a pentagonal shape to study its behavior under cyclic loading. The main objective of their study was to show and validate the ability of DEM to model railway ballast. Eliáš [116] modeled ballast as polyhedron to study its behavior under monotonic loading. Small number of particles are modeled due to the computational time issue. The author used a novel approach to generate random polyhedral particles using Vorni tessellation technique. Ahmed et al. [117] simulated the triaxial test of railroad ballast using polyhedron shape.

The third approach is introducing a rolling resistance moment at the particle's contacts. This approach was introduced by Jiang et al. [106]. The main idea of this approach is to add a rolling resistance moment in the spherical particle contact to resist the rolling motion. This represents the angularity and interlock properties of real ballast.

This approach is simpler and requires lower computational time compared to the previous two approaches [146]. The contact detection and contact force calculation are straight forward as the particle consists of one sphere with known radius center and position. The number of spheres is lower with respect to the multi-sphere approach. Therefore, less computational time is needed to detect the contacts and calculate the contact forces. There are many studies not related to railway engineering which used this approach [161, 162]. Irazábal et al. [146] recently used this approach with an application to railway engineering to study the lateral resistance of railroad ballast using DEM. Table 5, shows a comparison between the used particle shapes in modeling railroad ballast using DEM. Table 6, summarizes the used particle shapes in the literature to model the railroad ballast.

Table 5: Comparison of Ballast Shapes Used in DEM Models

3D Ballast Shape	Advantages	Disadvantages	Solutions to Disadvantages
Spheres	Simple shape. Most contact models developed for spherical shapes. Low computational time.	Particle behavior is unrealistic due to weak contact interlocking (rolling motion).	Implementation of complex rolling resistance moments to simulate the real interlocking ballast behavior.
Spherical clumps	Represent the real shape of ballast. Realistic behavior of ballast due to strong interlocking.	Many spheres of different sizes are required. Computational time depends on the number of spheres in the clump. Applying the contact bond model between the spheres in a clump to account for particle breakage and increases the computational time.	Simplified clump shapes with low number of spheres.
Polyhedrons	Represent the realistic shape of ballast with edges, faces and corners.	Massive computational time is needed to calculate and detect the contacts. Low number of well-defined contact models are available.	Eliminating the edges that take most of the computational time in contact detection and calculation [163]

Table 6: Summarized the Used Particle Shapes for Railroad Ballast in DEM Models

Ballast Shape	References
Spheres or Circles	[80, 118, 136]
Spherical or circular clumps	[17, 50, 119-128, 130-135, 141, 142, 159, 160, 164, 165]
Polyhedrons or polygons	[116-118, 128, 129, 139, 144, 147-151, 166, 167]

In this study, a spherical shape with a rolling friction resistance approach is used to model the behavior of railroad ballast using DEM. Because it requires lower computational time compared to others as discussed above. A calibration test is done using DEM in this study; to ensure the simulated material by this approach represents ballast behavior (4.3.1.3).

3.8 Particle Size Distribution

There is no specific or recommended Particle Size Distribution (PSD) to be used for railroad ballast, as it depends on the standards and specifications used in the design process as discussed in section 2.2.3. However, the most general used and recommended PSD of railroad ballast is gradation with a particle size range almost of 10-60 mm.

From the literature, particle size of modeled railroad ballast through box test using DEM varied. Lim and McDowell [80] used a constant particle size of spheres with diameter of 36.25 mm (average ballast size). Hossain et al. [120], Chen et al. [160] and Ngo et al. [17] used PSD based on the Australian standards (S 2758.7—1996). Ji et al. [139] used PSD based on the Chinese standards 2008.

There is a number of publications in the literature which used DEM to study the influence of different PSD on ballast behavior through different tests including box tests.

Pakalavan et al. [168] investigated the influence of different ballast PSD used by different railway associations like American (AREMA No.4), European, British and Indian on ballast shear strength through direct shear test. They concluded that the Indian standard gradation has the highest shear strength compared to the European, American (AREMA No. 4) and British standard gradation.

Bian et al. [78] used DEM to investigate the effect of different ballast PSD on the settlement behavior of railroad ballast under repetitive loading. Through large scale half-track model, the authors used in their study the common ballast gradations from different railway associations such as Rail Infrastructure Corporation (RIC) and Queensland in Australia, France and American Railroad Engineering and Maintenance of Way Association's (AREMA) in the United States. They found that under repetitive loading, ballast layer with particle size distribution of AREAM No.24 had the least track settlement with respects to the others.

Vizcarra et al. [136] used DEM to study the effect of PSD on ballast settlement under loading through box test. They compared between two different gradations. The first gradation is in accordance to Brazilian standards [169] identified by them as "Gradation B". The second gradation is by Indraranta et al. [170] as an enhancement to the Australian Standard [171] identified by them as "Gradation A". They concluded that PSD of railroad ballast affects its deformation behavior under monotonic loading.

AREMA gradations are used commonly worldwide [8]. Therefore, AREMA No. 24 gradation is used in this study.

3.9 Simulated Loading Types and Loading Cycle Number

From the literature, most of the studies related to railroad ballast modeling using DEM through box test simulate train loading as a pure continuous loading as shown in Table 7. The actual train loading is not a pure continuous sinusoid. The train consists of a number of cars. Each car has typically four axles with different spacing. Each axle exerts a load on ballast layer. The loading from the train is not a pure sinusoidal and depends on different parameters. For instance, car length, car weight, axle spacing and time between passing trains.

There are few studies which simulate the behavior of railroad ballast under simulated train loading and haversine through different models other than box test as shown in Table 8. However, as recommended by [172] that haversine can represent one single axle loading only. A number of loading axles cannot be represented by haversine [8].

From the literature, DEM was used through box test to understand the short-term behavior of railroad ballast under a small number of loading cycles. Long term behavior of ballast after a large number of loading cycles is not yet understood using DEM through box test. The used number of loading cycles in box test using DEM is very low compared to experimental work as shown in Table 7. Ngo et al. [17] and Chen et al.[160] used 500,000 and 200,000 loading cycles in their experimental box tests respectively. However, the maximum number of loading cycles used in DEM to understand the mechanical behavior of railroad ballast is 6000 for a two dimensional box test model and 4000 for a three dimensional box test model by [120] and [17] respectively, because DEM requires huge computational time. Computational time of a DEM model limits the researchers from various perspectives to be considered in the modeling process. For example, the number of loading cycles, particle shape, particle

breakage, simulation dimension and loading type. It is very difficult to simulate ballast

behavior using DEM under a large number of loading cycles using three-dimensional

scale and complex particle shapes including particle breakage. Some studies used a

large number of loading cycles but in two-dimensional scale. Others used complex

particle shapes and included particle breakage but for a low number of loading cycles.

It is difficult to consider all the perspectives of realistic modeling of railroad ballast in

one DEM simulation as shown in Table 8. It is a trade-off between realistic simulation

and computational time.

Table 7: Loading Types and Number of Loading Cycles Used in DEM Models of Box
Test to Understand Railroad Ballast Behavior

Loading Cycles Number	Loading Type and Frequency	Reference
1	Sinusoidal - [3,40] kN - 3Hz	[80]
20	Sinusoidal - [3,40] kN - 3Hz	[119]
6000	Sinusoidal - [9-99] – kN	[120]
1	Sinusoidal - [3,40] kN - 3Hz	[121]
1000	Sinusoidal [24-221] kN-20 Hz	[160]
4000	Sinusoidal [0-202] kN -15 Hz	[17]
800	Sinusoidal - [3-40] kN - 3,6,10,20,30 Hz	[139]
4	Simulated train loading from [173]	[128]
15	Sinusoidal - [3,40] kN - 3Hz	[142]

Table 8: Parameters Affecting the Computational Time for Different DEM Models Used to Understand the Mechanical Behavior of Railroad Ballast

DEM Model	Loading Cycles Number	Particle Shape	Particle Breakage	Model Dimension	Loading Type and Frequency	Reference
Box Test	1	Sphere	No	3D	Sinusoidal [3,40] kN 3Hz	[80]
Track-Three Sleepers	200	Circle	Yes	2D	Sinusoidal [0,20.67] kN 1 Hz	[118]
Box Test	20	Clump	Yes	3D	Sinusoidal [3-40] kN 3Hz	[119]
Box Test	6000	Clump	Yes	2D	Sinusoidal [9-99] kN	[120]
Box Test	1	Clump	No	3D	Sinusoidal [3-40] kN 3Hz	[121]
Triaxle Test	1000	Clump	Yes	2D	Sinusoidal [50-424] kN 10, 20, 30 and 40Hz	[123]
Track-Three Sleepers	2000	Polyhedral	No	3D	Simulated train loading developed in the same study	[174]

Cont. Table 8: Parameters Affecting the Computational Time for Different DEM Models Used to Understand the Mechanical Behaviour of Railroad Ballast

DEM Model	Loading Cycles Number	Particle Shape	Particle Breakage	Model Dimension	Loading Type and Frequency	Reference
Box Test	1000	Clump	No	3D	Sinusoidal [24-221] kN 20 Hz	[160]
Half Track	300	Polyhedral	No	3D	Simulated train loading from [175]	[78]
Track-Three Sleepers	200	Clump	Yes	2D	Sinusoidal [0-62] kN	[16]
Box Test	4000	Clump	No	3D	Sinusoidal [0-202] kN 15 Hz	[17]
Box Test	800	Polyhedral	No	3D	Sinusoidal [3-40] kN 3,6,10,20,30 Hz	[139]
Box Test	15	Clump	Yes	3D	Sinusoidal [3-40] kN 3Hz	[142]
Triaxle Test	2000	Polyhedral	No	3D	Haversine [0-165.4] kPa	[150]
Track-One Sleeper	32	Polyhedral	No	3D	Haversine [0-51,103] kN	[151]

3.10 DEM Software Packages

Cundall and Strack [70] are the first people who computationally implemented DEM with a code named "BALL". Then, a variety of DEM packages have been used to computationally implement DEM with advanced criteria including huge number of distinct particles in different loading and environmental conditions.

DEM software packages are different in functionality and capabilities. For example, PFC, YADE, LMGC90 and BLOCKS3D need coding skills. PFC and EDEM support clumping and clustering of spherical particles and BLOCKS3D allow the usage of polyhedral shapes. Table 9 below, describes the DEM packages software that have been used to model the behavior of railroad ballast using DEM in the literature.

In this study, EDEM software by DEM solutions is used because it supports the usage of spherical particles. Easy in use with a simple software interface in comparison to other software. Additionally, it can be customized using the Application Programming Interface (API).

Table 9: Types and Names of the Used Software in the Literature to Model Railroad Ballast using DEM

Software Type	Software Name	References
Open Source	YADE	[116, 129, 141]
	LMGC90	[143]
Commercial	PFC by Itasca	[16, 17, 80, 118, 120-127, 130-135, 138, 142, 159, 160, 165, 176, 177]
	EDEM by Dem Solutions	[50, 136, 140]
In house	BLOCKS3D by the University of Illinois [178-180]	[128, 144, 147-151, 166, 167]
	Interactive graphical software by Ahmed et al. [117]	[117]

3.11 Understanding Ballast Behavior using DEM Through Box Test

This study uses DEM to model the mechanical behavior of railroad ballast through box test as described above. This section concentrates on reviewing the literature about using DEM to understand the mechanical behavior of railroad ballast through box test. The chapter does not highlight the researches form the literature about understanding ballast behavior using DEM via other tests like uniaxial and triaxial tests.

Discrete element models of box tests in the literature were used to understand railroad ballast behavior from various perspectives; utilizing the advantages of DEM in visualizing the microscopic and macroscopic behaviors through a comprehensive insight to particle displacement and contact force distribution during the simulation.

This subsection presents an extensive literature about understanding the mechanical behavior of railroad ballast using DEM via box test from various perspectives.

3.11.1 Ballast Breakage

After long term service, ballast particles break. There are two types of ballast breakage (2.5). Corner breakage and particle splitting breakage. Lackenby et al. [33] found that corner breakage occurred mostly under dilation condition (low confining pressure) and splitting across particle breakage occurred mostly under contraction condition (high confining pressure).

However, most of the studies model the short-term mechanical behavior of railroad ballast using low number of loading cycles as discussed in section 3.9. Large number of load cycles is not used in DEM modeling due to the computational time issue. Number of researches did not include particle breakage in their DEM model of box test due to the high requirement of computational time as shown in Table 10.

However, many researches presented the importance of considering ballast breakage in DEM models [118, 123].

Table 10: The Usage of Particle Breakage in DEM of Railroad Ballast Through Box Test

Particle Breakage	Reference
Including particle breakage	[119, 120, 128, 142]
Not including particle breakage	[17, 80, 121, 139, 160]

Ballast breakage is modeled in DEM using two approaches. The first approach is to identify a finite bond tensile strength between the particles of the clumps. The breakage failure happens on the bond between the particles in each clump. When the acting contact stress is more than the bond tensile strength, bond breakage occurs. This approach is used when ballast is modeled as spherical clumps. This approach was presented by [123, 128, 159]. Zhang et al. [128] used a complex particle shape with bonded spheres to represent railroad ballast shape and breakage respectively. This approach is very time consuming. They studied the effect of bond strength (10 and 30 MPa) used in DEM model on the permanent deformation of ballast. They visualized that most of the broken bonds were under the sleeper. They found that low bond strength between spheres in one clump produced additional settlement to ballast layer. Some studies [119, 142] used box test to investigate ballast abrasion (corner breakage). They simulated ballast as unbreakable clumps of large particles with attaching smaller

bonded spheres (asperities). However, this approach failed to model particle splitting breakage. But it succeeds in modeling the ballast abrasion (corner breakage).

The second approach is to identify a tensile strength (critical stress) of the clump by which after this tensile stress the cluster original geometry is replaced by different smaller sized fragments. This was presented by different researchers using circular clumps [16, 118, 120, 181] and polyhedron [116]. Hossain et al. [120] used this approach in their DEM of railroad ballast using box test. They used a value of 10 MPa as a critical stress of the clumps. They obtained from the DEM the same conclusion of Lackenby et al. [33] described above.

In this study, ballast breakage is not considered due to the high requirement of computational time.

3.11.2 Settlement Behavior

Most of researchers studied the ballast settlement behavior under cyclic loading using pure sinusoidal loading type through DEM of box test. Few researchers studied the behavior of railroad ballast settlement under dynamic loadings. From the literature, box test was used intensively to study the settlement behavior of railroad ballast using DEM. The settlement behavior of railroad ballast includes vertical and lateral settlement.

The conclusions of the DEM simulations regarding ballast settlement behavior are almost in good agreement with experimental work. Ballast beneath the sleeper displaces downward and beside the sleeper displaces upwards.

However, some of the studies included in their simulations different parameters related to railroad ballast; to investigate their influence on ballast settlement as discussed below and summarized in Table 11. For instance, ballast particle shape,

ballast fouling, geotextile reinforcement, under sleeper pads, loading frequency and confining pressure.

Lim and MacDowell [80] and Lu and MacDowell [119] were the first authors who introduced the modeling of box test using DEM. Their main concern was on validating their DEM model and showing the importance of DEM in visualizing the microscopic behavior of railroad ballast. Lu and MacDowell [121] discussed the effect of geometrical shapes on ballast settlement and rotation under sinusoidal cyclic loading. They were the first authors who showed how DEM can be utilized to visualize the railroad ballast particle displacement and rotation. Ballast displacement was shown as vectors and the thickness of the vector is proportional to the displacement magnitude of the particle. They pointed out that ballast displacement behavior using clumps is almost similar to the box test results obtained by [182].

Hossain et al. [120] discussed ballast settlement using DEM through box test model under sinusoidal cyclic loading and different confining pressures. They emphasized on the significance of confining pressure in reducing ballast settlement. They concluded that around 2000 cycles ballast settlement is maximum at all confining pressures. The same conclusion was observed by Chen et al. [160].

Ngo et al. [17] studied the influence of geogrid on fresh and fouled ballast settlement behavior; experimentally using process simulation test and numerically using DEM under cyclic loading. They observed that geogrid reduced ballast vertical and lateral settlement for all fouling indices. Li and McDowell [142] studied the influence of under sleeper mat on ballast settlement behavior using DEM through box test. They found that under sleeper mat reduced ballast settlement and particle abrasion under sleeper.

Zhang et al. [128] presented the settlement behavior under simulated train loads of heavy haul vehicle passage through DEM model of box test. Ballast was modeled using complex clumps with bonded spheres to represent ballast shape and breakage respectively. This approach is very time consuming as they include large number of particles in one simulation. Furthermore, including particle breakage is an additional calculation to the DEM simulator. They showed the effect of modeling particle breakage using different bond strengths (10 and 30 MPa) on the ballast settlement behavior. The maximum sleeper settlement for one haul car passage was in the range of 0.83-1 mm.

Ji et al. [139] investigated the influence of cyclic loading frequency on ballast settlement behavior. They found that cyclic load frequency affects ballast settlement behavior. Maximum settlement was observed for high load frequency.

Table 11: Purpose of DEM of Box Test Studies from the Literature

Main Purpose of DEM of Box Test	Reference
Validation	[80]
Validation and influence of modeling particle abrasion on ballast vertical settlement	[119]
Influence of confinement on ballast vertical settlement	[120]
Influence of particle shape on ballast vertical settlement	[121]
Influence of confinement on ballast vertical and lateral settlement	[160]
Influence of geogrid and ballast fouling on ballast vertical and lateral settlement	[17]
Influence of loading frequency on ballast vertical settlement	[139]
Influence of particle shape and breakage on ballast vertical settlement	[128]
Influence of under sleeper pads on ballast vertical settlement	[142]

3.12 Gap of Knowledge Related to DEM of Railroad Ballast

DEM is a powerful tool for understanding and visualizing the mechanical behavior of railroad ballast. DEM can visualize the microscopic and macroscopic behavior of railroad ballast through a comprehensive insight into the contact force distribution and particle displacement during loading. DEM can study the effect of different parameters of railroad ballast like particle shape, particle size distribution, particle breakage and fouling on the mechanical behavior of railroad ballast.

Many Researchers used DEM to understand the mechanical behavior of railway ballast. Most of the DEM models for railroad ballast were used to calibrate material properties or validate experimental tests. For example, particle crushing test [80, 183, 184], uniaxial test [80, 116, 125, 138], triaxial test [122, 123, 126, 137, 144, 150, 183], direct shear test [79, 124, 129, 135, 141, 167, 185, 186] and box test [17, 80, 119-121, 128, 136, 139, 142, 160, 177]. Some researchers modeled ballast layer under a number of sleepers [16, 118, 127, 174, 187] and under one sleeper [78, 143, 166, 167] to represent the track/half-track condition using DEM for a low number of loading cycles.

However, Full track analysis under dynamic train loading for a large number of loading cycles is not fully understood using DEM. The main limitation of DEM is the massive requirement of computational time despite the advancement of computational resources. The effect of dynamic loading due to track and rail irregularities on the mechanical behavior of railroad ballast has not been fully investigated yet. Most of the studies on modeling the mechanical behavior of railroad ballast modeled ballast under quasit-static loading.

The length scale and dimension of the DEM model and number of loading cycles are a trade-off between realistic modeling and computational time. Large-scale and three-dimensional ballasted track DEM model using a large number of loading

cycles reflect the real ballasted track condition. Nevertheless, it is very difficult to model this case using DEM as it requires huge computational time.

From the literature, DEM was used mainly to validate experimental tests related to railroad ballast for a small-scale model. Most of the studies modeled the behavior of railroad ballast for short term using a low number of load cycles under a pure continuous sinusoidal loadings.

3.13 Research Novelty

As discussed above, most of the researchers used DEM to model railroad ballast behavior under pure continuous sinusoidal loading through box test. A train consists of a number of cars. Each car has a number of axles with different spacing. Each axle applies a load on the track substructure. The train loading is not a pure continuous sinusoidal loading. The train loading depends on the train weight, car length, axle number and axle spacing.

In this study, DEM of box test is used to model the behavior of railroad ballast under different simulated train loadings; to understand the mechanical behavior of railroad ballast under different simulated train loadings. Moreover, it is used to investigate the influence of simulated train loading on the mechanical behavior of railroad ballast.

In this work, the simulated train loadings include a more realistic train loading simulated utilizing the BOEF theory; and sinusoidal loading based on train speed and axle spacing. The results from a more realistic simulated train loading utilizing the BOEF theory are compared with those from sinusoidal loading.

CHAPTER 4: MODELING METHODS AND PROCEDURES

4.1 Introduction

Ballast is the main element of a ballasted railway track. Ballast layer has significant functions. It acts as a loading platform as it distributes and transfer the train loads to subgrade layer. It plays a vital role in maintaining the track alignment and stability. After service, ballast deforms and degrades. Maintenance of ballast material is required. Maintenance activity is costly and requires large operational time. Understanding the mechanical behavior of ballast behavior leads to efficient maintenance and better design. From the literature, experimental and modeling approaches are used to understand the mechanical behavior of railroad ballast.

Large scale experimental apparatuses are needed to understand the railroad ballast mechanical behavior under the real conditions. Indraratna et al. [10] recommend avoiding the use of conventional tests for granular material as they rottenly produce confusing results due to the large granular particles size relative to test sample size. Large scale experimental instruments are used for several tests like uniaxial, triaxial and box test. Large scale triaxial and box tests are commonly used in evaluating and understanding the mechanical behavior of railroad ballast experimentally.

Significant effort in modeling the ballast is done in the literature to understand the mechanical behavior of railroad ballast. Field and large-scale experimental tests are used to evaluate and understand the real mechanical behavior of railroad ballast. Nevertheless, testing ballast behavior either in the field or in the lab is an expensive exercise. Alternatively, modeling the mechanical behavior based on theoretical models that reflect the real mechanical behavior is introduced. The main significant advantages of modeling approach are the conservation of cost and work in comparison to the experimental approach. Modeling approaches can be used to understand and evaluate

the behavior of railroad ballast under different loading conditions and material properties. Furthermore, modeling develops the knowledge and tools needed for predictions. Such tools have the potential to make huge financial savings within the design constraints.

There are two different types of modeling methods used to model the mechanical behavior of railroad ballast based on the problem-solving type; analytical and numerical. The key concerns and limitations of each modeling method is described in the previous chapter.

In this study, the numerical Discrete Element Method is used to model the behavior of railroad ballast.

From the literature, most of the researches related to understanding the mechanical behavior of railroad ballast using DEM used sinusoidal loading to simulate train loading. Sinusoidal loading is a pure continuous function. Train loading is not pure continuous sinusoid. The train loading has a different shape than sinusoidal. Based on many factors such as car length, car weight, axle number and axle spacing. In this study, the influence of simulated train loading on modeling the behavior of railroad ballast using DEM is investigated. Analytical modeling utilizing the Beam on Elastic Foundation (BOEF) theory is used to simulate a more realistic train loading. The numerical Discrete Element Method is used to model the behavior of railroad ballast under different simulated train loading. The results from more realistic simulated train loading utilizing BOEF theory are compared with those from sinusoidal loading.

Simulating the entire track is computational and time expensive activity. Therefore, small box portion of real track is simulated by box test as illustrated in Figure 23. Box test was used extensively in the literature to understand the mechanical behavior of railroad ballast as described in the previous chapter.

In this study, the modeling process is done into two parts using two modeling methods (Figure 24). Part 1, using analytical modeling to simulate the more realistic train loading utilizing Beam on Elastic Foundation (BOEF) theory. Part 2, using numerical Discrete Element Method (DEM) to model the behavior of railroad ballast under different simulated train loading via box test. In discrete element modeling of railroad ballast, the model setup is done first. Then, the simulated material of railroad ballast using DEM is calibrated using angle of repose test; to ensure the right assigned and used properties of railroad ballast in the model. After that, EDEM software is customized through EDEM Application Program Interface (API) to support force control mode. Ballast material is created, and preloading is applied. Finally, simulated train loading cases are defined and applied through developed force control mode in EDEM. There are two different simulated train loading cases used in this study as described below (4.3.6). Case 1 is a more realistic train loading simulated based on BOEF theory. Case 2 is a sinusoidal loading based on train speed and axle spacing. The modeling process is summarized and demonstrated in Figure 25.

This chapter discusses the modeling methods and procedures used to model the behavior of railroad ballast under different simulated train loadings.
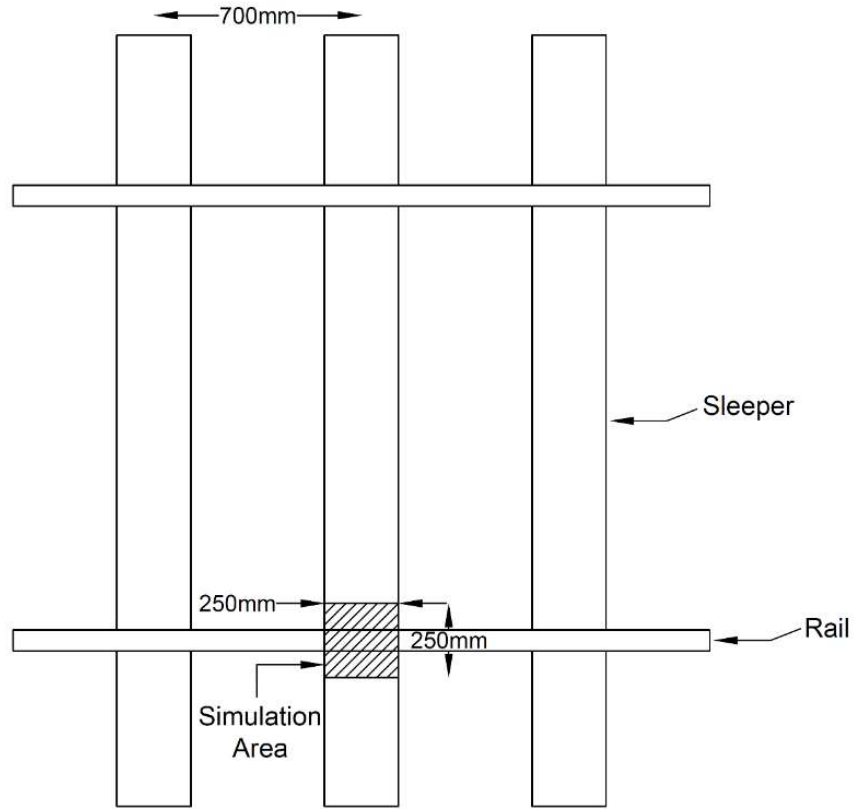
Figure 23: Box simulation area of a railway track.
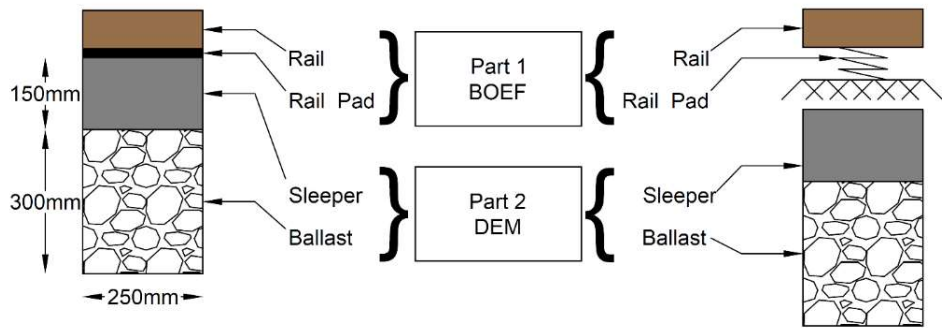
Figure 24: Modeling methods.
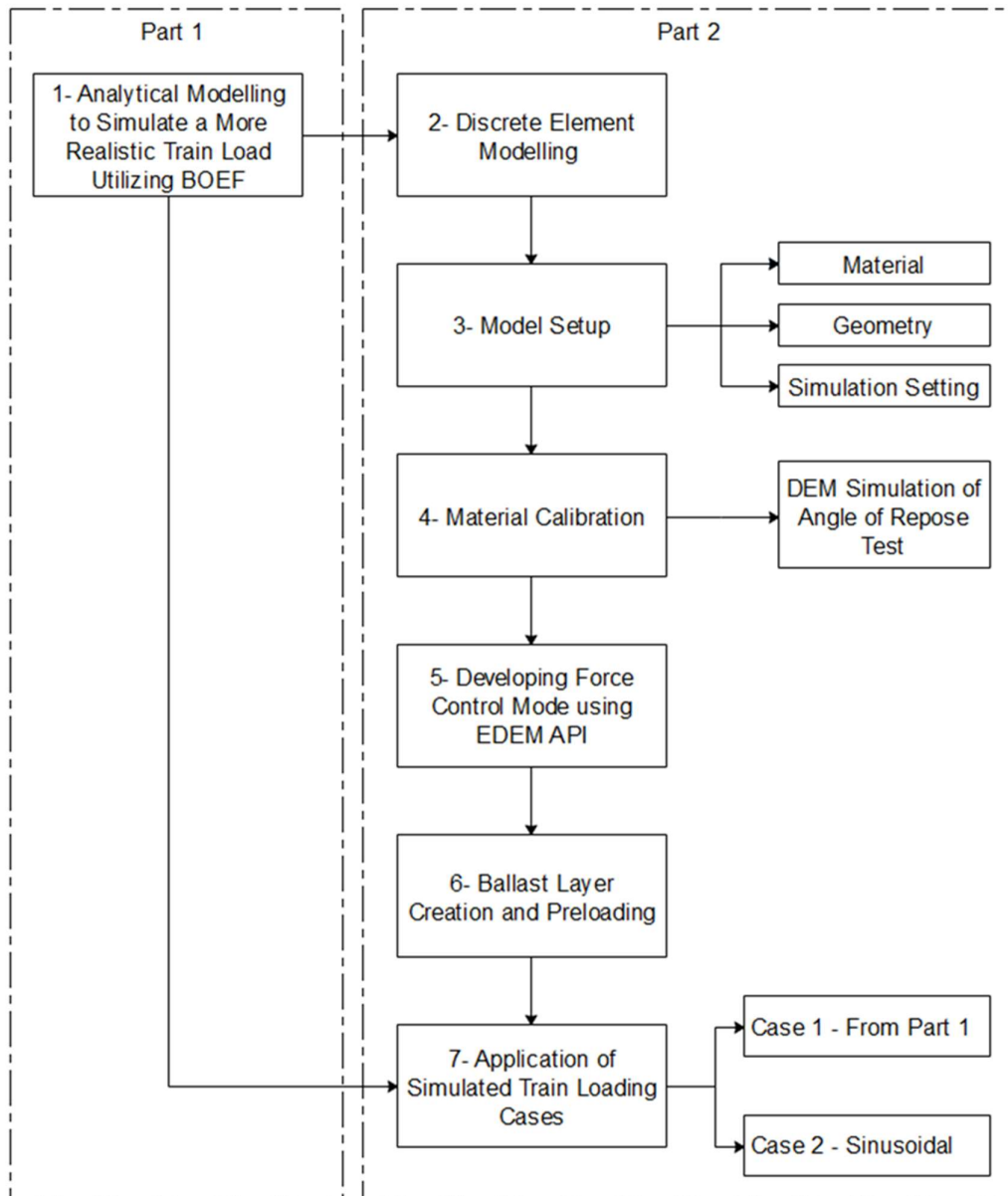
Figure 25: Modeling process.

4.2 Part 1: Analytical Modeling Utilizing BOEF Theory

4.2.1 Introduction

Analytical models of ballasted tracks are founded on mathematical models. These models describe the mechanical behavior of each track element based on its characteristics. There are two approaches to analytically model a ballasted track based

on support nature; continuous or continuous discretely supported models as shown in Figure 26.
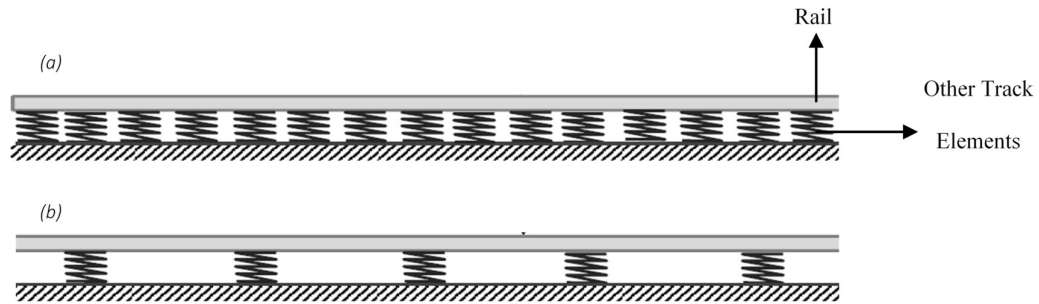
Figure 26: Analytical models for ballasted track where rail is (a) continuously supported (b) discretely supported.

In the first approach, rails are modeled as beams on a continuously supported foundation. Although, the first approach does not show all the features of ballasted track such as sleeper spacing, it determines the most significant properties of its mechanical behavior [188]. The second approach counts for sleeper spacing where rails are modeled as discretely supported beams. The first analytical model for ballasted track was introduced by Winkler [69] and identified as Beam on Elastic Foundation (BOEF). Where the ballasted track is modeled as continuous Bernoulli beam representing the rails, supported by continuous and elastic foundation known as Winkler foundation as shown in Figure 26 (a). The Winkler foundation is modeled as continuous linear elastic springs representing the other track elements underneath the rails (i.e. Rail pads, sleeper, ballast and sub-ballast).

From the literature, the ballasted track elements have been analytically modeled using different structural elements based on their characteristics. In general, rails are modeled as beams based on two beam theories; Euler-Bernoulli and Timoshenko beam theories [189, 190]. Sleepers are modeled as rigid masses. Other track elements such as rail pads and ballast layer are modeled as mass-spring systems. The track subgrade is modeled either as a rigid foundation or half space. More information about the ballasted track analytical models can be found in [191].

In this study, the BOEF theory is utilized to simulate a more realistic train loading that will be used as an input parameter in part 2 (DEM of simulation box test) as shown in Figure 27. The rail is modeled as Euler-Bernoulli beam discretely supported by rail pads to count for the sleeper spacing. The rail pad is modeled as a spring with constant stiffness (k_{pad}). Measurement point is the location of DEM simulation box test. Figure 27, describes the infinite BOEF model.
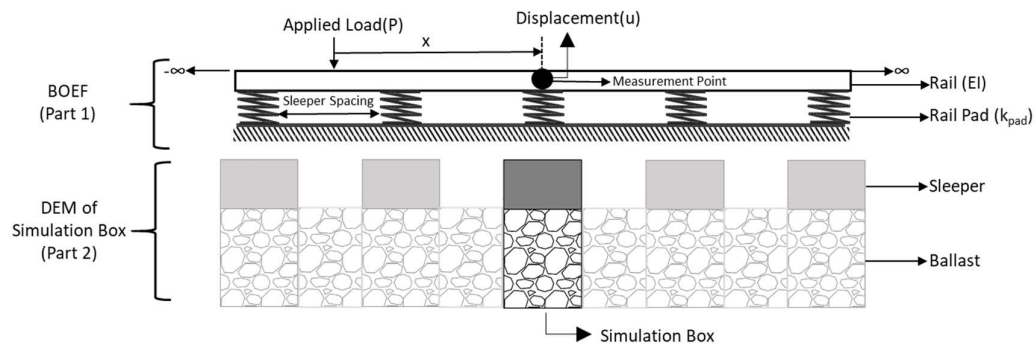
Figure 27: Infinite BOEF model used in this study to simulate train loading.

4.2.2 Solving the Governing Differential Equation

Governing equation of the system (Figure 27) is a homogenous linear Ordinary Differential Equation (ODE) to the fourth order (equation 4.1).

$$EI\frac{d^4u}{dx^4} + k_{pad}u = 0 \tag{4.1}$$

where, EI is the rail bending stiffness, k_{pad} is the rail pad stiffness and u is the displacement response.

To simplify the solving process, the infinite beam splits into two semi-infinite beams (Figure 28). Analysis is taken into consideration for the right part.
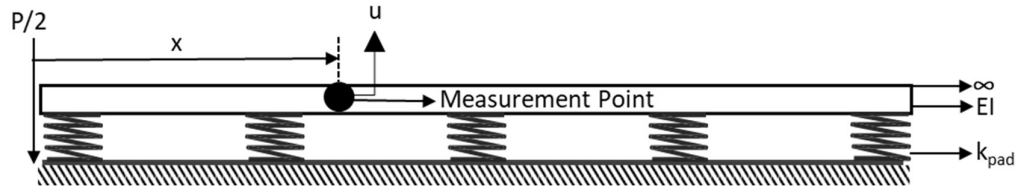
Figure 28: Right part of infinite BOEF model.

With the following boundary conditions:

$$at\ x = 0 \Rightarrow \theta = 0\ and\ F = \frac{-P}{2}$$

$$at\ x \to \infty \Rightarrow u \to 0$$

where θ is the rotation and P is the applied force

The solution of equation 4.1 can be written as

$$u = e^{\alpha x} \tag{4.2}$$

substitution of equation 4.2 in equation 4.1 gives:

$$EI\alpha^4 + k_{pad} = 0, \qquad \alpha = \sqrt[4]{-4\lambda} \qquad (4.3)$$

where,

$$\lambda = \sqrt[4]{\frac{k_{pad}}{4EI}}$$

and the values of the roots are

$$\alpha = (1+i)\lambda, \qquad \alpha = (-1+i)\lambda, \qquad \alpha = (-1-i)\lambda \ and \ \alpha = (1-i)\lambda$$

The solution can be written as shown in equation 4.4

$$u = A_1 e^{(1+i)\lambda x} + A_2 e^{(-1+i)\lambda x} + A_3 e^{(-1-i)\lambda x} + A_4 e^{(1-i)\lambda x} \qquad (4.4)$$

where A_1, A_2, A_3 and A_4 are constants. Equation 4.4 can be simplified into

$$u = e^{\lambda x}(A_1 e^{i\lambda x} + A_4 e^{-i\lambda x}) + e^{-\lambda} \ (A_2 e^{i\lambda x} + A_3 e^{-i\lambda x}) \qquad (4.5)$$

using the relationships of:

$$e^{i\lambda x} = \cos(\lambda x) + i\sin(\lambda x)$$

$$e^{-i\lambda x} = \cos(\lambda x) - i\sin(\lambda x)$$

equation 4.5 can be written as

$$u = e^{\lambda x}[(A_1 + A_4)\cos(\lambda x) + (iA_1 - iA_4)\sin(\lambda x)]$$
$$+ e^{-\lambda x}[(A_2 + A_3)\cos(\lambda x) + (iA_2 - iA_3)\sin(\lambda x)] \qquad (4.6)$$

Equation 4.6 can be simplified with introducing new constant parameters

$$u = e^{\lambda x}[B_1 \cos(\lambda x) + B_2 \sin(\lambda x)] + e^{-\lambda x}[B_3 \cos(\lambda x) + B_4 \sin(\lambda x)] \qquad (4.7)$$

where B_1, B_2, B_3 and B_4 are constants which are complex and can be found by applying the boundary conditions. By applying the first boundary condition which says that as $x \to \infty \Rightarrow u \to 0$. B_1 and B_2 can be found which are equal to zero because at that boundary   condition

78

$$x \to \infty \Rightarrow e^{-\lambda x} \to 0 \ and \ e^{\lambda x} \to \infty.$$

Using the values of B_1 and B_2 equation 4.7 can be written as

$$u = e^{-\lambda x}[B_3 \cos(\lambda x) + B_4 \sin(\lambda x)] \tag{4.8}$$

Recalling the relationships for slope (θ), moment (M) and shear (F)

$$\theta = \frac{du}{dx}, M = EI\frac{d^2u}{dx^2} \ and \ F = \frac{dM}{dx}$$

and applying the second boundary condition at

$$x = 0 \Rightarrow \theta = \frac{du}{dx} = 0 \ and \ F = \frac{dM}{dx} = \frac{-P}{2}$$

to equation 4.8

$$\frac{du}{dx} = [-\lambda e^{-\lambda x}B_3(\cos(\lambda x) + \sin(\lambda x))] + [\lambda e^{-\lambda x}B_4(\cos(\lambda x) - \sin(\lambda x))] = 0$$

$$\frac{du}{dx} = -\lambda B_3 + \lambda B_4 = 0$$

$$\therefore B_3 = B_4 \tag{4.9}$$

The second boundary condition is used to find the values of the constants B_3 and B_4

at

$$x = 0 \Rightarrow F = \frac{dM}{dx} = \frac{-P}{2}$$

$$M = EI\frac{d^2u}{dx^2} = EI \ [2\lambda^2 e^{-\lambda x}(B_3\cos(\lambda x) + B_4 \sin(\lambda x))] \tag{4.10}$$

The differentiation of equation 4.10 with respect to x gives the following:

$$\frac{dM}{dx} = 2EI\lambda^3 e^{-\lambda x}[B_3(\cos(\lambda x) + \sin(\lambda x)) - B_4(\cos(\lambda x) + \sin(\lambda x))] \tag{4.11}$$

applying the boundary condition in equation 4.11 which gives

$$4EI\lambda^3 Bt = \frac{-P}{2}$$

where

$$Bt = B_3 = B_4 \tag{4.12}$$

Equation 4.12 can be simplified to find the value of Bt

$$Bt = \frac{-P}{8EI\lambda^3}$$ (4.13)

Back substitution of Bt from equation 4.13 into equation 4.8, provides the general solution

$$u = \frac{-P}{8EI\lambda^3} e^{-\lambda x}[\cos(\lambda x) + \sin(\lambda x)]$$ (4.14)

Equation 4.14 can be used to find the vertical displacement at distance "x" from the applied force. The simulated train loading (F_{train}) at the measurement point can be obtained by multiplying equation 4.14 by the rail pad stiffens (k_{pad}) using the following relationship

$$F_{train} = uk_{pad}$$ (4.15)

4.3 Part 2: Discrete Element Modeling of Railroad Ballast

4.3.1 Ballast Material Setup

4.3.1.1 Material Properties

The first step in setting up the simulation is defining the material properties. EDEM requires from the user to define the properties of two types of materials used in the simulation; bulk and equipment materials. It is essential to define the material properties correctly that represent the material behavior. The bulk material in this simulation is railroad ballast material. While, the equipment materials are box and sleeper material (4.3.2.1).

Contact models that are used to calculate the contact forces between distinct elements are mainly based on the material properties. There are different contact models used in modeling railroad ballast as discussed previously in section 3.6. In this study,

the Hertz-Mindlin contact model is used based on the recommendation of Di Renzo and Maio [132]. Besides that, it is the default contact model in EDEM.

Most of the studies related to DEM of railroad ballast did not consider the particle breakage in their simulation and used low number of loading cycles due to huge requirement of computational time as described in section 3.11.1. In this study, particle breakage of railroad ballast is not considered to minimize the high requirement of computational time.

Railroad ballast has certain material properties. Most of them are well know from the literature and can be used directly in the simulation. Other ballast material properties cannot be used directly in the simulation. They require certain modifications since the contact mechanism in DEM is a simplification of the real scenario. For example, Youngs Modulus of railroad ballast. Railroad ballast has a value of Youngs Modulus almost equal to 30 GPa [6, 7]. From the literature, a smaller value of Youngs Modulus is used because the contact surface area in DEM is much greater than the real case as shown in Figure 29. Some material properties in the literature are defined based on various calibrations with experimental tests. For example, material properties related to particle scale such as coefficient of restitution, coefficient of static friction and coefficient of rolling friction.

Figure 29: Geometry of contact for (a) real and (b) simulated cases.

The required bulk material properties are different form DEM software package to other. EDEM requires six bulk material properties; Poisson's ratio, solid density, Young's modulus or shear modulus, coefficient of restitution, coefficient of static friction and coefficient of rolling friction. In EDEM, either Young's modulus or shear modulus of the material is defined. Table 12 summarizes the required ballast material properties in EDEM software, the used values in the literature for each parameter and the used values for each parameter in this study. The used material properties for railroad ballast is assigned in EDEM as shown in Figure 30.

Table 12: Values of Railroad Ballast Material Properties Used in the Literature and in
This Study

Parameter	Definition	Values Used in the Literature	Values Used in This Study
Poisson's ratio	"Poisson ratio is the ratio of transverse contraction strain to longitudinal extension strain in the direction of stretching force" [192]	• In the range of 0.18-0.2 [193, 194]. • 0.2 [117]	0.2
Solid Density	Sometimes called particle density. It is the ratio of total solids mass to their volume.[195]	• In the range of 2500-2700 kg/m^3 [194]. • 2600 kg/m^3 [80, 139].	2600 kg/m^3
Young's Modulus	Is the measure of the material stiffness. It is the ratio of the stress applied to the strain formed in a material in the elastic region.	• In the range of 2.4 – 24.0 GPa [117]. • Irazábal et al. [146] suggested a minimum value of 17.7 GPa for spherical shapes	17.7 GPa (correspondent to a Shear Modulus of 7.5 GPa).

Cont. Table 12: Values of Railroad Ballast Material Properties Used in the Literature and in This Study

Parameter	Definition	Values Used in the Literature	Values Used in This Study
		Interaction properties between ballast particles	
Coefficient of Restitution	Is the ratio of the relative velocity of the two particles after collision to the relative velocity of the two particles before collision.	• It is well known in the literature as 0.4 [193]. • 0.2 [136]. • 0.4 [146].	0.4
Coefficient of Static Friction	Is ratio of static friction force to the applied normal force	• In the range of 0.577 and 0.839 [194]. • 0.5 [136]. • 0.6 [196]. • 0.6 [146]	0.6
Coefficient of Rolling Friction	Is ratio of force that resists the rolling motion to the applied force that cause rolling motion	• 0.25 [146]	0.25
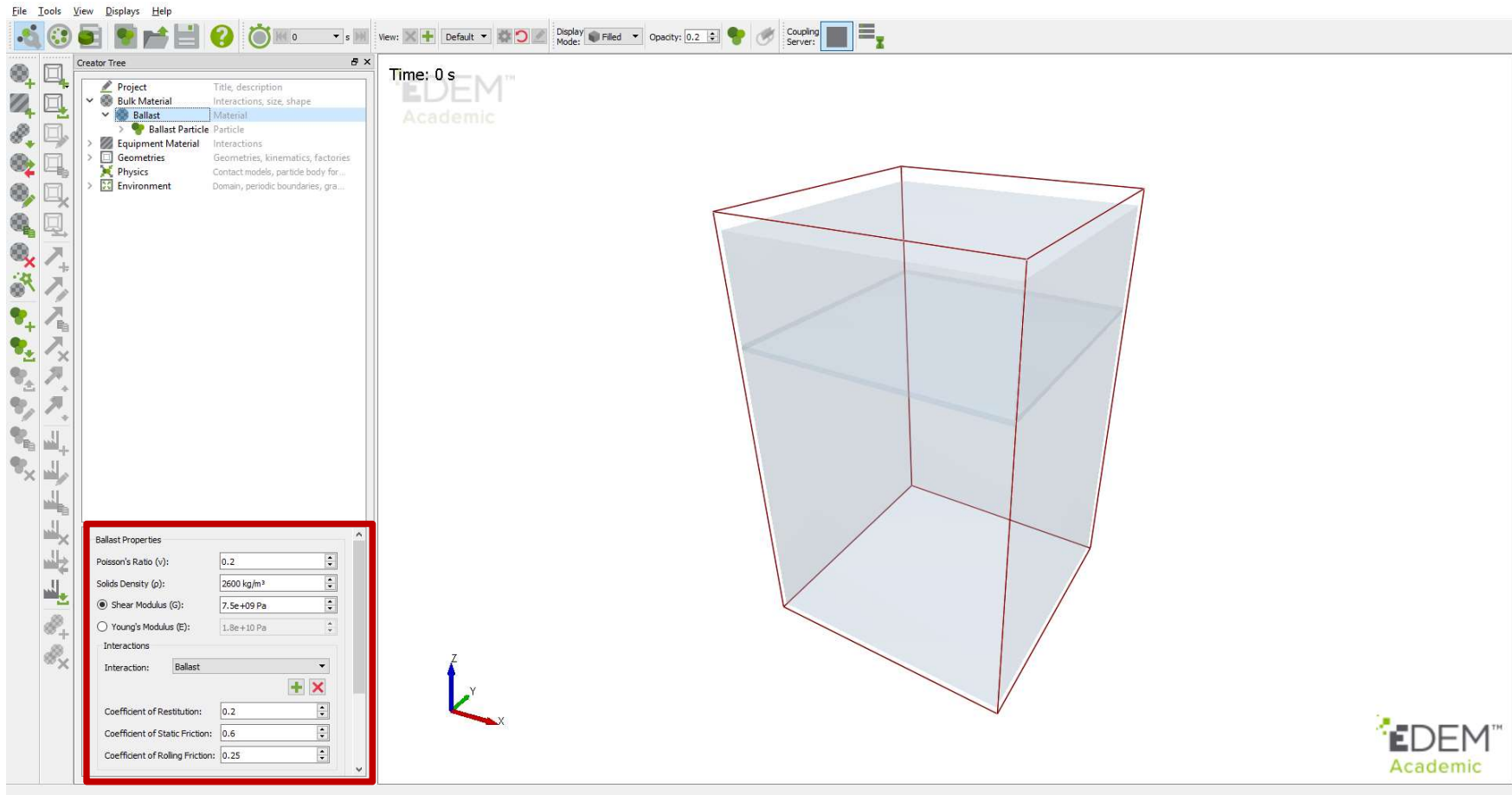
Figure 30: Input parameters assigned in EDEM for ballast material properties.

4.3.1.2 Particle Shape and Size Distribution

There are different shapes and approaches used in the literature to model railroad ballast using DEM. From the literature, railroad ballast particles were modeled based as polyhedrons, spheres or multi-sphere (clump).

Polyhedrons can represent the ballast shape including particle angularity. However, the contact detection and calculations are complicated for the polyhedrons. A contact detection algorithm and contact models need to be defined. There is a low number of contact models for polyhedrons compared to spheres. There are three types of contacts that need a proper mathematical representation for polyhedron; face to face, face to edge and edge to edge. Although the complex particle shape using polyhedrons represents the real ballast shape, it costs huge computational time.

Spheres are used mostly in modeling railroad ballast using DEM. Because most of contact models are based on spherical shapes. Modeling ballast behavior requires lower computational time compared to polyhedrons. The contact detection algorithm and models are well defined in the literature for spherical shapes.

Spheres does not reflect the angular shape of railroad ballast. Multi-sphere and rolling resistance approaches are used to model railroad ballast. In multi spheres approach, the number of spheres used impacts on the computational time. Representing the real ballast shape requires a complicated DEM simulated particle shape. Whether using spheres or polyhedrons. Although the complexity of a particle shape represents the real shape of the ballast particle, it requires a huge computational time. The comparison between the different shapes and approaches are discussed in detail in section 3.7.

In this study, a spherical shape with a rolling friction resistance approach is used. The main advantage of this approach is the low computational time compared to multi-

sphere and polyhedrons approaches as discussed above. The contact detection and contact force calculation are straight forward as the particle consists of one sphere with known radius center and position. The number of spheres is lower with relative to multi-sphere approach.

There are various particle size distributions used for railroad ballast worldwide as discussed in section 3.8. The most common and used gradation for railroad ballast is AREMA gradations [8]. In this study, the common AREAM No. 24 gradation is used.

In EDEM, there are five options to define the size distribution of the particle; fixed, random, normal, log-normal and user defined distributions. The "user defined" option is used to define AREMA No.24 gradation in EDEM. In this option, one particle size is created and EDEM creates different particles' sizes based on radius scale and mass percentage defined by the user. First, the particle of ballast is created with a radius of 37.5 mm (largest radius in AREMA No.24 distribution) as shown in Figure 31. Then, the defined radius scale and mass percentage of other particle sizes are defined in EDEM based on AREMA No.24 gradation (Figure 31). Figure 32, shows the used PSD of ballast material based on AREMA No.24 gradation.

Table 13, summarizes the used material properties of railroad ballast used in this study.
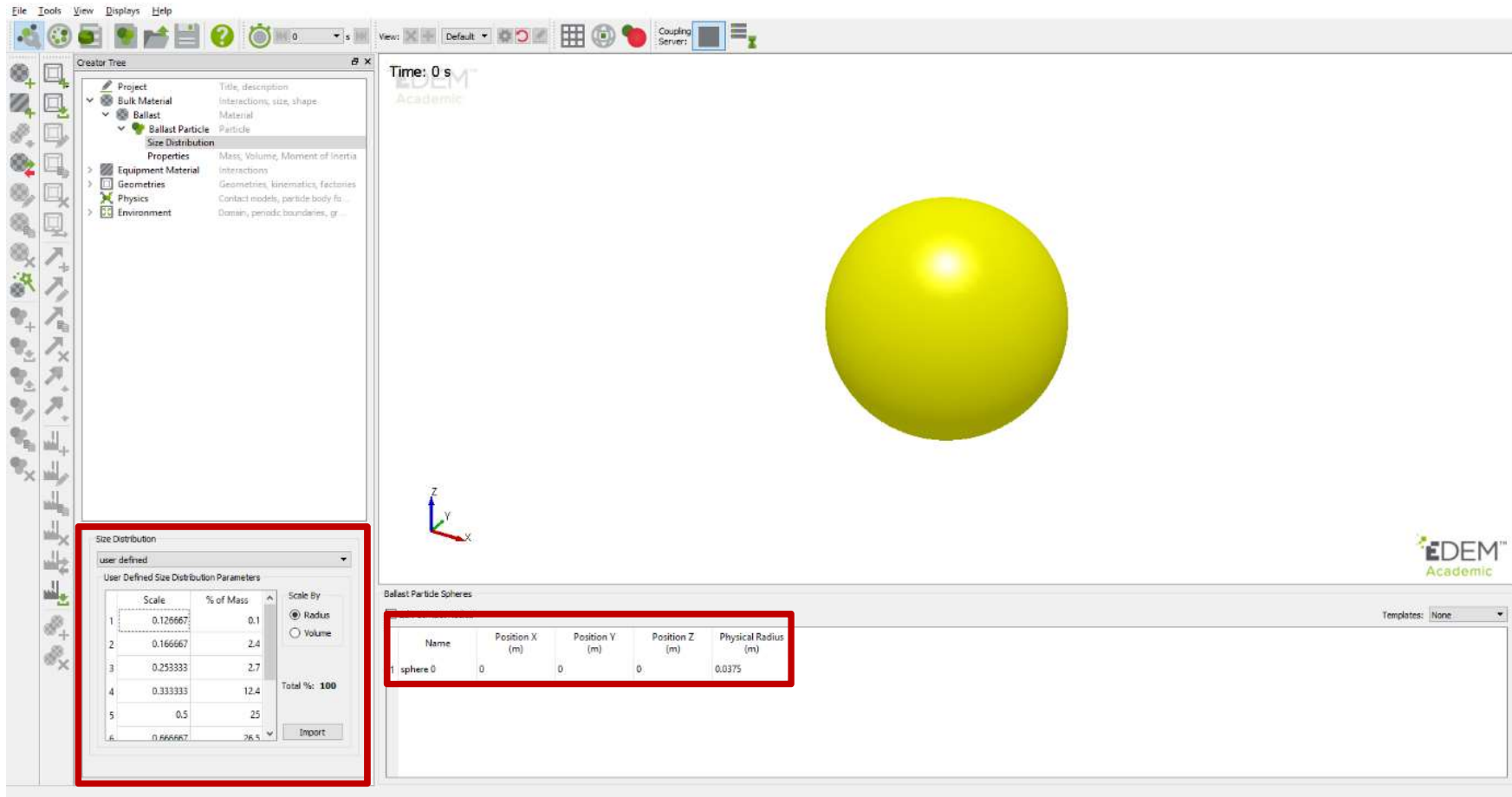
Figure 31: Sphere with diameter of 75 mm and AREMA No. 24 gradation used to simulate railroad ballast material.
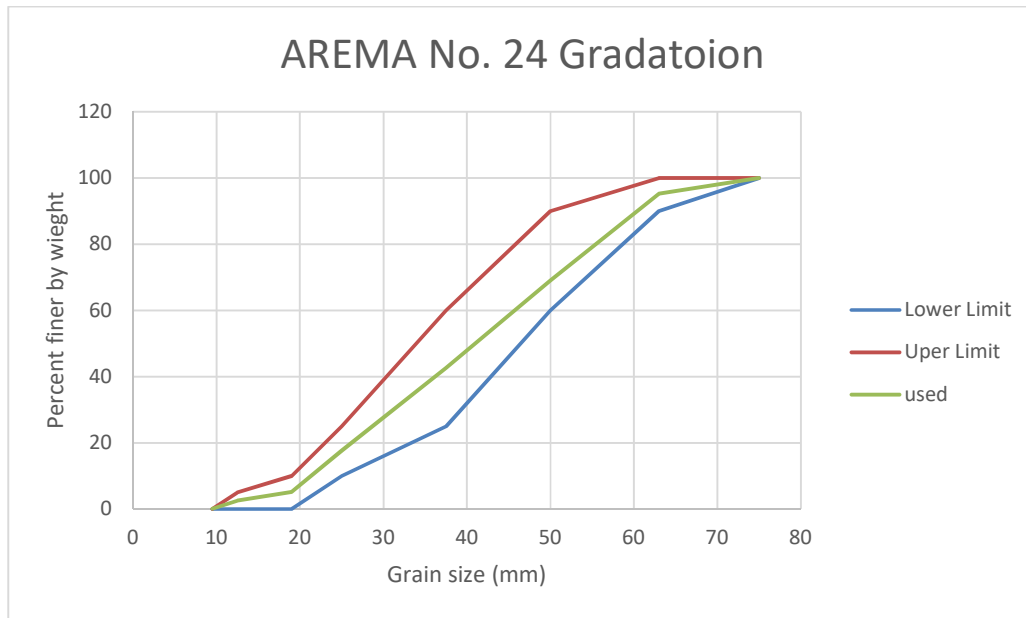
Figure 32: Used particle size distribution to simulate railroad ballast according to AREMA No.24 gradation.

Table 13: Summary of the Used Values of Ballast Material Properties in DEM Simulation

Input used Parameters	Value
Passions ratio	0.2
Solid Ballast density	2600 kg/m^3
Youngs Modulus	17.7 GPa
Shear Modulus	7.5 GPa
Coefficient of Restitution	0.4
Coefficient of Static Friction	0.6
Coefficient of Rolling Friction	0.25
Particle Shape	Spheres
Particle Size Distribution	AREMA No.24
Contact Model	Hertz-Mindlin

4.3.1.3 Ballast Material Calibration

In DEM, it is significant to use the right material properties that represent the material behavior. Some of the ballast material properties are well known and can be used directly in DEM simulation. However, number of ballast material properties related to particle scale are difficult to be measured experimentally due to its small scale. For instance, coefficient of restitution, coefficient of static friction, coefficient of rolling friction and particle shape. Therefore calibration test is required to ensure the accuracy of the material properties and simulation results [197].

Coetzee [182] presented a review on the calibration methods used to identify the material properties for DEM simulations including particle size, shape and distribution. There are two main calibration methods. The Direct Measuring and Bulk calibration methods.

The Direct Measuring method, where the material properties inputted in DEM model directly after measuring them at particle or contact level. For example, Young's modulus, coefficient of restitution, coefficient of static friction, coefficient of rolling friction and particle shape. It is very difficult to measure those parameters at contact or particle level, especially for small and irregular shape as the case of railroad ballast.

The second calibration method is the Bulk method, where field or experimental test are done and then the numerical model is repeated by adjusting material properties until the results are in a good agreement with field/experimental test. The most commonly tests are angle of repose, uniaxial test and triaxial test. The method does not require the complex instruments to measure the material properties at a particle or contact level and assumptions and modifications can be done relative to contact models and particle shape respectively. It is a time expensive activity to do the numerical simulation many times until the numerical results are in a good agreement with

experimental results. Most of DEM simulations of railroad ballast was used for calibration purpose using Bulk calibration method as described previously in section 3.12.

In this work, the bulk calibration method using angle of repose test is used. Angle of repose is defined as the angle between the horizontal plane and the maximum slope of a stable soil pile [198]. The angle of repose is different from a material to another. The angle of repose of a material is influenced by number of particle properties like particle shape [199-201], friction and rolling coefficients [202, 203]. However, it is not influenced by particle density, Poisson's ratio or Young's Modulus [204]. Railroad ballast has a typical angle of repose equal to 40 degrees [165]. There are different methods to measure the angle of repose of a material experimentally. Beakawi Al-Hashemi and Baghabra Al-Amoudi [205] reviewed the different experimental approaches used in the literature for measuring the angle of repose of granular materials including a comprehensive comparison between them.

Chen et al. [165] used angle of repose test in his DEM simulation to calibrate railroad ballast material properties. The same test was used later by Irazábal et al. [146].

In this study, the geometrical set up of the test used is the same as in reference [165] as shown in Figure 33. Although the values of the ballast material properties in Table 13 are taken from literature, this calibration is required to ensure the accurate representation of ballast material. Furthermore, to show the validity of representing ballast irregular particle shapes as spheres with coefficient of rolling resistance.

The calibration test is done using the ballast material properties in Table 13. The variable parameter is the coefficient of rolling resistance. The calibration test is done two times to investigate the influence of rolling friction coefficient on representing ballast shape. One time with zero value for coefficient of rolling friction and the other

time with 0.25 value. The zero value of rolling friction coefficient represents the pure

spherite of particle shape. The 0.25 value represents the angularity of particle shape.

Results of this calibration is discussed in section 5.2.1 below.
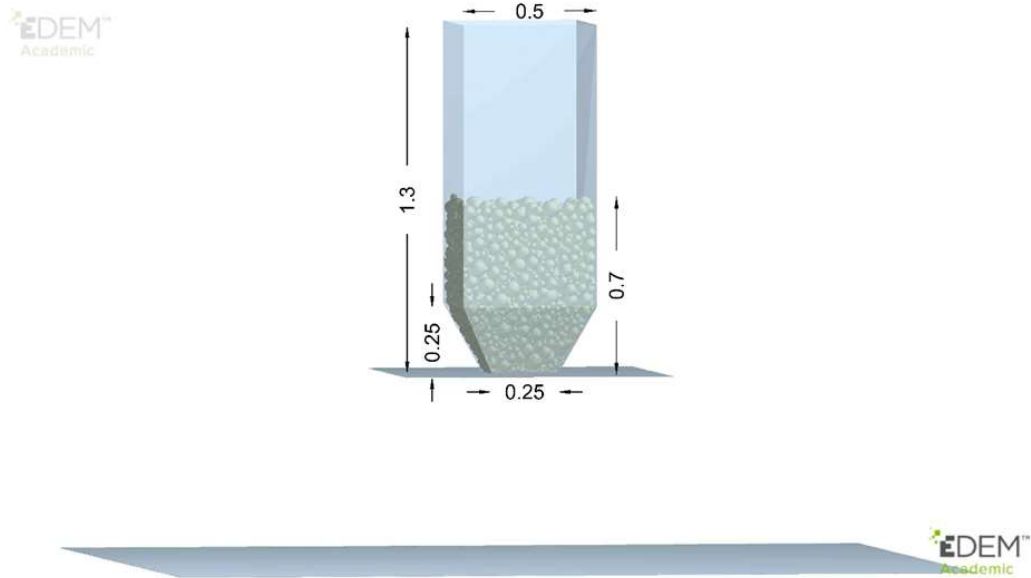
Figure 33: Set up of angle of repose test using DEM.

4.3.2 Box Test Setup

4.3.2.1 Equipment Material Properties

Equipment material is the second type of material in EDEM that needs to be

defined and assigned before starting the simulation. Equipment material is assigned

only to geometries. The equipment material has different properties compared to bulk

material. It does not have a related particle shape or particle size distribution. In this

simulation, there are two equipment materials used; steel for the box and concrete for

the sleeper. The used values for the material properties for both materials are typical to

what is known in the literature. There is not enough literature on the interaction properties between equipment and ballast materials using DEM, default values from EDEM are used. Table 14, summarizes the properties of equipment materials used in this simulation.

Table 14: Equipment Material Properties Used in DEM Simulation

Parameter	Steel		Concrete	
	Literature	Used	Literature	Used
Poisson's ratio	• Common	0.3	• Common	0.25
Solid Density	• Common	7850 kg/m^3	• Common	2400 kg/m^3
Young's Modulus (Shear Modulus)	• Common	26 GPa (10 GPa)	• Common	30 GPa (12 GPa)
Interaction properties between Equipment materials and ballast				
Coefficient of Restitution	• 0.25 [8]	0.25	----------------	0.5 (default value in EDEM)
Coefficient of Static Friction	• 0.7 [8]	0.7	• 0.7247 [206]. • 0.1-0.8 [207] • 0.5-0.9 [208] • Has marginal influence of the simulation results [208]	0.5 (default value in EDEM. No lateral forces are applied)
Coefficient of Rolling Friction	0.001 by Vizcarra et al. [8]	0.001	----------------	0.01 (default value in EDEM)

4.3.2.2 Geometries Setup

After defining the properties of the equipment materials. The dimensions of the geometries need to be defined. In EDEM, there are three geometrical shapes. Box, cylinder and polygon. In this study, box shape is used. The sleeper is created as a closed box. The box is created as an open box (upper face "Face1" is eliminated) to allow for sleeper vertical movement as shown in Figure 34. The equipment materials are assigned. Concrete material for sleeper and steel material for box. In EDEM, geometry is defined either as a physical or virtual. The virtual geometry does not interact with anything in simulation and is used mainly to create particles. While, the physical geometry interacts with the particles in the simulation and can be used to create particles. Particle creation is described in the below section. Both of sleeper and box are defined as physical geometries. The dimensions of the sleeper and box are defined and created as shown in Figure 35.
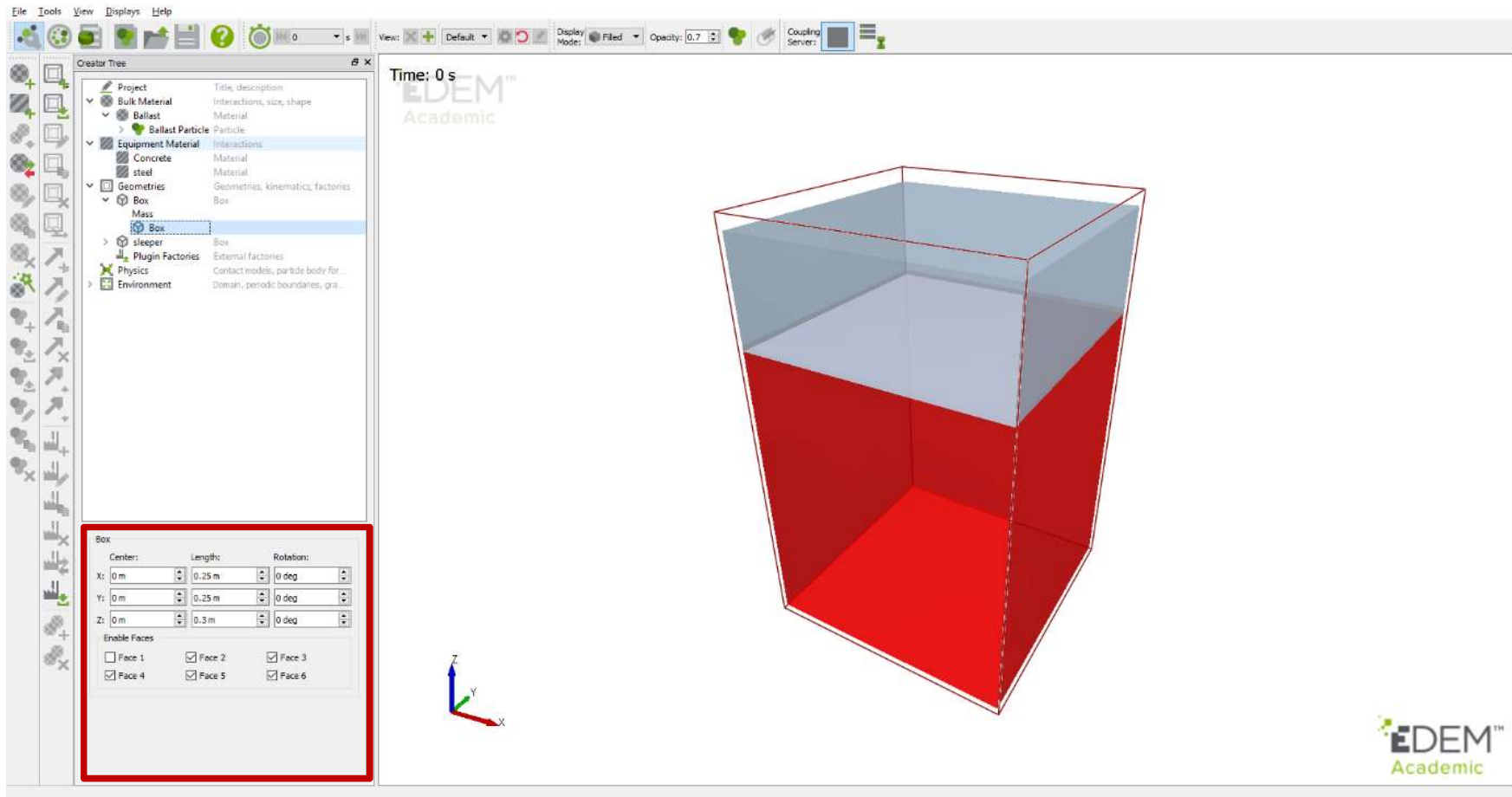
Figure 34: Box assigned parameters in EDEM.
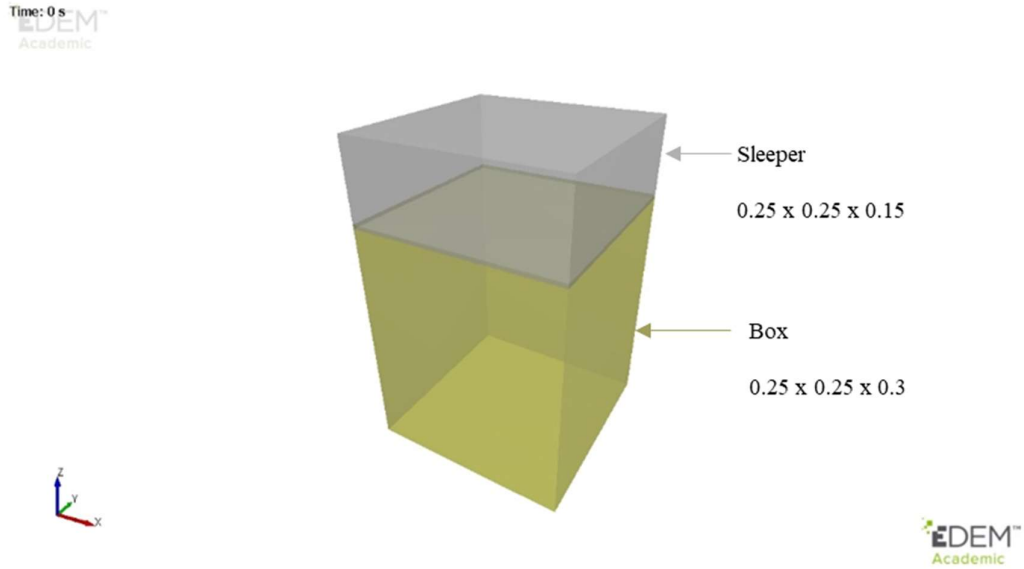
Figure 35: Box test geometrical set up used in EDEM (dimensions in meters).

4.3.3 Simulation Setting

EDEM requires various parameters related to simulation setting to be defined before starting the simulation (Figure 36). For instance, integration method, time step, simulation time, data save point, grid cell size and simulator engine. Each parameter and the used value are discussed below.
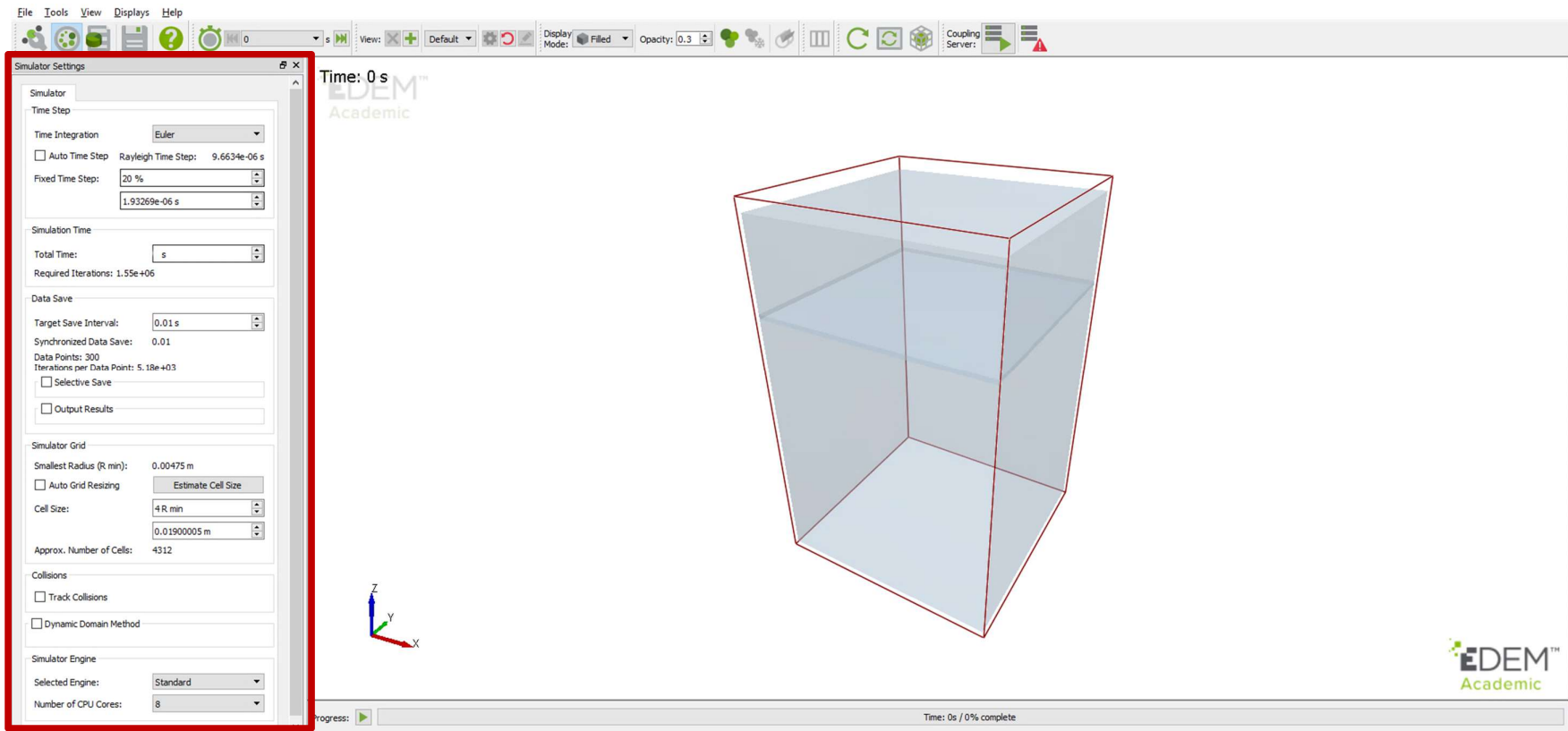
Figure 36: Simulation settings in EDEM.

4.3.3.1 Integration method

Time numerical integration is used to calculate numerically the particle velocity and position from Newton's second law. There are different schemes of numerical integration used in DEM as discussed in section 3.4.

There are two types of integration schemes in EDEM; Euler and Verlet. Euler integration scheme is the default one. Verlet scheme cost an additional 10% of computational time in EDEM compared to the Euler scheme [209].

In this study, Euler integration scheme is used due to its simplicity and low requirement of computational time as described previously (3.4).

4.3.3.2 Time step

EDEM requires to define the time step used in the simulation before starting the simulation. Time step is the amount of time where EDEM performs contact detection, calculates and updates particles positions iteratively during the simulation. It is crucial to choose the appropriate time step in DEM simulation [81, 82]. There are two principles that should be considered in choosing the appropriate time step; excessive overlapping and propagation of surface wave disturbance.

Simulation with a large time step has low number of saved data and calculation iterations compared to simulation with a small time step. Large time step requires low computational time. Large time step may produce inaccurate simulation results [83]. As particles behave unsteadily in the simulation with a large time step due to excessive overlapping between particles as shown in Figure 37. At the initial time the objects approach each other with certain velocities. After one large time step, their positions are updated with an apparent overlapping. This produces a large contact force which leads to incorrect calculations of particle positions. Too small-time step could provide accurate results but needs a huge computational time and produces huge saved data.

Therefore, the value of time step should be chosen to produce accurate results in an efficient computational time. The typical time step used in DEM simulations is in the range of 1×10^{-4} to 1×10^{-6} seconds.

The movement of granular particle is influenced on the immediate contacts with its neighbors and the wave disturbance from far particles. This wave is called surface wave and identified as Rayleigh wave. The time step should be small enough to avoid the influence of wave disturbance from each particle to be propagated to other than neighbor particles. Large time step causes wave disturbance of each particle propagates to its neighbors' particles and other faraway particles. This leads to inaccurate results. Figure 38 illustrates the influence of Rayleigh wave disturbance in small- and large-time step. Where, in small step (Figure 38 a) particle 2 is moved due to the contact and wave disturbance from particle 1. In large time step (Figure 38 b), the wave disturbance caused by particle 1 propagates to more than its neighbor (particle 2) reaching to particle 3. This causes the incorrect positions of particles and simulation results.

Therefore, a suitable time step is calculated based on the Rayleigh wave time (T_R) using the below equation.

$$T_R = \frac{\pi R \left(\frac{\rho}{G}\right)}{(0.1631\upsilon + 0.8766)} \tag{4.16}$$

where, T_R is the Rayleigh time, R is the particle's radius, ρ is the particle density, G is the shear modulus of the material, υ is the Poisson's ratio.

The Rayleigh wave time is estimated from the Rayleigh wave speed. A fraction of the Rayleigh wave time is taken as a time step. The fraction of Rayleigh wave time ensures the realistic overlapping between particles (realistic contact forces) and avoids the disturbance of the Rayleigh wave to be propagated to more than the neighbor particles. This produces more stable and accurate results. The Rayleigh wave time

depends on different material parameters. Therefore, it is important to choose the right material parameters of railroad ballast as discussed later in this section. It depends on particle radius, density, shear modulus and Poisson's ratio. The default and recommended value of this fraction by EDEM is 0.2 (20% of T_R). EDEM calculates T_R based on the defined material properties. Besides, the used time step in the simulation is based on the fraction factor. In this study, the default fraction factor of 0.2 (20%) is used. The used time step is 1.93269×10^{-6} seconds.
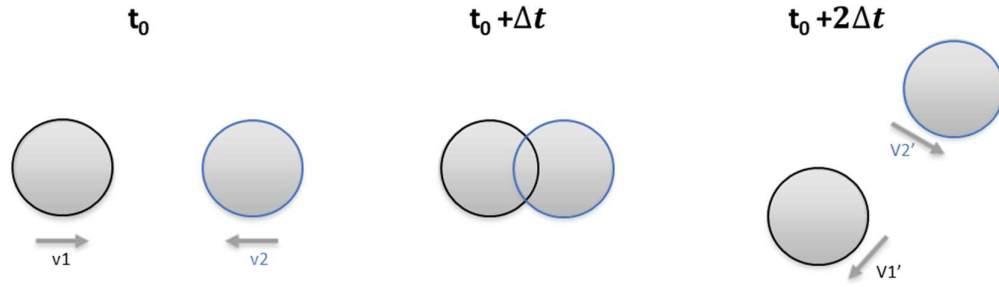
Figure 37: Influence of large time step on particle contact mechanism.
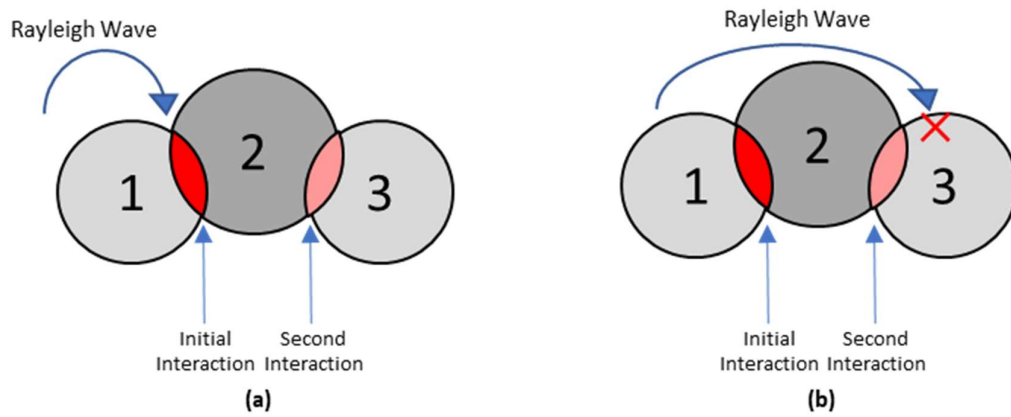
Figure 38: Influence of Rayleigh wave disturbance using (a) small and (b) large time steps.

4.3.3.3 Simulation Time and Data Save

The simulation time is the total amount of time in seconds that the simulation is run. In EDEM, the simulation time for each simulation is defined by the user. In this study, the simulation time is not fixed. Each loading case has its own simulation time to complete 1000 loading cycles. The simulation time for each case is discussed below in section 5.2.3. EDEM calculates the required iterations automatically once the

simulation time step and the simulation time are defined. The number of iterations is defined as the ratio of the simulation time to the time step.

Data save is the amount of time where simulation data is saved. The data save is an option provided by EDEM. The larger the data saves, the lower computational time is required, where less data is saved and vice versa. The default value of the data save in EDEM is 0.01 seconds. In this study, 0.01 seconds is used as a data save. Once data save value is defined, EDEM automatically calculates the number of data save points and number of iterations per data point based on the simulation time, the time step and the data save time. EDEM provides a selective save option where certain selected data is saved (e.g. particle and geometry related data). In this study, this option is not used as all data is needed.

4.3.3.4 Simulation Grid Cell Size and Simulator Engine

Contact detection between particles is done by different approaches. There are two methods to detect contact between particles. The grid and tree based as described in section 3.5. Most of DEM software packages use the grid-based algorithm including EDEM. In grid-based approach, the simulation domain is divided into grid cells. EDEM searches for possible particle contacts in each cell. Then, EDEM identifies the contact details.

It is necessary to define the grid cell size. The grid cell size does not affect the simulation result. It influences the computational time. The typical grid cell size is in the range of 3-6 of R_{min} (minimum particle radius). Cell grid size below 2 of R_{min} requires huge computational time. The estimated grid cell size in this study is equal to 4 of R_{min} which is 0.0190 m as shown in Figure 36.

In EDEM, the simulator can run in two modes Central Processing Unit (CPU) or in Graphics Processing Unit (GPU). This is based on the license type and

computational resources. The computer used in this study has an i9 intel CPU which consists of 14 cores and a "NVIDIA GeForce GTX 1080Ti" GPU. The best scenario to reduce the computational time is to use both modes in ruining EDEM i.e. CPU and GPU modes running in parallel. EDEM default license includes the usage of CPU mode only using 8 cores. It is optional to increase the number of CPU cores or add GPU mode to EDEM license. However, any additional core of CPU or usage of GPU mode are considered as an additional option and cost to the license.

The additional cores to the license have a marginal influence on the computational time. From 8 cores to 12 cores the computational speed increases by a factor of 1.5. Regarding GPU, EDEM 2018 does not support the GPU mode using API. In this stud, API is used to customize the control mode in EDEM as described in 4.3.4. Therefore, EDEM default license is used in this study. EDEM default license includes the usage of 8 cores of CPU mode, EDEM Application Programming Interface (API) for user Defined Libraries and Default CAD Import Option.

4.3.4 Control Mode

There are two modes of control used in the experimental tests; displacement and force control modes.

Displacement control mode is defined as the application of a load on the material using displacement with a specified rate where the failure of the material occurs in a non-destructive way. Non-destructive failure means that the material can surpass the load after this point. The displacement control mode is used to monitor specific material properties under fatigue. For example, the change of material stiffness during the test.

Force control mode is the application of a load on the material using a force with a specified rate until the failure of the material (destructive failure) occurs. After

this failure, the material cannot surpass the load anymore. The force control represents the real field condition and it is used commonly to obtain the ultimate strength of the material [210].

From the literature, most of experimental work and DEM models used to understand the mechanical behavior of railroad ballast via box test, used the force control mode. It represents the field condition and provides a descriptive data for the ultimate failure of ballast layer (2.5).

In this study, the force control mode is used. Although EDEM software supports the use of displacement control mode, EDEM can be customized to support the force control mode using Application Programming Interface (API) through C++, which is the basic language of the software.

4.3.4.1 Aim and Description of the Validation Exercise

This exercise aims to show the concepts of the developed subroutine that uses force control in EDEM software using the API via C++ language. Different C++ codes are written and customized to represent the different input simulated loading to be used in this study via EDEM (Appendix).

By default, EDEM can define linear and sinusoidal translations to geometry based on displacement control. The displacement control requirements in EDEM differ from normal software interface and coupling interface using API via C++. In the normal software interface EDEM requires the start time, end time, velocity and acceleration to define the geometrical motion. In the coupling interface, EDEM requires the total translation and velocity per time step to define the geometrical motion.

In this exercise, the DEM simulation is used for the illustration and validation purposes. The illustration includes the set of equations and C++ program algorithm

used to make EDEM work in a force control mode. The validation is done by validating the developed set of equations with the results obtained from the simulation.

The DEM model of this exercise consists of a small cubical box with a volume of 0.1 m^3 and a square plate with side dimension of 0.1 m (Figure 39). The box is filled with spherical particles. After the particles reached the equilibrium state, the plate compresses the particles using the force control mode. All the parameters used in this exercise related to the simulation are the default parameters by EDEM.
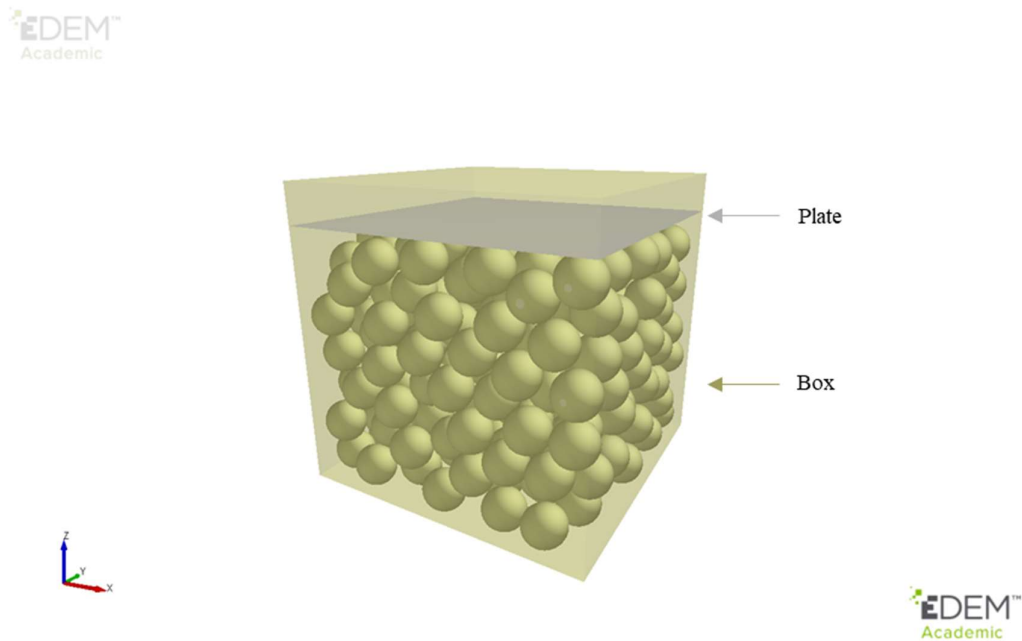
Figure 39: DEM simulation of a small box used for the force control mode exercise.

4.3.4.2 Set of Equations

In force control mode, there are two forces applied on a geometry at contact (compression scenario). The top force is the input (application) force. The bottom force is the contact (response) force between the material and the geometry.

The system that needs to be solved consists of a mass (geometry) and two forces (Figure 40). The input force (F^i) from the top is a virtual force in EDEM. The response force (F^c) from the bottom is the total contact forces on the geometry. The response force is known from EDEM.
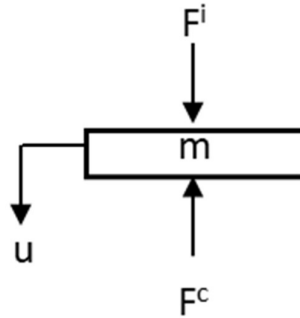
Figure 40: Free body diagram of the geometry at contact.

The governing equation of the above system is homogenous linear Ordinary Differential Equation (ODE) of the second order.

$$m\frac{d^2u}{dt^2} + F^i = F^c \qquad (4.17)$$

with an initial value of

$$u(0) = 0 \text{ and } \frac{du}{dt}(0) = 0$$

where m is the geometry mass, u is the displacement response, F^c is the contact force and F^i is the virtual input force. The different simulated train loading (4.3.6) are used as F^i. At time (t), F^c is the only unknown parameter. To find F^c, a numerical integration is required.

There are several types of numerical integration schemes. Euler numerical integration is used to be consistent with the default EDEM simulation settings (4.3.3.1). EDEM uses Euler integration scheme as a default option for particles' positions calculations.

To solve equation 4.17 numerically, the second order ODE is converted to first order ODE. This is done by introducing new variable z

$$z = \frac{du}{dt} \tag{4.18}$$

$$\frac{dz}{dt} = \frac{d^2u}{dt^2} \tag{4.19}$$

and initial value of $z(0) = 0$.

Substituting equations 4.18 and 4.19 to 4.17 gives

$$m\frac{dz}{dt} + F^i = F^c \tag{4.20}$$

Solve for $\frac{dz}{dt}$ using the initial value of $z(0) = 0$, the acceleration (a) of the geometry at time t is equal to

$$a(t) = \left[\frac{dz}{dt}\right]_t = \frac{F_t^c - F_t^i}{m} \tag{4.21}$$

where F_t^i is known and F_t^c is obtained from EDEM.

Euler numerical integration method with a time step of Δt is used to find the velocity of the geometry (v) at time t+1

$$v(t+1) = z_{t+1} = z_t + \left[\frac{dz}{dt}\right]_t \Delta t \tag{4.22}$$

Integrating equation 4.22 with respect to t and using equation 4.18, the translation of the geometry (u) at time t+1 is equal to

$$u_{t+1} = u_t + [\frac{du}{dt}]_t \Delta t \tag{4.23}$$

equation 4.23 can be written as

$$u_{t+1} = u_t + z_t \Delta t \qquad (4.24)$$

Both velocity (equation 4.22) and translation (equation 4.24) of the geometry are known

at time t+1.

The previous equations (equations 4.21, 4.22 and 4.24) are used in EDEM

coupling interface to simulate the movement of the geometry based on force control.

EDEM simulates the translation and velocity of the geometry at each timestep that

corresponds to the required predefined force (F_i).

Different C++ codes are written and customized to represent the different input

loading types used later in this study through EDEM. The different input loading types

include: constant loading used in the preloading process; sinusoidal loading used in

Case 2; simulated train loading utilizing BOEF used in Case 1. The C++ codes for the

previous loading types are shown in the Appendix.

The validation of this code is done by validating equation 4.17, where the

predefined input force (F^i) is known and the response contact force (F^c) is obtained from

EDEM. The validation results of this exercise for different predefined loading force

types are discussed in section 5.2.2.

4.3.4.3 C++ Program Algorithm

The algorithm of C++ program that is written to customize EDEM using the

previous equations to work in force control mode is described below:

1. Defining the essential C++ libraries (e.g. iostream)

2. Defining EDEM library (e.g. IEDEMCoupling.h) that allows the user to use all the

    EDEM related functions in C++ and initialize the coupling.

3. Defining the parameters used in the C++ code (e.g. geometry translation)

4. Initializing the coupling between EDEM and C++ source code via API using "IEDEMCoupling coupling" function in C++ via EDEM coupling interface.

5. Default displacement control of EDEM is used.

6. Geometry moves down with a predefined velocity.

7. Contact force from particles close to the predefined force (F^c=0.98 F^i).

8. Stop displacement control mode and use force control mode.

9. F^c and u of the geometry at time (t) is obtained from EDEM using "coupling.getGeometryForces" and "coupling.getGeometryTranslation" functions respectively, in C++ via EDEM coupling interface.

10. F^i at time (t) is calculated based on the applied force type (e.g. constant, sinusoidal, simulated train loading from BOEF).

11. Geometry acceleration at time (t) is calculated using equation 4.21.

12. Geometry velocity and position are updated for the next time step (t+1) using equations 4.22 and 4.24 respectively.

13. Simulate the geometry translation using the calculated velocity and position form 12 using "coupling.setGeometryMotion" function in C++ via EDEM coupling interface.

14. Back to step 9 until the end of simulation time.

4.3.5 Ballast Layer Creation and Preloading

It is essential to ensure the initial ballast status in ballast creation stage using DEM with relative to field condition. In the field, the required bulk density of railroad ballast should be more than 1400 kg/m^3 with accordance to Australian standards (AS 1141.4). Navaratnarajah and Indraratna [211] reported that the typical field density of railroad ballast is 1560 kg/m^3 that corresponds to a void ratio of 0.73 approximately. The initial void ratio of railroad ballast is in the range of 0.6-0.8 [35]. From the

literature, ballast particles are created and compacted to different void ratios using DEM (e.g. 0.65 [128],0.67 [120],0.69 [136] and 0.82 [17]).

In EDEM, particles are created using geometrical factories. There are two types of factories; static and dynamic. The static factory creates particles while the simulation is paused. The particles are created first then the simulation is run. Dynamic factory creates particles during the simulation. The simulation is not paused during particle creation.

To create particles in EDEM, a geometrical factory needs to be defined. In this simulation the physical box geometry is used as a dynamic factory to create the particles. The dynamic factory type is used as it is closer to the reality where ballast material is poured in a box. The input mass is 29.25 kg which is calculated based on a field bulk density of 1560 kg/m^3 [211] and a box volume of 0.25×0.25×0.3 cubed meters.

The default generation rate in EDEM is 5000 kg/s. The value of generation rate is defined based on the number of trails. In this study, the used generation rate is 700 kg/s. A larger number of generation rate (more than 700 kg/s) gives a warning message that the factory is not large enough to create particles at this rate. A smaller number of generation rate (less than 700 kg/s) requires more time to create the particles. At each time step EDEM tries to create the particles based on the defined rate (20 times default value of maximum attempts to place particles). This rate is converted to mass per time step after starting the simulation. The particles are created right after starting the simulation. The factory settings used in this simulation is shown in Figure 41.

In this simulation, the particles are created and reach equilibrium after 3 seconds of the simulation time with a total number of 4842 particles. The created material has a void ratio of 0.7 that corresponds to a bulk density of 1531 kg/m^3. Figure 42 shows the

particle creation process at the first and last stages of the simulation. Figure 43 shows

the mass of the created particles during the simulation.
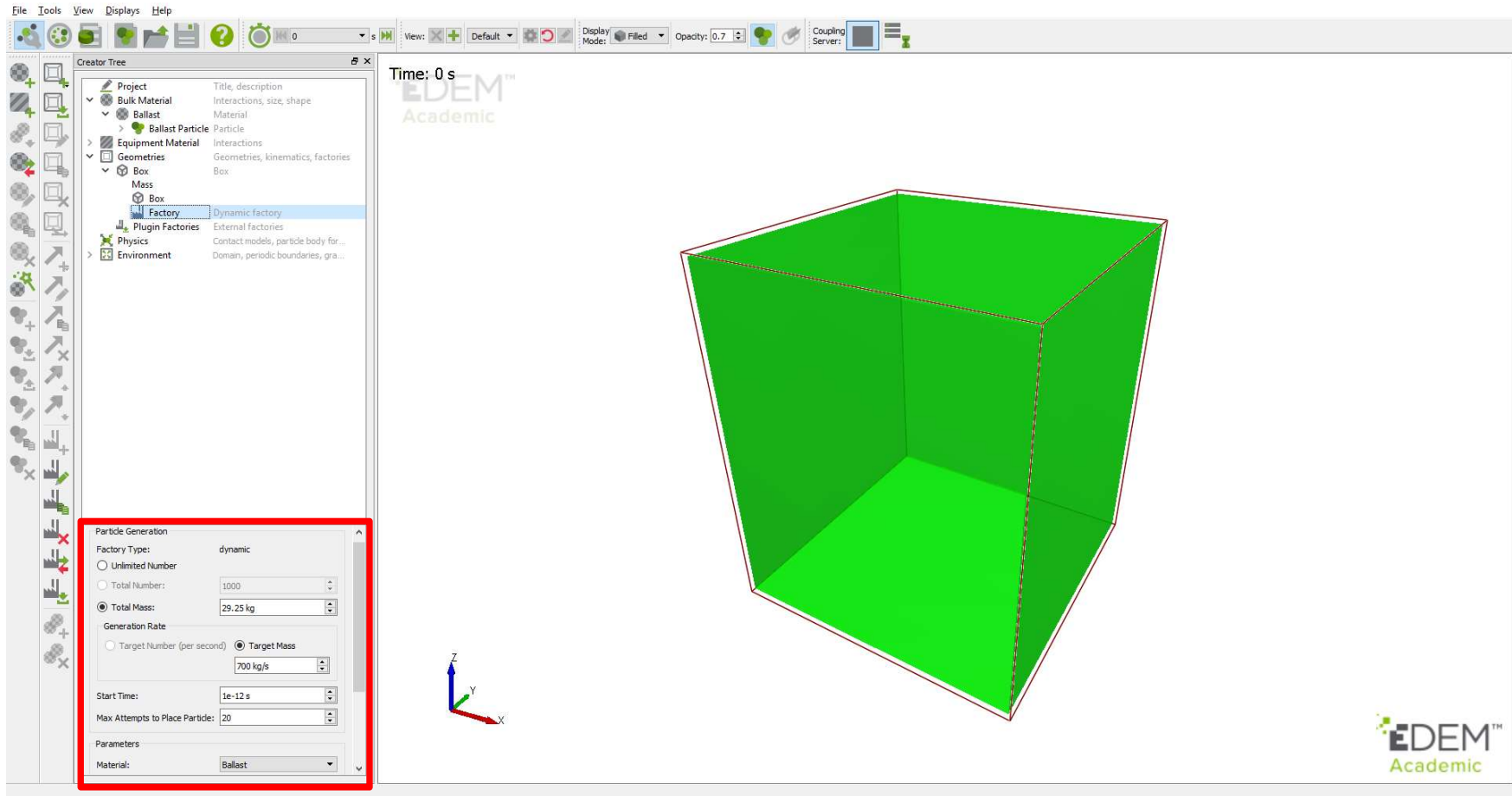
Figure 41: Factory required parameters for particles creation.
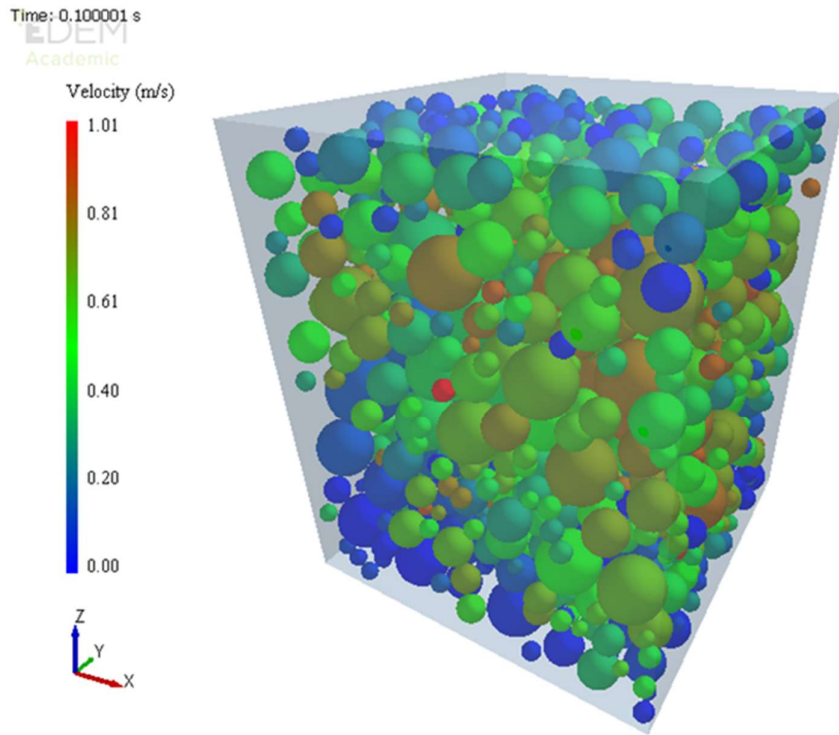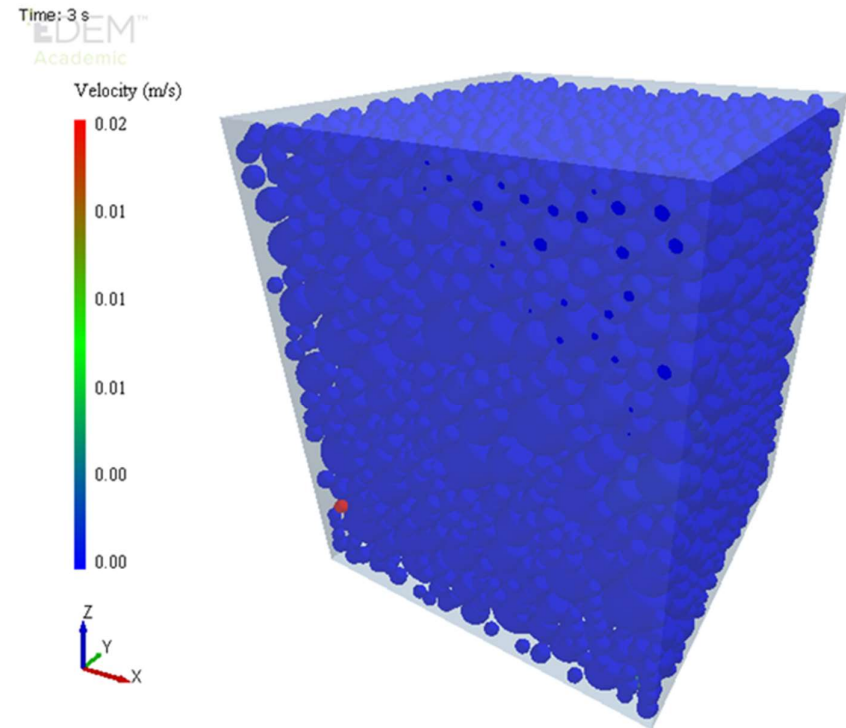
Figure 42: Particle creation at (a) 0.01 and (b) 3 seconds
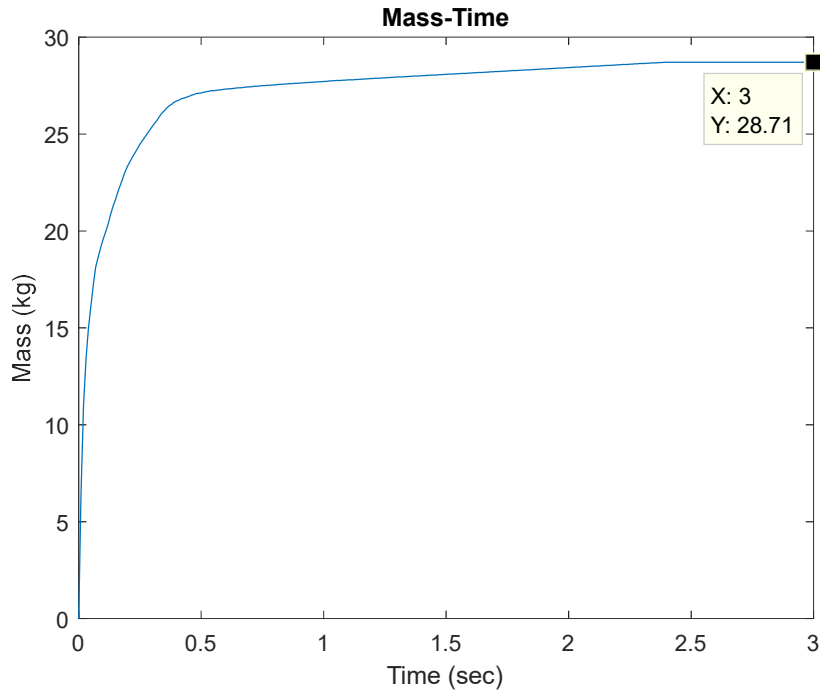
Figure 43: Created mass of particles during the simulation time.

Then, preloading stage is applied to ballast material. In the field, ballast layer is exposed to a static load and live load. The static load consists of the weight of rails and sleepers. The live load is the train load. From its name, the preloading stage is the stage before the passages of trains; and it represents the static load. It is essential to consider the preloading stage in the simulation before applying the simulated train loading. The preloading calculation is done for the simulated box. Figure 44, shows the distribution of the static load by sleeper and rail exerted on the simulation box.
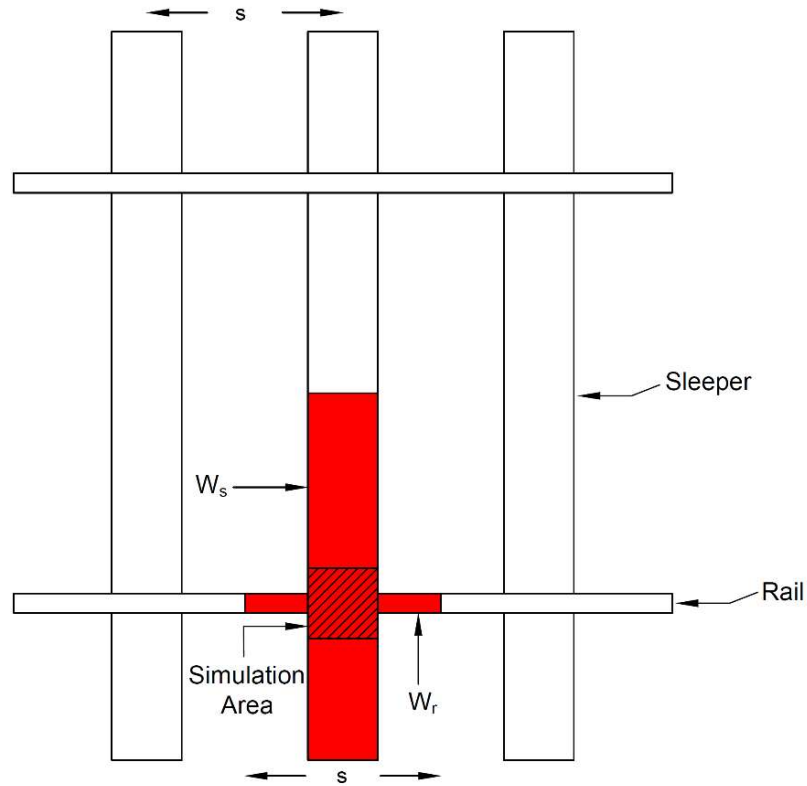
Figure 44: The weight distribution of sleeper (Ws) and rail (Wr) on the simulation box.

The preloading value is calculated based on typical weights of rail and concrete sleeper. Rail typically weighs 65 kg/m [8]. Concrete sleeper typically weighs 360 kg [8]. The typical spacing between sleepers (s) is 0.7 m [80]. The value of preloading (P_r) is calculated based on below equation:

$$P_r = 9.81 \times \left[(W_r \times s) + \left(\frac{W_s}{2} \right) \right] = 2212.16 \text{ N} \tag{4.25}$$

where, P_r is the preloading (N), W_r is the typical weight of rail per unit length (kg/m), W_s is the typical weight of concrete sleeper (kg), s is the typical spacing between sleepers (m).

The constant value of preloading force is used in the force control mode using the developed set of equations (4.3.4) via EDEM API. EDEM supports the displacement mode of geometries. The EDEM API is an additional interface used in EDEM to allow users for any further customizations. In this study, the API is used to customize EDEM to support the force control mode. C++ is used as it is the basic language of EDEM. The main logic behind customizing EDEM via API using C++ language is described in details in section 4.3.4.

The preloading stage takes 2 seconds of simulation time to achieve the equilibrium state of ballast particles (Figure 45). The increment of the total force on the sleeper bottom in the initial stage of the simulation is due to the transition from displacement control to force control mode; where in the displacement control the acceleration of the geometry is zero (inertial force of the geometry is zero) then it increases to a value at a small timestep. This increment causes the sudden increase in the total force; due to the significant contribution of the inertial force at that timestep. Therefore, the simulation is done for 2 seconds to achieve the equilibrium state of ballast particles.
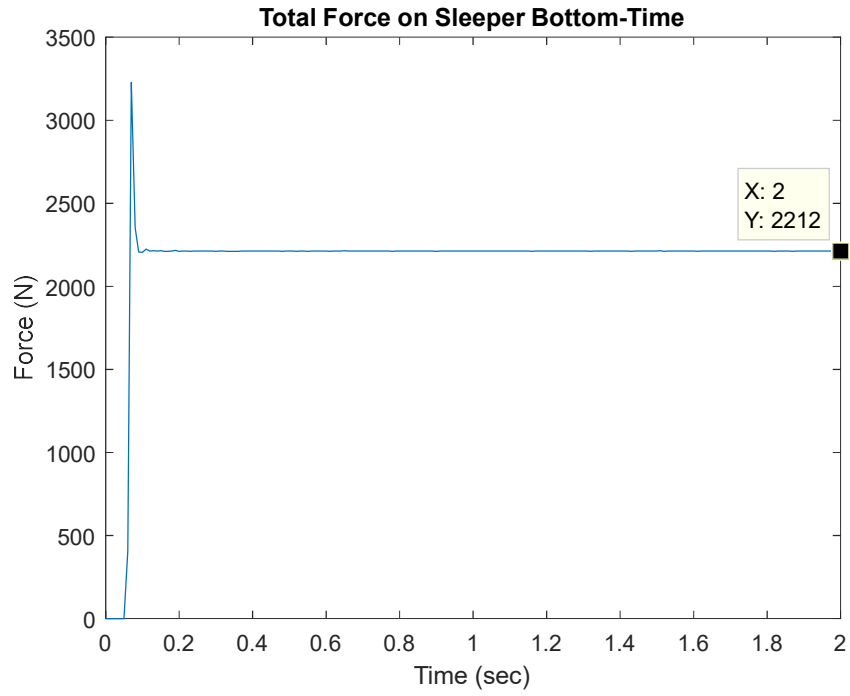
Figure 45: Total force on the sleeper bottom during the preloading stage for the 2 second simulation time.
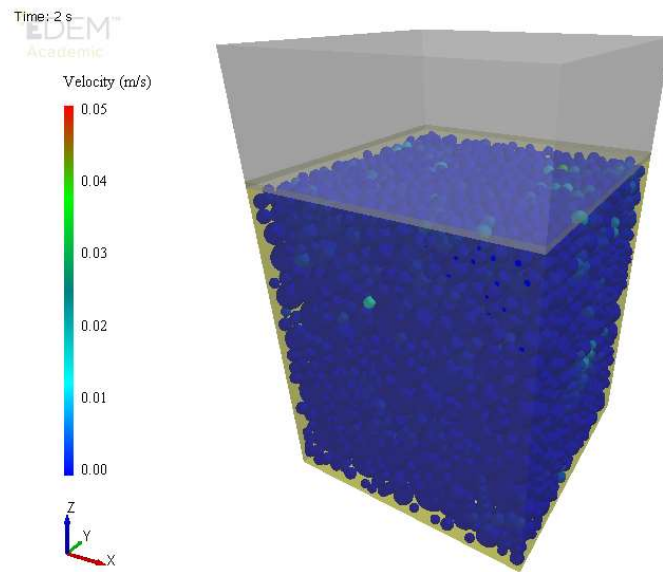
Figure 46: End of preloading stage at 2 second of simulation time.

4.3.6 Simulated Train Loading

4.3.6.1 Loading Cases

     As discussed above that most researchers in the literature simulated the train loading as a pure continuous sinusoid based on axle spacing and train speed; unlike the actual loading induced by the trains. The loading induced from the train is not a pure sinusoid. There are various parameters affect the train loading like train speed, car length, car weight and axle spacing.

     To investigate the influence of simulated train loading on the behavior of railroad ballast using DEM; Beam on Elastic Foundation (BOEF) theory is utilized to simulate a more realistic train loading. The results from more realistic simulated train loading are compared with those from sinusoidal loading.

     Discrete Element method is used to model the behavior of railroad ballast under two simulated train loading cases via Box Test. The train loading cases is simulated for an infinite train that passes a measurement point on the track. The measurement point is the simulation box.

     There are two loading cases used in this study as described in Table 15. Case 1 is the more realistic train loading simulated utilizing Beam on Elastic Foundation (BOEF) theory as described in section 4.2. For this case, the simulated train has different axle spacings and same car length as shown in Figure 47. The description of the parameters in Figure 47 is given in Table 16.

Table 15: Description of the Two Loading Cases Used in This Study

Case	Description
Case 1	Simulated infinite train loading utilizing BOEF theory
Case 2	Simulated infinite train loading as sinusoidal loading with frequency based on axle spacing of L_1
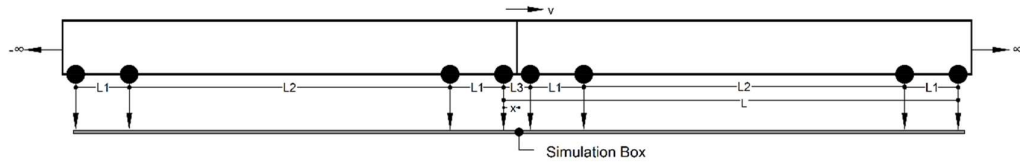
Figure 47: Simulated train dimensions.

Table 16: Description of the Parameters in Figure 47

Parameter	Description
L	Typical spacing between the first axle of two consecutive train cars
L_1	Typical spacing between the two front and rear axles
L_2	Typical spacing between the second and third axles
L_3	Typical spacing between the fourth axle and first axle of two consecutive train cars
x	
v	The train velocity

Case 2 is a sinusoidal loading type with a frequency based on a typical axle spacing of L_1 that equals to 2.5 m and a train speed of 100 km/h (Doha Metro maximum train speed); which corresponds to a loading frequency of 11.11 Hz. From the literature, most of the calculated frequency of sinusoidal load is based on the axle spacing of L1 and in the range of 1.5-2.6 m.

Aursudkij et al. [48, 212] presented that the usual loading frequency for a normal train is in the range of 8 – 10 Hz and for a high speed train it may extend to 30 Hz; assuming an axle spacing of 2.6 m and a train speed of 75-94 km/h. Indraratna et al. [123] used sinusoidal loading with various ranges of frequencies 10, 20, 30 and 40 Hz in their triaxial test using DEM. Their cyclic loading frequencies were calculated based on an axle spacing of about 2 m that corresponds to different train velocities (73, 145, 218 and 291 km/h). Chen et al. [160] used a sinusoidal loading with a frequency of 20 Hz in their DEM simulation of box test. The frequency was calculated based on an axle spacing of 2.02 m which corresponds to a train velocity of 146 km/h. Ngo et al. [17] used sinusoidal loading in their DEM simulation of box test. In their study, they used an axle spacing of almost 1.5 m of a train speed of 80 km/h that corresponds to a frequency of 15 Hz.

4.3.6.2 Number of Loading Cycles

The number of loading cycles used in the literature for modeling the behavior of railroad ballast using DEM varied as shown in Table 7. In the field, ballast deformation and degradation occurs after a large number of loading cycles, beyond 100,000 [120] . Ngo et al. [17] And Chen et al.[160] used 500,000 and 200,000 loading cycles in their experimental tests respectively. However, the maximum number of loading cycles used in DEM to understand the mechanical behavior of railroad ballast is 6000 for a 2D model and 4000 for a 3D model by [120] and [17] respectively. This

is due to the huge requirement of the computational time by DEM which is the main limitation. Therefore, the number of loading cycles used in this study is 1000 loading cycles.

CHAPTER 5: ANALYSIS, RESULTS AND DISCUSSION

5.1 Introduction

This chapter includes two main sections; analysis and results and discussion. In the analysis section, the analysis of several perspectives used in this study and described in the previous chapter are discussed. The perspectives are ballast material calibration, control mode and simulated train loading. These perspectives are required to simulate the behavior of railroad ballast under different train loading using DEM. These perspectives produce results that require analysis. More information about the previous perspectives can be found in the previous chapter.

In the results and discussion section, the main results of this study are highlighted and discussed. The section is divided into two subsections; macroscopic behavior and microscopic behavior. The first two subsections highlight the results of this study related to ballast behavior under different simulated train loading cases using DEM.

5.2 Analysis

5.2.1 Ballast Material Calibration

The angle of repose test is used to calibrate ballast material properties using DEM as described in section 4.3.1.3.

The calibration test is done using the ballast material properties given in Table 13. The calibration test is done two times. One time with zero value of coefficient of rolling friction and the other time with 0.25 value; to investigate the influence of rolling friction coefficient on representing ballast shape. The zero value of rolling friction coefficient represents the pure spherite of particle shape. The 0.25 value represents the angularity of particle shape.

In calibration simulation, the particles are created inside the hopper. After reaching the steady state of the particles, the particles are freely deposited from a square

hopper with 25 cm side, located at 0.7 m above the ground. The angle of repose is measured for both cases as shown in Figure 48.

The angle of repose for the first simulation is 8 degrees (Figure 48 a). The angle of repose for the second simulation is 40 degrees (Figure 48 b). The ballast material properties in the second simulation represent the behavior of railroad ballast. Because it develops a typical angle of repose for railroad ballast [165]. This simulation ensures the validity of ballast material used in Table 13 to represent ballast in DEM.

Therefore, the material properties in Table 13 are used in this study as a representation of ballast material using DEM.
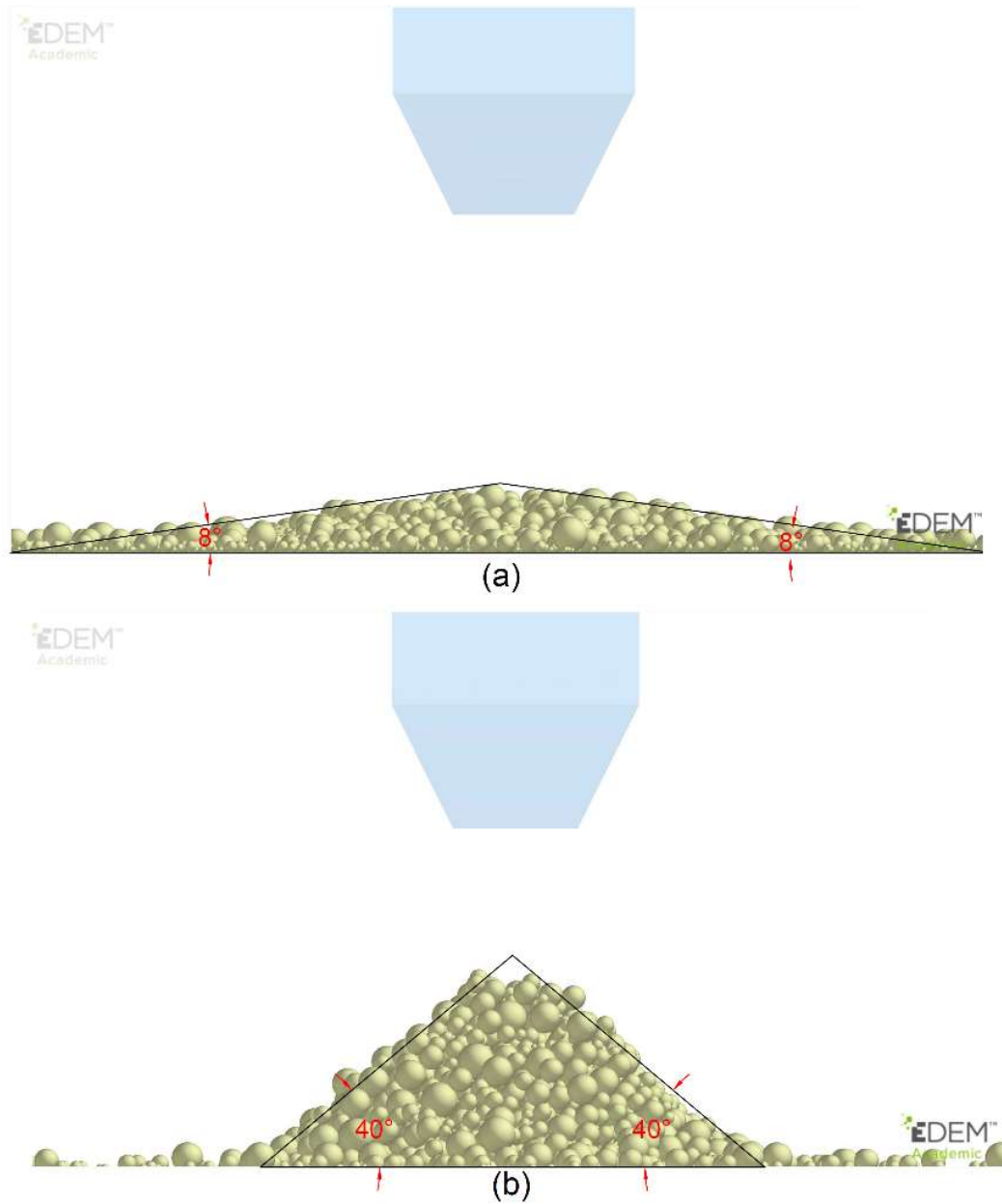
Figure 48: Measured angle of repose for (a) spheres with zero value of coefficient of rolling friction and (b) spheres with 0.25 value.

5.2.2 Control Mode

Although EDEM software supports the use of displacement control mode, EDEM can be customized to support force control mode using Application Programming Interface (API) through C++ as discussed in section 4.3.4.

In this study, a subroutine program is developed to allow the use of force control mode in EDEM through EDEM API; based on a developed set of equations (4.3.4.2) and program algorithm (4.3.4.3). The validation exercise aims to show the concepts of using force control in EDEM software using the API through C++ language as described in section 4.3.4.1. Different C++ codes are written and customized to represent the different input loading application types to be used in EDEM as shown in Appendix. The developed set of equations are described in section 4.3.4.2. The C++ code algorithm is discussed in section 4.3.4.3.

There are three predefined types of loading applications used in this study. Those loadings represent the predefined input force (F^i). Constant loading, sinusoidal loading and more realistic simulated train loading utilizing BOEF theory. The constant loading is required and used in the preloading stage as described in section 4.3.5 . The other two types of loading are used to study the influence of simulated train loading on behavior of railroad ballast using DEM as described in section 4.3.6. The three loading types used in this exercise are for validation purpose only.

In this exercise, the plate starts moving downward based on displacement control mode until it is in contacts with the particles; where the plate starts to move based on force control. The movement of the plate is based on force control mode using EDEM API. The validation of this code is done by validating equation 4.17. In other words, the sum of the inertial force (ma) and predefined input force (F^i) equals to the response contact force (F^c). The predefined input force (F^i) is known and the response

contact force (F^c) is obtained from the simulation using EDEM. The inertial force (ma) is calculated based on the difference of F^c and F^i. Then the inertial force is added to the predefined force (F^i) to compare the summation with the response contact force (F^c) and validate equation 4.17. The simulation time for this exercise is two seconds.

The results show good agreement between the summation of the inertial force and F^i with F^c as shown in Figure 49, Figure 50 and Figure 51 for constant loading, sinusoidal loading and simulated train loading respectively. For the sinusoidal loading type (Figure 50), two simulations with different frequencies are used to ensure the validity of the developed code for low and high loading frequency. Low frequency equals to 1 Hz and high frequency equals 20 Hz. As expected at high frequency inertial force of the geometry is more than at low frequency due to the dynamic effects (higher gematrical acceleration results to higher inertial force).

The increment of the total force on the sleeper bottom in the initial stage of the simulation for the all loading types is due to the transition from displacement control to force control mode; where in the displacement control the acceleration of the geometry is zero (inertial force of the geometry is zero) then it increases to a value at a small timestep. This increment causes the sudden increase in the total force; due to the significant contribution of the inertial force at that timestep.
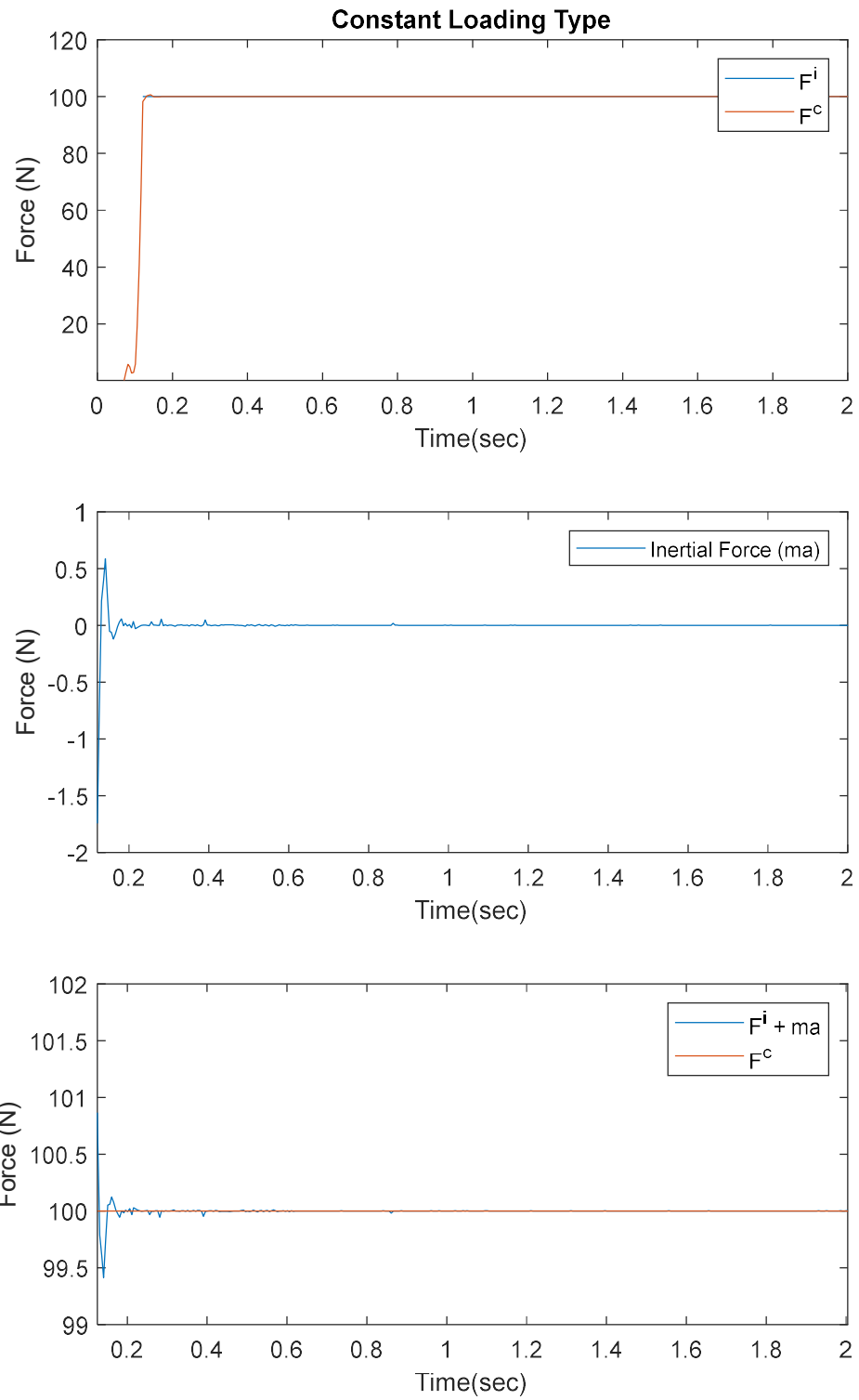
Figure 49: Validation of constant loading type.
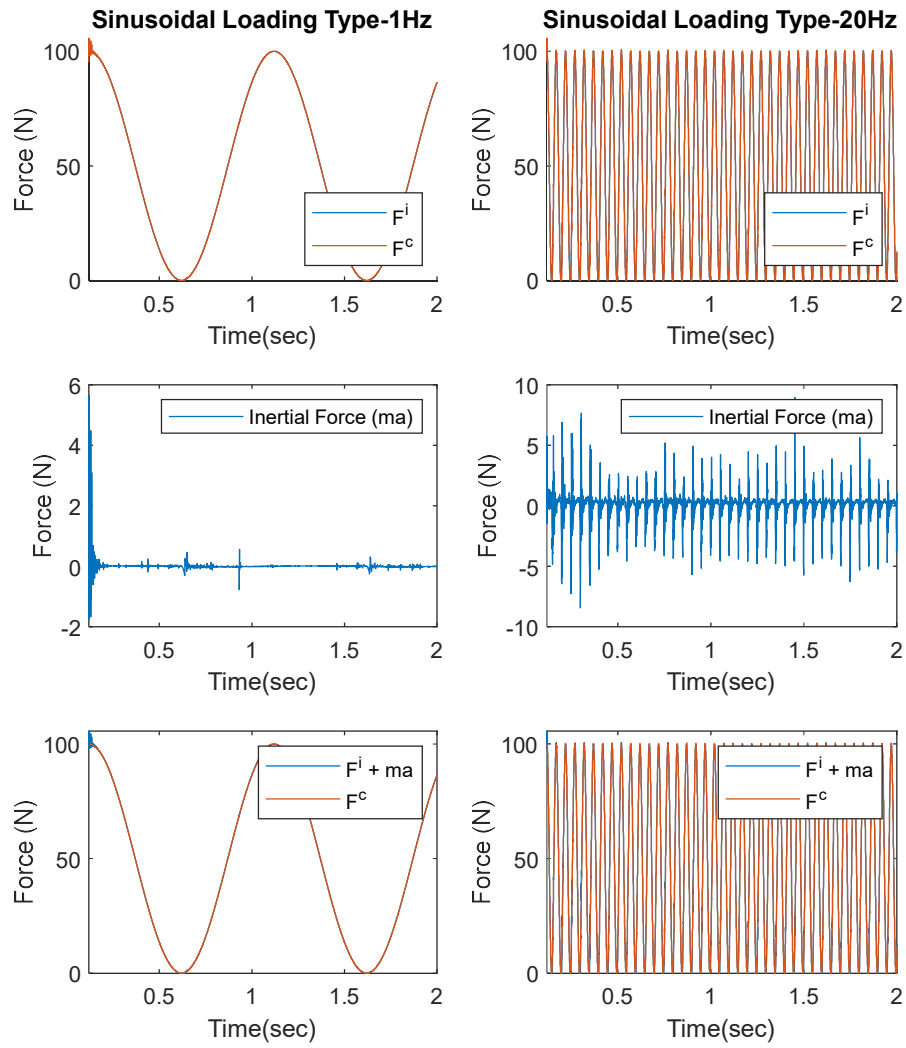
Figure 50: Validation of sinusoidal loading type.
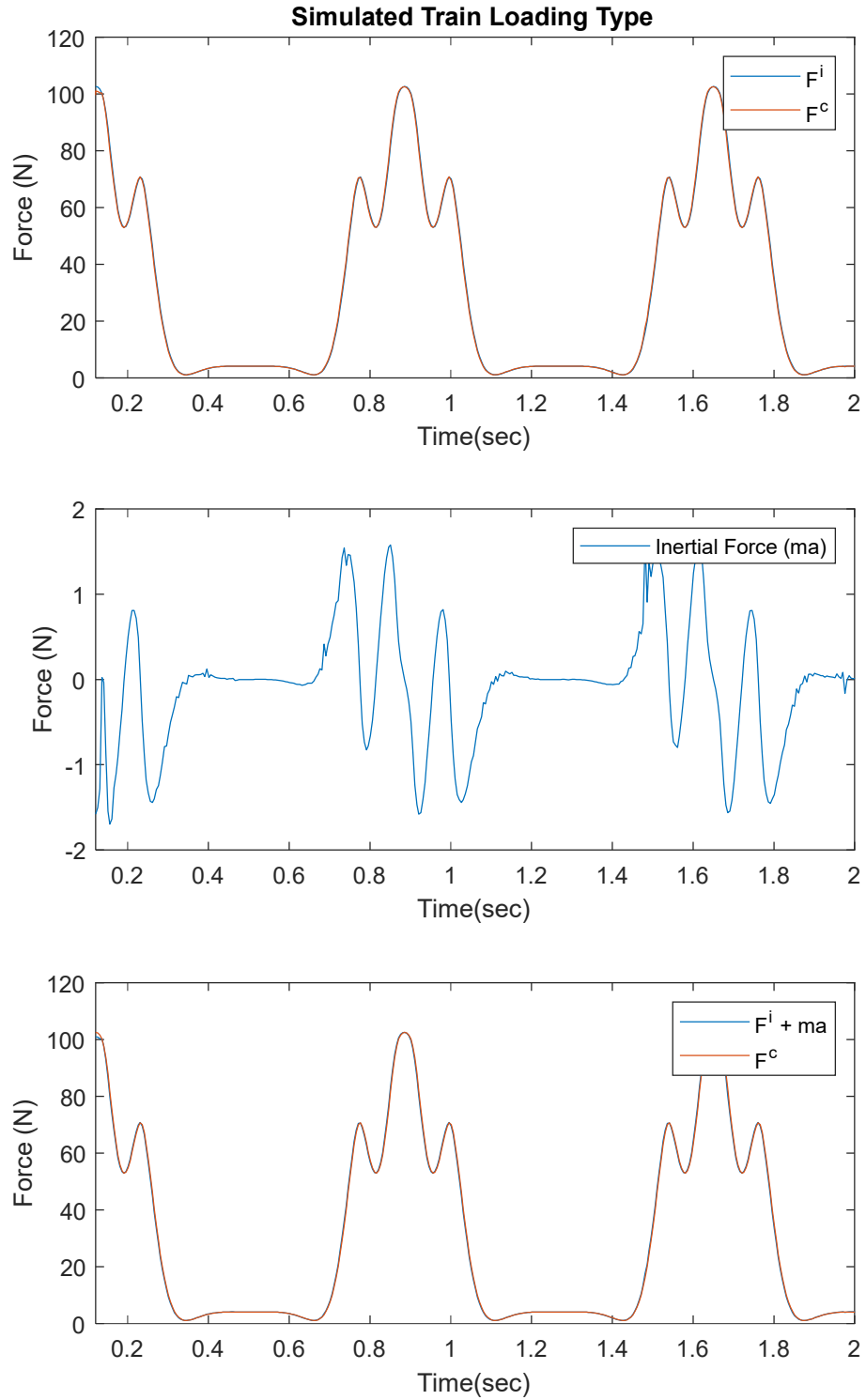
Figure 51: Validation of simulated train loading type.

5.2.3 Simulated Train Loading

In this study, two loading cases are used to investigate the influence of simulated train loading on railroad ballast using DEM (4.3.6). The loading cases are described in Table 15. Each loading case is described below in a particular section. As discussed previously in section 4.3.4, all the loading cases are applied in EDEM using the developed force control code mode through EDEM coupling via EDEM API.

Case 1 is the more realistic train loading simulated utilizing the Beam on Elastic Foundation (BOEF) theory as described in section 4.2. Case 2 is a sinusoid loading with a frequency calculated based on simulated train speed and axle spacing.

5.2.3.1 Simulation Time

Each loading case has a certain simulation time to complete 1000 loading cycles as shown in Figure 52. The simulation time is the estimated required time used in EDEM, to complete 1000 cycles for each loading case. A total of 281 seconds of simulation time is required to complete the simulations of the two loading cases. Each loading case is simulated to complete 1000 loading cycles. However, in the below sections the loading cases are shown for the first 2 seconds for illustration purpose.
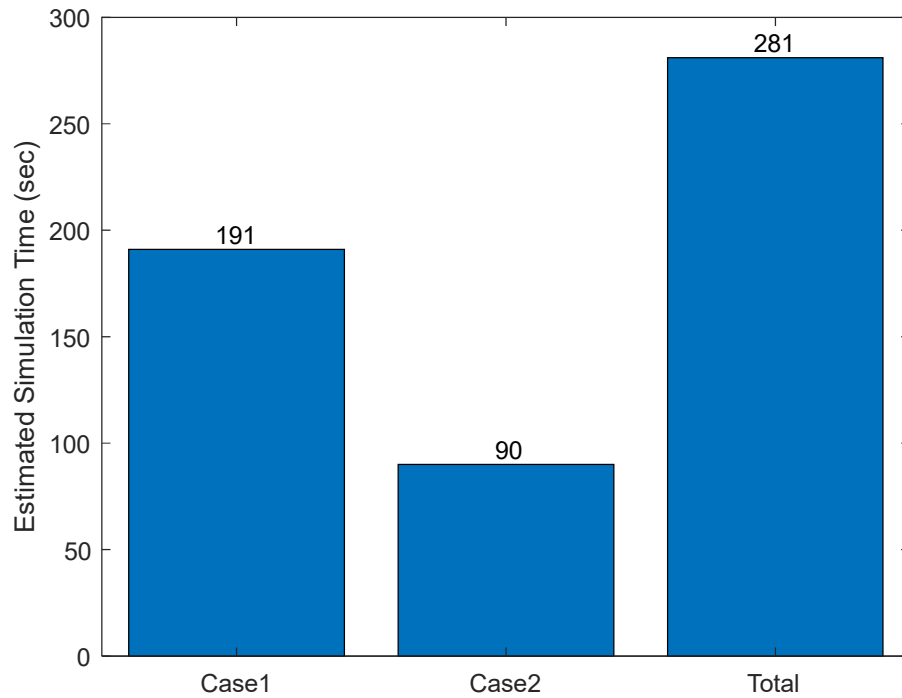
Figure 52: Required simulation time for each loading case to complete 1000 loading cycles.

5.2.3.2 Loading Cases

Case 1 is the more realistic train loading type simulated utilizing BOEF theory as discussed in section 4.2. Case 2 is a sinusoid loading type with a frequency based on the simulated train speed and most commonly used axle spacing (L_1) in the literature as described in section 4.3.6.1. For fair comparison purpose, the peak to peak amplitude of the sinusoidal loading case is taken from Case 1; where point A is the maximum loading point and B is the minimum loading point.

The simulated loadings for Case 1 and Case 2 are shown in Figure 53 and Figure 54 based on the parameters given in Table 17 and Table 18 respectively. Point A and

point B in Case 1 are used as a rang of the peak to peak amplitude for loading Case 2 for fair comparison purpose. Point C, represents the flying sleeper phenomenon due to the more realistic simulated train loading utilizing BOEF theory. Points A, B and C represent loading values equal to -5.40×10^4 N, -696.82 N and -2.21×10^3 N respectively
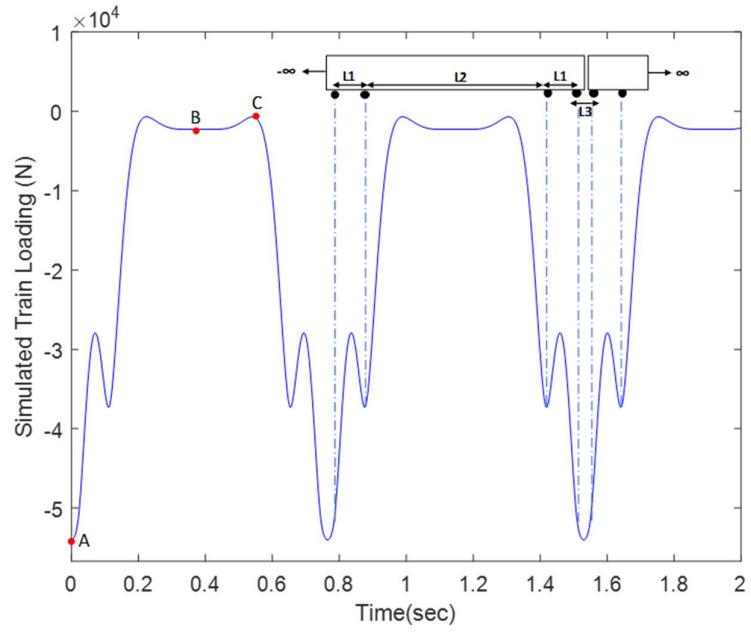
Figure 53: Case 1.
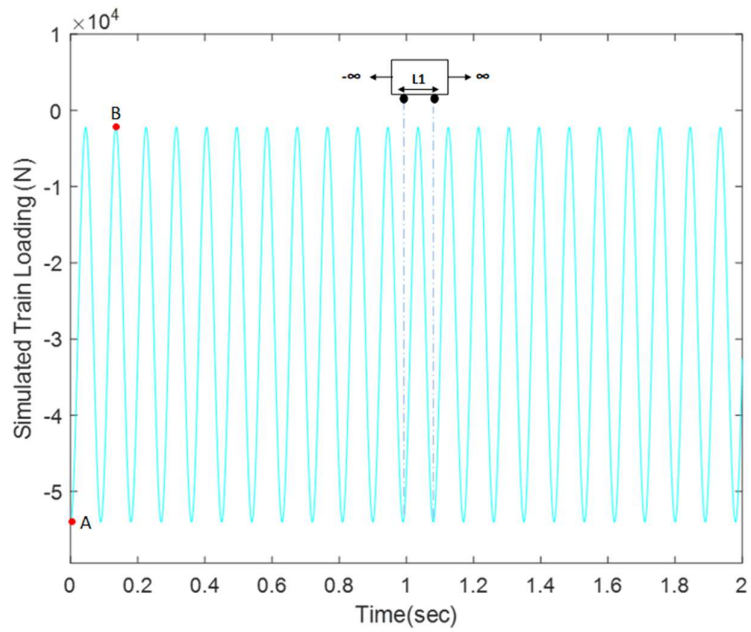
Figure 54: Case 2.

Table 17: Parameters Used to Simulate Loading Case 1

Used Parameter	Value
Rail Bending Stiffness (EI - $N.m^2$)	5×10^6
Rail Pad Stiffness (k_{pad} - N/m)	20×10^6
Wheel load (P - N)	73575 corresponds to 15 ton of axle load
Train Velocity (v- km/h)	100
L_1 (m)	2.5
L_2 (m)	15
L_3 (m)	1.25
x (m)	0.625

Table 18: Parameters Used to Simulate Loading Case 2

Used Parameter	Case 2
Train Velocity (v- km/h)	100
Maximum Loading Point (A-N)	5.4×10^4
Minimum Loading Point (B-N)	2.2×10^3
Frequency (f -Hz)	$f = \frac{v}{L_1} = 11.11$

5.3 Results and Discussion

Discrete Element Method is a powerful numerical tool in understanding the mechanical behavior of discontinuous material like railroad ballast. The main advantage of DEM is, its ability to visualize the macroscopic and microscopic behavior of railroad ballast. In this study, the DEM is used to simulate the mechanical behavior of railroad ballast under different simulated train loading cases using box test.

In this section, the mechanical behavior (macroscopic and microscopic) of railroad ballast under different simulated train loading cases are discussed and compared. Furthermore, the section highlights the influence of simulated train loading cases on the mechanical behavior of railroad ballast using DEM. Moreover, this section presents the computational time taken to complete the total simulations for two different loading cases.

The section is divided into three subsections; macroscopic behavior, microscopic behavior and computational time.

5.3.1 Macroscopic Behavior

In this subsection, the macroscopic behavior of railroad ballast under different simulated train loading is discussed and compared. The comparison is based on Case 1; where loading Case 1 is a more realistic train loading simulated utilizing BOEF (sections 4.2). The main parameter used for discussion and comparison of the macroscopic behavior of railroad ballast is ballast layer displacement. The influence of different simulated train loading cases for 1000 loading cycles on ballast displacement is discussed and compared.

To measure the displacement of ballast layer, it is not practical to take the average displacement of distinct ballast particles at each time step/cycle and compare the results; therefore, the displacement of ballast layer is measured and represented by the displacement of sleeper which can be obtained easily in EDEM.

5.3.1.1 Ballast layer Displacement

There are two simulated train loading cases used in this study; Case 1 and Case 2. Case 1 is a more realistic simulated train loading, simulated utilizing the BOEF theory. Case 2 is a sinusoidal loading with a frequency based on the simulated train speed and axle spacing of L_1, frequently used in the literature. The Absolute

Displacement (AD) of ballast layer under both loading cases for1000 loading cycles is shown in Figure 55.

The AD versus the number of loading cycles is used to compare the results between the two loading cases; and to investigate the influence of simulated train loading on ballast mechanical behavior using DEM as shown in Figure 55. The AD of the sleeper is taken at each cycle for each loading case. The AD for the two loading cases has the same increasing trend relative to cycle number as shown in Figure 55. The AD of ballast layer increases with the number of loading cycles for both loading cases. This trend agrees with the literature [17, 35, 118, 139, 213, 214].

At the initial 10 loading cycles for both cases, the ballast layer displaced rapidly with a high rate of change as shown in Figure 56 (a) ; while at the last 10 loading cycles ballast displaced gradually as shown in Figure 56 (b). At the initial stage, the rapid ballast layer displacement occurs due to the initial particle rearrangement. However, the gradual settlement of ballast layer at the last stage of loading is due to the ballast layer densification. This agrees with the experimental observation of Ngo et al.[17] that ballast layer under cyclic loading undergoes three stages. Initial rapid displacement, gradual displacement and stabilization. The stabilization stage is not observed in this simulation due to the low number of applied loading cycles.

Therefore, ballast layer compaction is required to reduce the initial displacement. In the field, ballast layer undergoes a compaction process before traffic operations to reduce this type of displacement. The compaction process is done by different methods like natural stabilization (number of train passes at a slower speed of traffic trains), dynamic stabilization (application of vertical load with lateral vibration of rails using specialized equipment) or crib compaction (vertical vibration of compactor plates placed at crib and shoulder of ballast with application of vertical load

using specialized equipment) for new ballast [215]. For old ballast, compaction is done during ballast maintenance by tamping or stone blowing processes using vibratory tines.
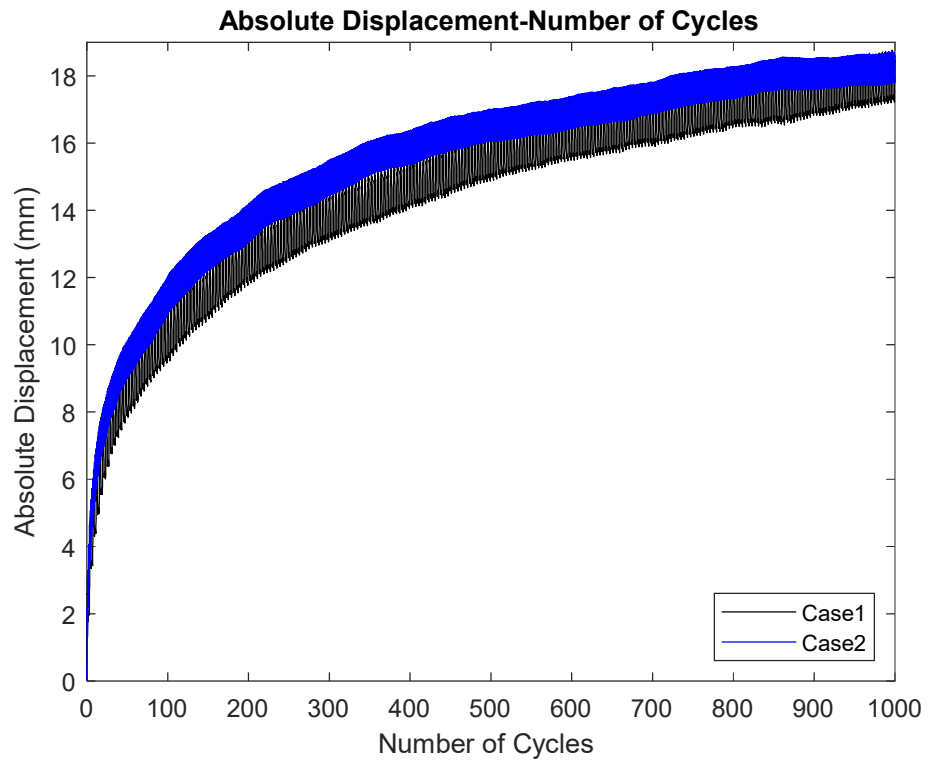
Figure 55: Absolute displacement of ballast layer versus loading cycles for the two loading cases.
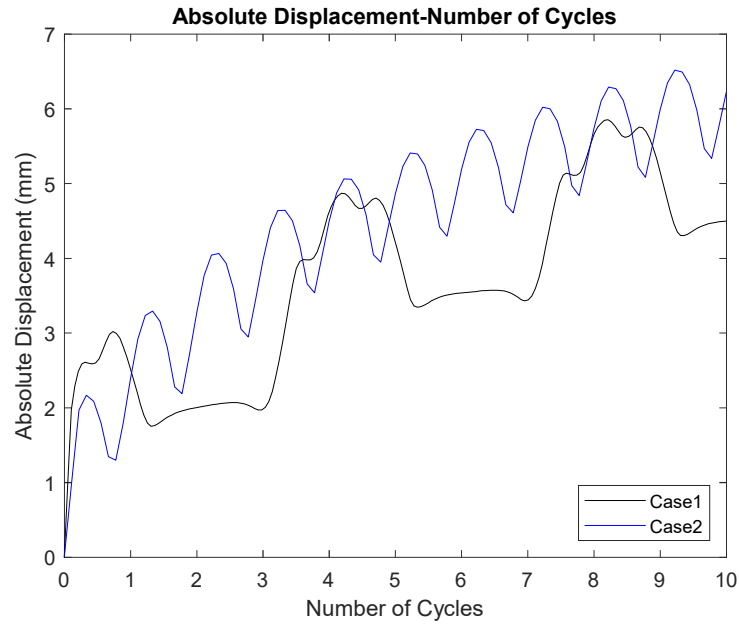
(a)
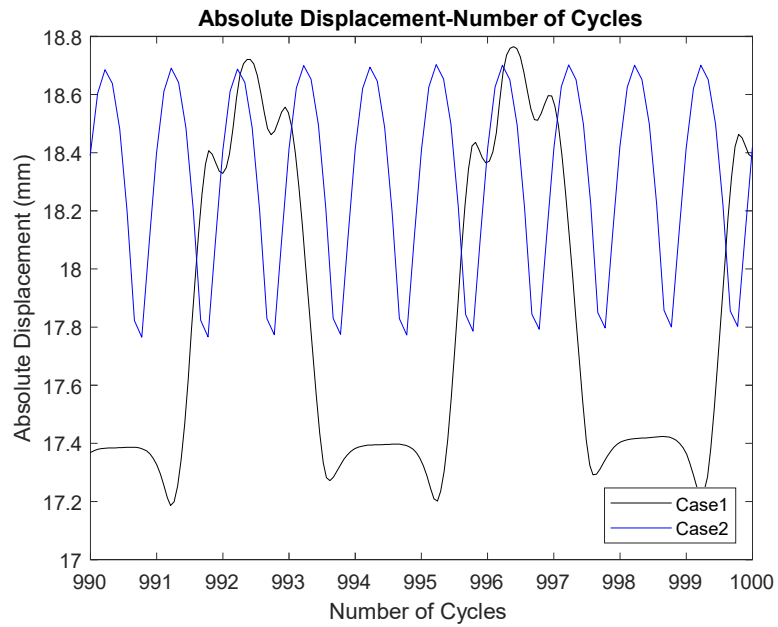
(b)

Figure 56: Absolute displacement of ballast layer at the (a) first 10 cycles and (b) last 10 cycles for the both cases.

For better representation and comparison between the results shown in Figure 55, the least square fitting method is used. The logarithmic function type is used to represent the AD of both loading cases with a close R^2 value to 1. The best fit logarithmic representation and equations of AD for both loading cases are indicated and showed in Figure 57 and Table 19 respectively.

As shown in Figure 57, the two loading cases result in a different AD of ballast layer. The highest values of AD of ballast layer in this study are 17.52 mm and 18.4 mm for Case 1 and 2 respectively. Loading Case 2 results in a higher displacement of ballast layer compared to loading Case 1. This can be explained due to the high frequency associated with loading Case 2 that introduces dynamic effects to the system, besides, the continuous full loading and unloading during the simulation; unlike Case 1 where there is a partial loading and unloading as well as some rest periods due to the different axle spacings of the simulated train. The dynamic effects from Case 2 do not only affect the macroscopic behavior of railroad ballast, they affect also the microscopic behavior of railroad ballast from a particle scale as will be discussed in the next sub section.

To have an idea about the agreement of the results from this study to the literature, the maximum AD of ballast layer from this study is compared to other studies in the literature. However, there are different study parameters used in the literature compared to this study e.g. study type, loading type and loading range. Therefore, the maximum AD of ballast layer form other studies from the literature that have a close study parameters to this study, are used for a comparison purpose. Ballast displacement in this study has good agreement with the literature as shown in Table 20.

The rate of change of the AD is not uniform for both loading cases. Both loading cases have almost a steep slope in the first 50 loading cycles due to the rapid initial

displacement of the ballast particles. Then, the slop of each loading case after the 50th cycle drops gradually; where rearrangement of ballast aggregates occurred at this stage. This agrees with the experimental observation of Ngo et al. [17].
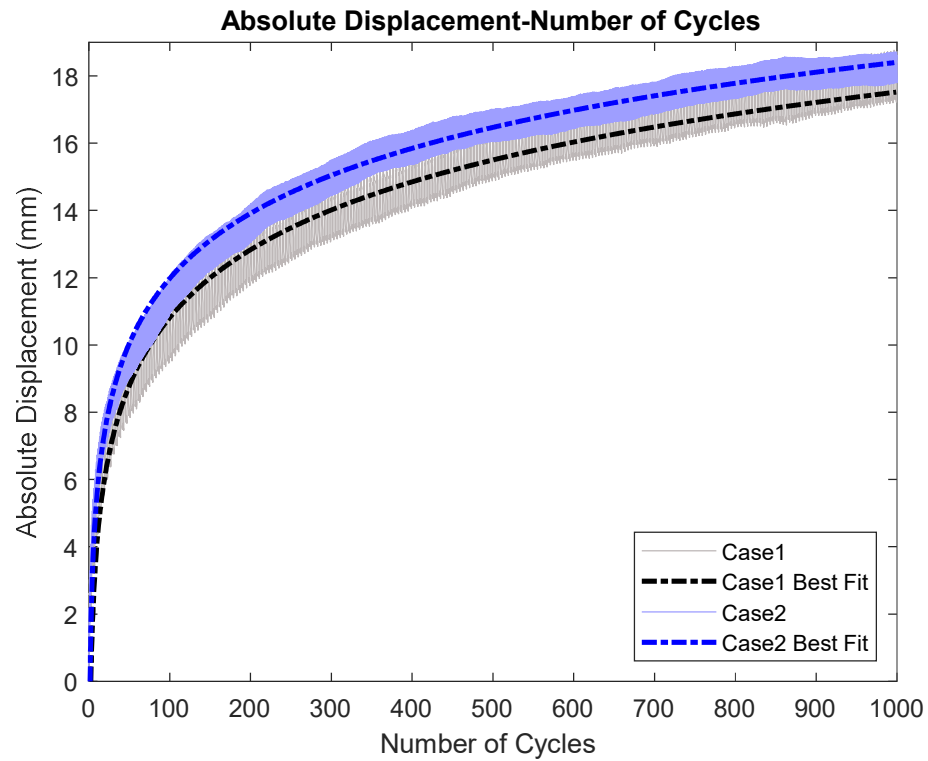
Figure 57: Best fit of the absolute ballast displacement versus cycle number for Case 1 and Case 2.

Table 19: Best Fit Equations and R^2 Values of the Absolute Maximum Ballast Displacement Versus Cycle Number for Each Loading Case

Case	Best Fit Equation	R^2 value
1	y = 2.9141 ln(x) - 2.6087	0.94
2	y = 2.7911 ln(x) - 0.8752	0.97

Table 20: Maximum Absolute Ballast Vertical Displacement Results from the Literature

Test	Study Type	Loading Type	Loading Range and Frequency	Maximum Absolute Ballast Vertical Displacement	Corresponding Loading Cycle Number	Reference
Box Test	Numerical using DEM	Loading cases (4.3.6)	[2.2-54] kN 11.11 Hz (4.3.6 & 5.2.3)	17.52 & 18.4 mm	1000	This Study
Box Test	Experimental	Sinusoidal	[3-40] kN 3 Hz	≈20 mm	1000	[35]
Box Test	Experimental	Sinusoidal	[3-40] kN 3 Hz	20 mm	1000	[213]
Track- Three Sleepers	Numerical using DEM	Simulated train loading	[0-14] kN	≈13-16 mm	1000	[174]
Box Test	Experimental	Sinusoidal	[3-10,20,30 and 40] kN 3 Hz	≈15-23 mm	1000	[214]
Box Test	Numerical using DEM	Sinusoidal	[0-202] kN 15 Hz	≈12-16 mm	1000	[17]

The percentage error of AD at each loading cycle is calculated, to compare the results of the sinusoidal loading case (Case 2) with the more realistic simulated train loading (Case1) as shown in Figure 58.

The calculation of percentage error of AD is based on the below equation:

$$PE_N = \frac{C_N^2 - C_N^1}{C_N^1} \times 100 \qquad (5.1)$$

where, PE_N is the percentage error at N which is the cycle number, C_N^2 is the value of the best fit of AD for Case 2 at the Nth cycle number and C_N^1 is the value of the best fit of AD for Case 1 at the Nth cycle number.

The simulated train loading type used in DEM of railroad ballast influences the mechanical behavior of railroad ballast. The maximum difference occurs at the initial stage of loading due to the high initial rapid displacement of ballast particles resulting from the dynamic effects associated to sinusoidal loading ; where a maximum difference of up to almost 14% is shown between the simulated train and sinusoidal loadings as indicated in Figure 58. The percentage error decreases with the loading cycle number to reach a minimum difference of almost 5% at the 1000th loading cycle. This due to the gradual displacement of ballast particles which resulted from the particles rearrangement and densification.
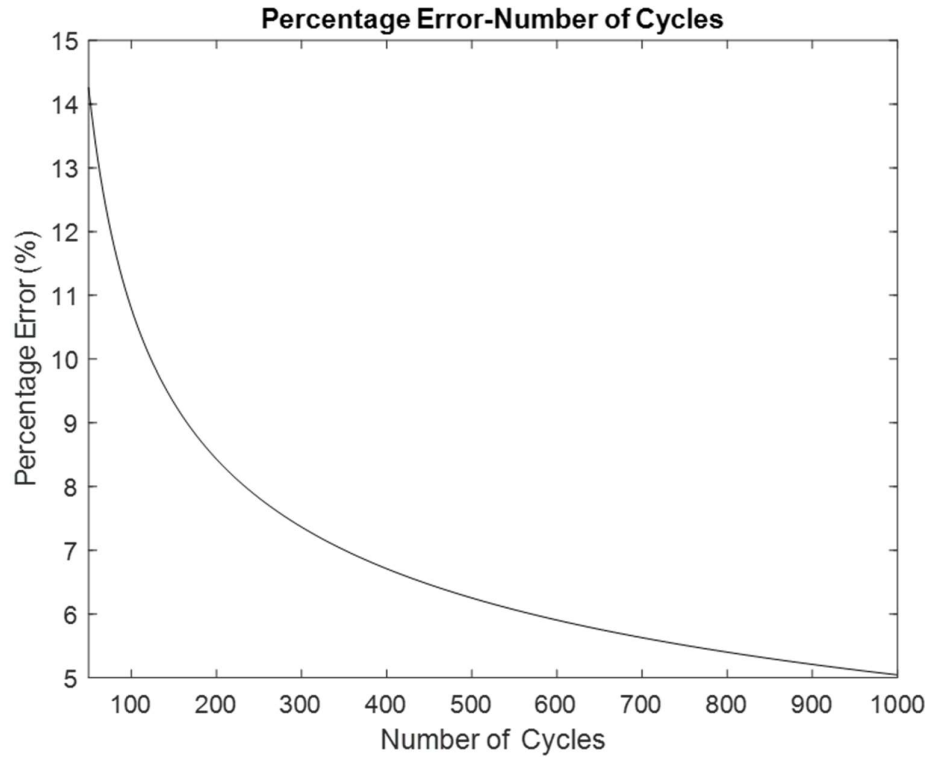
Figure 58: Percentage error between best fit functions of the AD of ballast resulted from the two loading cases.

5.3.2 Microscopic Behavior

Discrete Element Method is a powerful numerical tool in understanding the microscopic mechanical behavior of granular material like railroad ballast. It accounts for the discontinuity property of railroad ballast. The key advantage of DEM is that it provides a comprehensive insight to the velocity, displacement and force of distinct particle during the simulation unlike other modeling methods.

In this subsection, the microscopic mechanical behavior of railroad ballast under two loading cases is highlighted and discussed. Furthermore, this subsection

emphasized on the significance of DEM to understand and visualize the microscopic behavior of railroad ballast from a particle scale.

5.3.2.1 Particles' Velocities

The distribution of particles' velocities under the minimum and maximum loads at the 1000th cycle are shown in Figure 59 and Figure 60 for Case 1 and Case 2 respectively.

For all the cases, at the minimum load the particles' velocities are less than at the maximum load of the 1000th cycle. Moreover, particles velocities under the sleeper is higher than particles far way the sleeper. The particles velocities decrease as going down away from the sleeper bottom.

The different values of particle velocities for both loading cases highlight the influence of simulated train loading on the mechanical behavior of railroad ballast. The sinusoidal loading case (Case 2) results in a higher particle velocity at the maximum and minimum loads of the 1000th loading cycle compared to Case 1 as shown in Figure 61 ; due to the dynamic effects from Case 2.
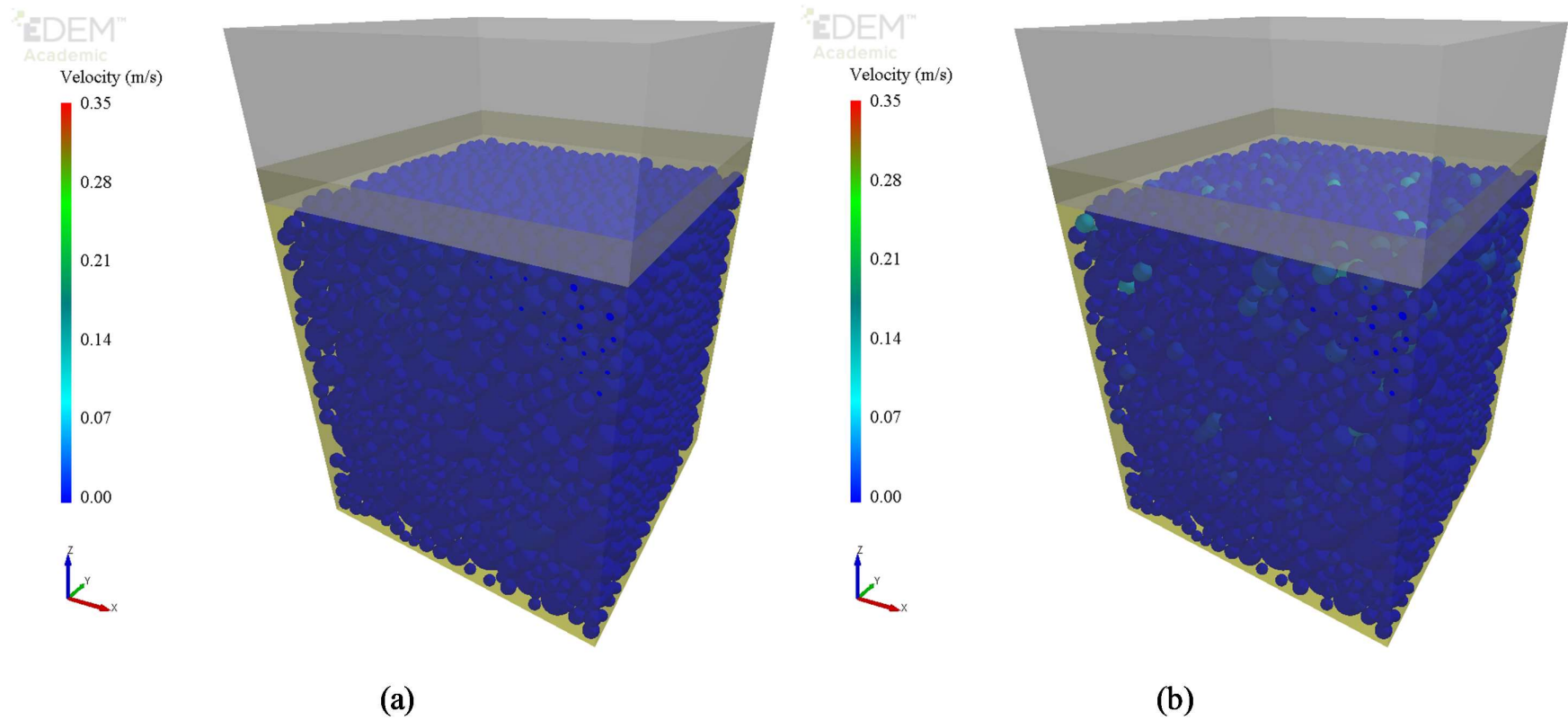
Figure 59: Particles velocities at the 1000th cycle for (a) minimum and (b) maximum loads of Case 1.
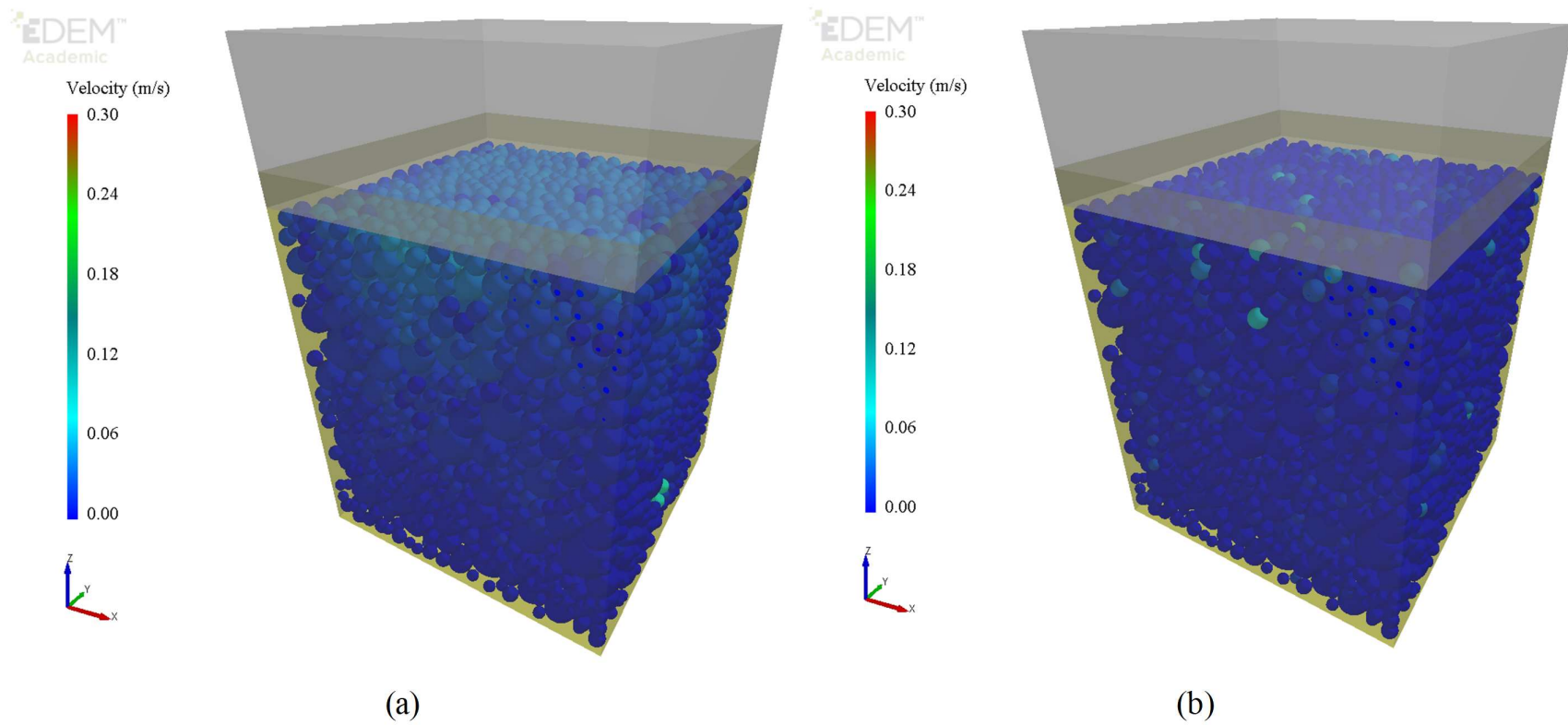
Figure 60: Particles velocities at the 1000th cycle for (a) minimum and (b) maximum loads of Case 2.
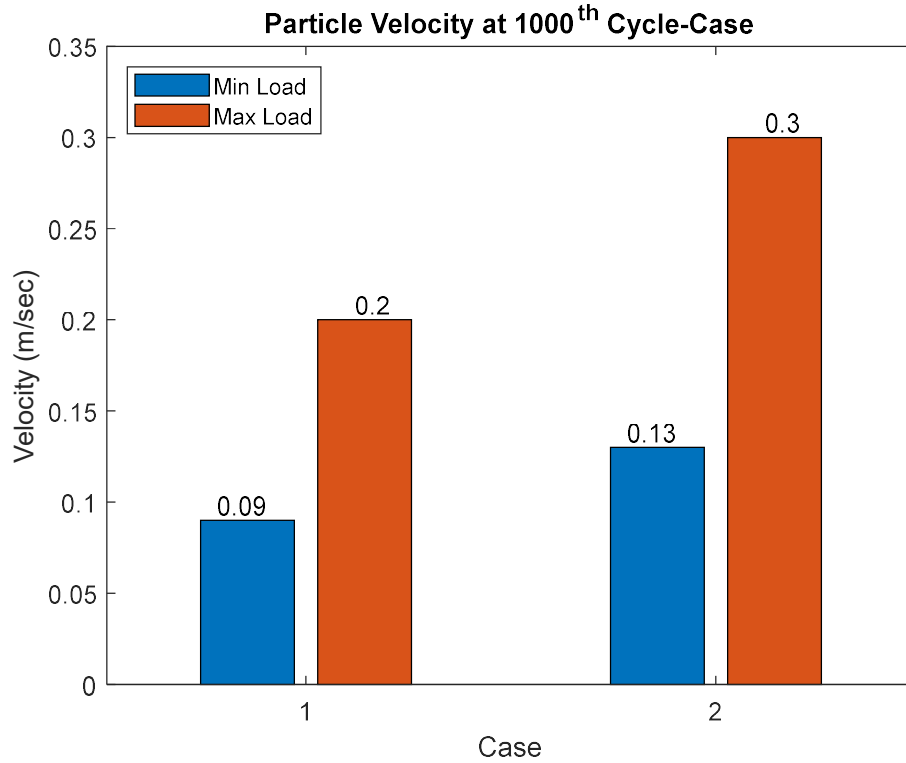
Figure 61: Maximum particle velocity for each loading case at the minimum and maximum loading of the 1000th cycle.

5.3.2.2 Particles' Displacements

The particles' displacements at the minimum and maximum loads of the 1000th cycle are depicted in Figure 62 and Figure 63 for Case 1 and Case 2 respectively. Particle displacement is represented by a vector. The direction of the vector represents the direction of the particle displacement.

For all the cases, at the maximum load, particles move downward and at the minimum load particles tend to move upwards. This can be clearly observed for loading

Case 2 (Figure 63); due to the high loading frequency that introduces dynamic effects to the system. This trend of particle movement agrees with the literature [80, 118].
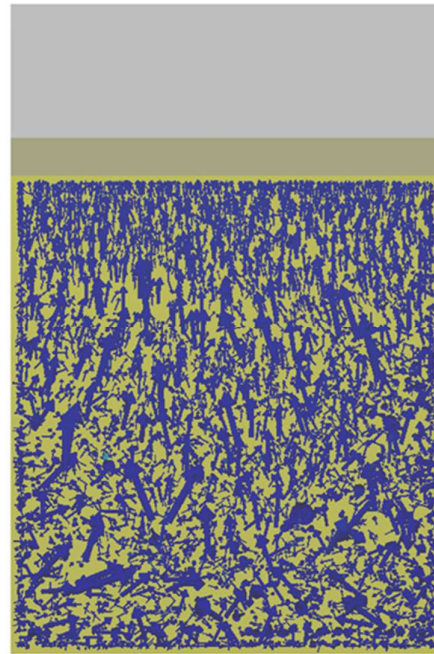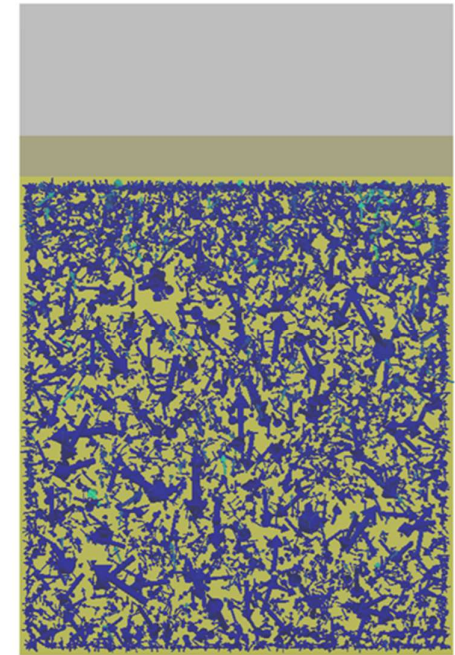
Figure 62: Particles displacements at the 1000th cycle for (a) minimum and (b) maximum loads of Case 1.
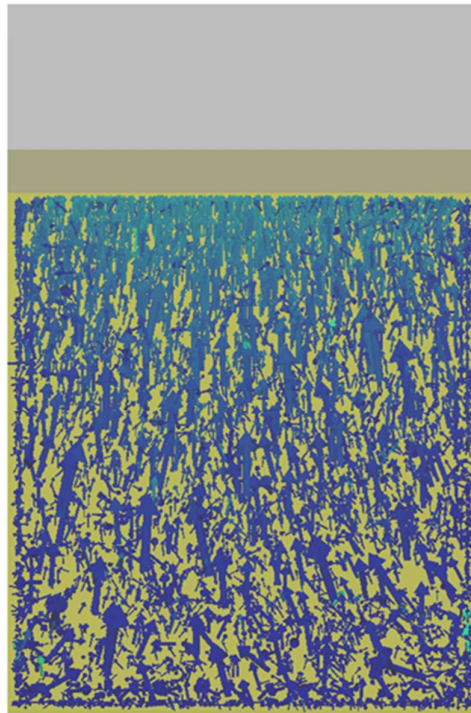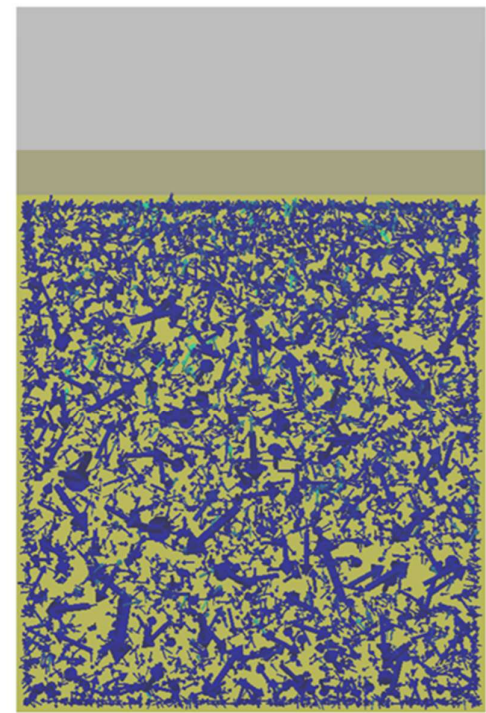
Figure 63: Particles displacements at the 1000th cycle for (a) minimum and (b) maximum loads of Case 2.

5.3.2.3 Particles' Forces

Particles' forces can also be visualized by DEM. The distribution of particle force under the minimum and maximum loads at the 1000th cycle are shown in Figure 64 and Figure 65 for Case 1 and Case 2 respectively. The particle total force is defined as the magnitude of the resultant forces on a distinct particle.

For all the cases, at the minimum load the particles forces are less than at the maximum load of the 1000th cycle. Moreover, particles forces under the sleeper are higher than particles far away from the sleeper. This trend agrees with the literature [80, 118].

The particle force at the maximum and minimum loads of the 1000th for Case 2 are higher than those Case 1 as shown in Figure 66. This is due to the dynamic effects from Case 2.
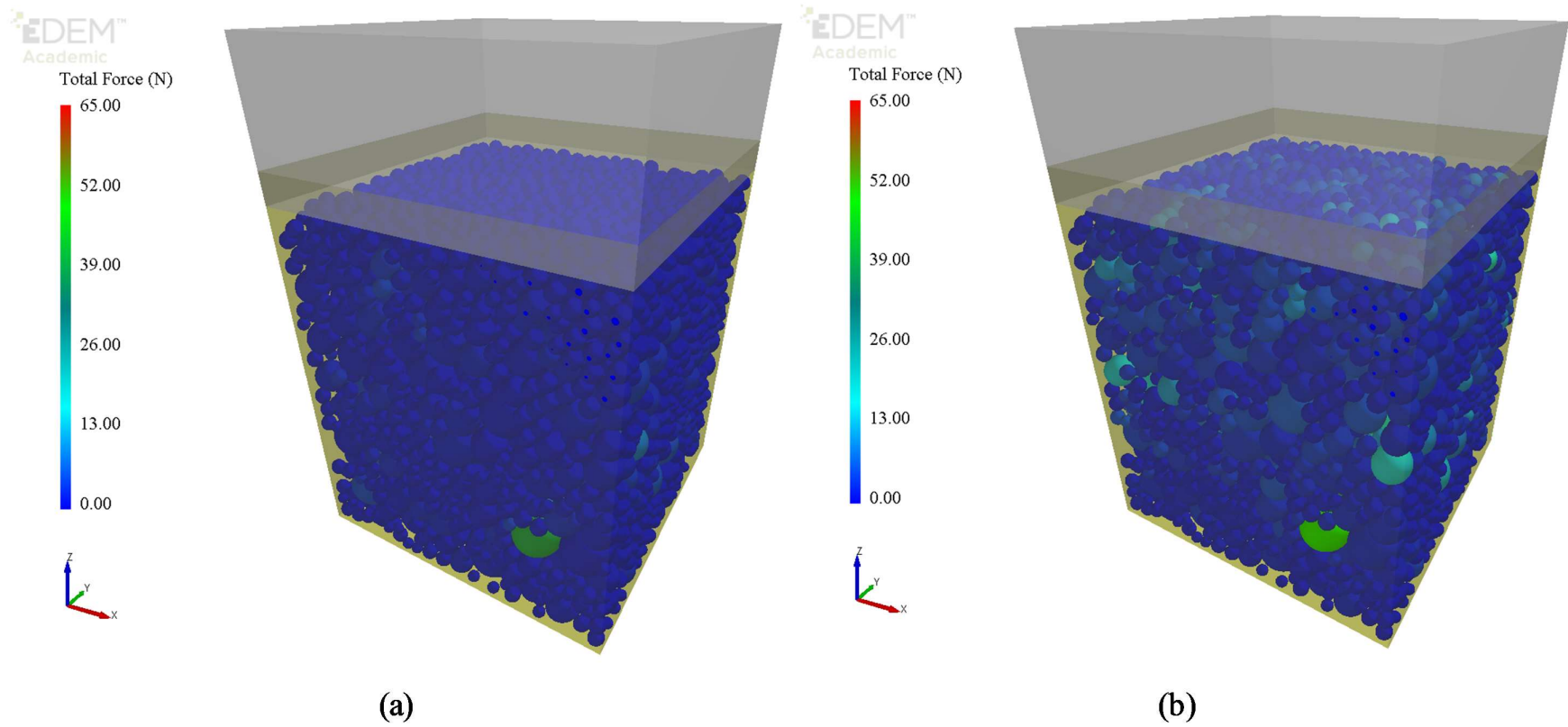
Figure 64: Particles forces at the 1000th cycle for (a) minimum and (b) maximum loads of Case 1.
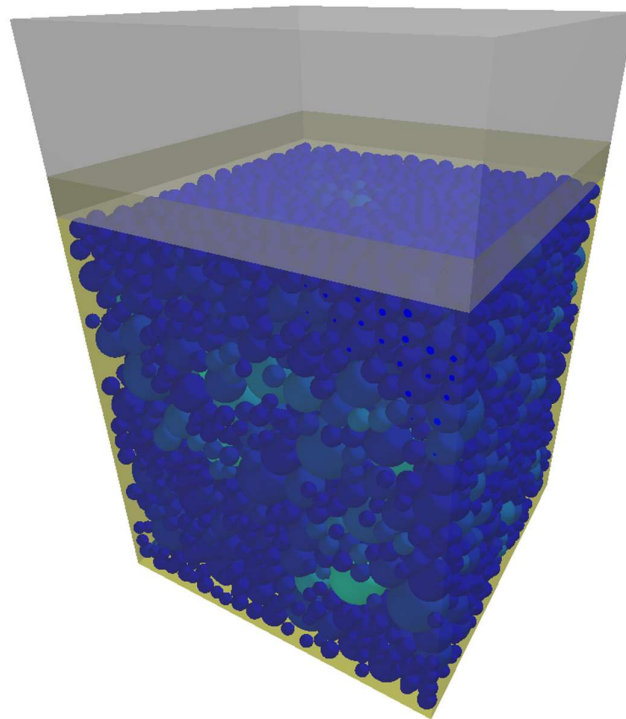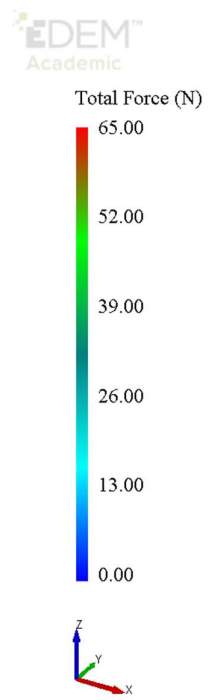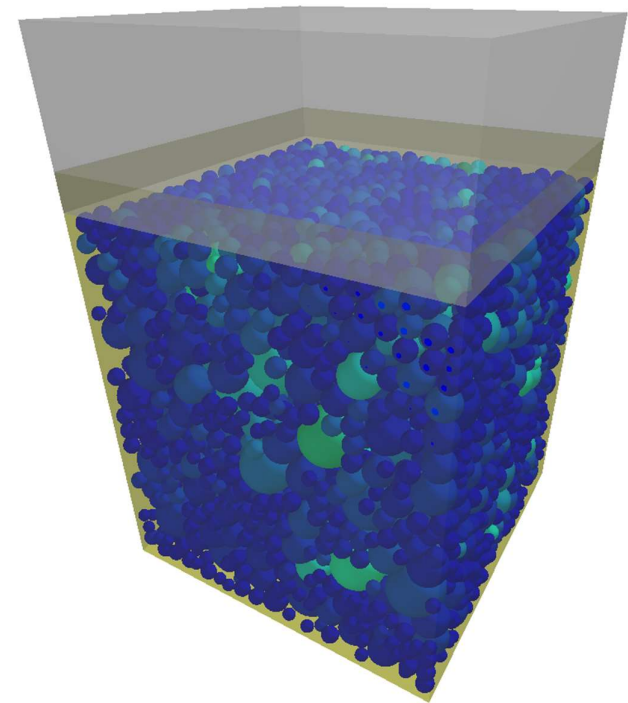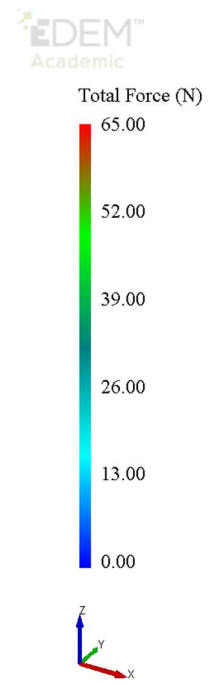
Figure 65: Particles forces at the 1000th cycle for (a) minimum and (b) maximum loads of Case 2.

Particle Force at 1000th Cycle-Case
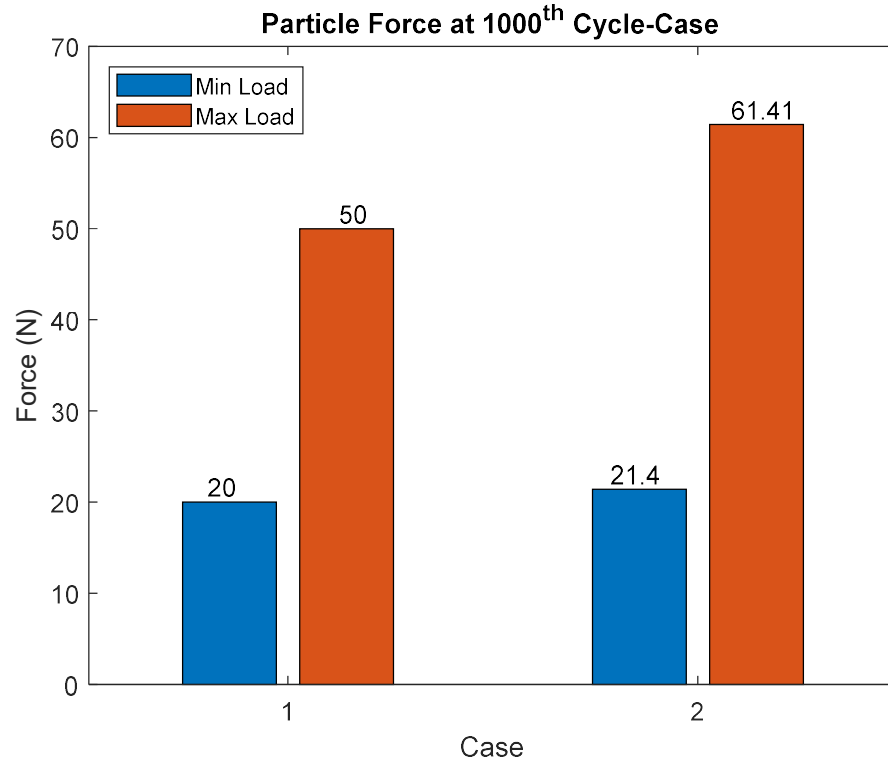
Figure 66: Maximum particle force for each loading case at the minimum and maximum loading of the 1000th cycle.

5.3.3 Computational Time

The computational time is defined as the processing time (actual time) taken to complete the simulation. The estimated computational time taken for each loading case to complete 1000 loading cycles are shown in Figure 67. The used computer in this study can simulate about 41 seconds of the simulation time (5.2.3.1) per day.
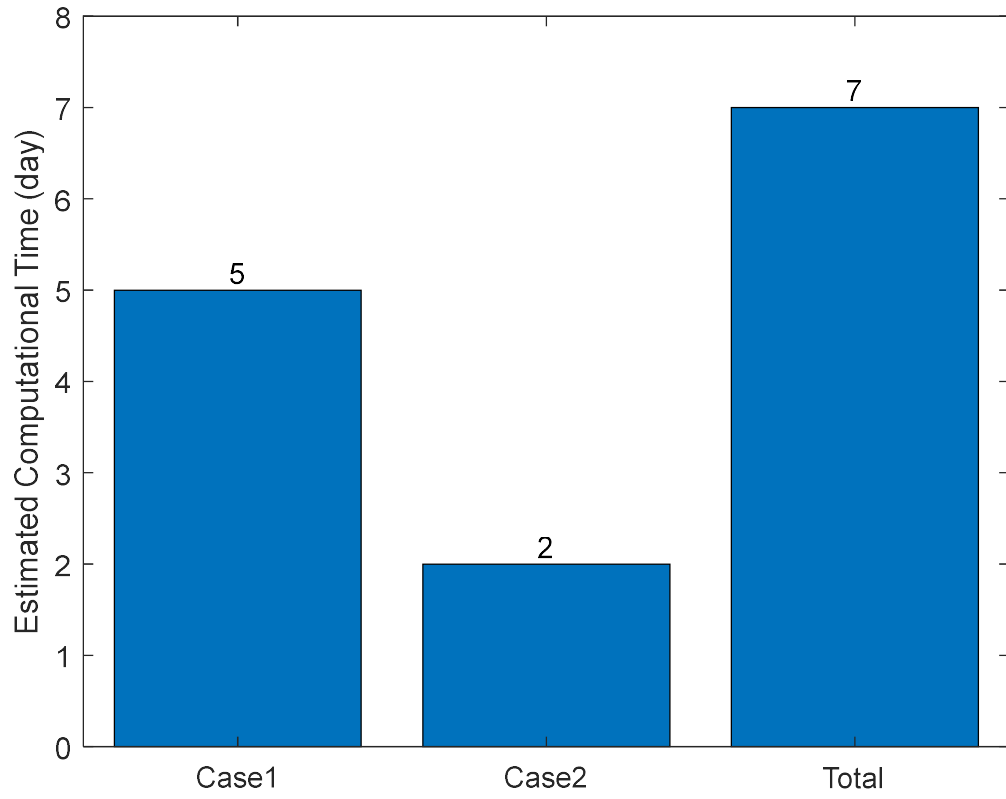
Figure 67: Estimated computational time for both loading cases.

CHAPTER 6: CONCLUSION AND RECOMMENDATIONS FOR FUTURE

WORK

Ballasted railway tracks have been used intensively around the world. Ballast is the key component of a ballasted track. Ballast layer deforms and degrades under repetitive traffic loading. Ballast layer requires periodical maintenance. Ballast maintenance is an expensive activity. Therefore, the research about understanding ballast mechanical behavior has been increased for better ballast layer design and efficient periodical maintenance.

In this work, Discrete Element Method (DEM) is used to model the behavior of railroad ballast. Modeling the entire track using DEM is computationally expensive. A box portion (box test) of the track is simulated.

DEM is a powerful tool to visualize and understand both the macroscopic and microscopic behavior of railroad ballast. It provides a comprehensive insight to the discontinuous material from particle scale. For instance, particle velocity, displacement and force. However, its main limitation is the computational time.

In this study, the bulk calibration method using angle of repose test is used; to ensure the accurate representation of ballast material used in DEM. Furthermore, to show the validity of representing ballast irregular particle shape as sphere with coefficient of rolling resistance. The obtained angle of repose is 40 degrees which is the typical value for railroad ballast. This ensures the validity of railroad material properties used in this work.

It is essential to use in DEM a simulated train loading that represents the real case scenario. The simulated train loading should represent the train loading.

From the literature, researchers used DEM to model railroad ballast behavior under pure continuous sinusoidal loading through box test. Train consists of number of

cars. Each car has a number of axles with different spacing. Each axle applies a load on the track substructure. The train loading is not a pure continuous sinusoidal loading. The train loading depends on train weight, car length, axle number and axle spacing.

This study aims to understand the mechanical behavior of railroad ballast under different simulated train loadings using DEM. Moreover, to investigate the influence of different simulated train loadings on the mechanical behavior of railroad ballast using DEM. EDEM software by DEM Solutions is used for the analysis. MATLAB is used for loading cases analysis. EDEM software is a useful tool to be used for DEM analysis. EDEM can be customized to support force control mode using Application Programming Interface (API) through C++. The EDEM API is an additional interface used in EDEM to allow users for any further customizations. A set of equations and program algorithm are defined to make EDEM work using force control. A Different C++ codes are written and customized to represent the different input simulated loading cases to be used in EDEM.

In this work, there are two simulated train loading cases. Case 1 is the train loading simulated utilizing Beam on Elastic Foundation (BOEF) theory to simulate a more realistic train loading. Case 2 is a sinusoidal loading with a frequency based on the commonly used axle spacing (L_1) in the literature and train speed of the simulated train. The results from the more realistic simulated train loading utilizing BOEF theory are compared with those from sinusoidal loading.

The simulated train loading type influences the mechanical behavior of railroad ballast where a maximum difference of up to almost 14% in the absolute displacement of the ballast layer is shown between the simulated train and sinusoidal loading.

Further investigations are required to account for large numbers of loading cycles (long-term behavior); dynamic loading associated to high train speed, wheels

and track irregularities; particle breakage (permanent deformation); and the actual scenario of train loading (finite train with rest periods). It is recommended to develop new numerical schemes that require low computational time compared to DEM; to model the long-term behavior of railroad ballast for a larger model scale (ballasted track consisting of a number of sleepers). Further research work is needed to study the influence of simulated train loading cases on the mechanical behavior of railroad ballast using large scale experimental testing.

REFERENCES

1. Givoni, M., C. Brand, and P. Watkiss, *Are railways 'climate friendly'?* Built Environment, 2009. **35**(1): p. 70-86.

2. Givoni, M., *Environmental benefits from mode substitution: Comparison of the environmental impact from aircraft and high-speed train operations.* International Journal of Sustainable Transportation, 2007. **1**(4): p. 209-230.

3. Song, M., et al., *Railway transportation and environmental efficiency in China.* Transportation Research Part D: Transport and Environment, 2016. **48**: p. 488-498.

4. Savolainen, V.V. and O.P. Hilmola, *The relative technical efficiency of European transportation systems concerning air transport and railways.* International Journal of Business Performance Management, 2009. **11**(1-2): p. 19-42.

5. Gautier, P.E., *Slab track: Review of existing systems and optimization potentials including very high speed.* Construction and Building Materials, 2015. **92**: p. 9-15.

6. Blanco-Lorenzo, J., et al., *Dynamic comparison of different types of slab track and ballasted track using a flexible track model.* Proceedings of the Institution of Mechanical Engineers, Part F: Journal of Rail and Rapid Transit, 2011. **225**(6): p. 574-592.

7. Esveld, C., *Modern Railway Track*. 2001, Zaltbommel MRT Press.

8. Li, D., et al., *Railway geotechnics*. 2015, London: CRC Press.

9. Selig, E.T. and J.M. Waters, *Track geotechnology and substructure management*. 1994: Thomas Telford.

10. Indraratna, B., D. Ionescu, and H.D. Christie, *Shear behavior of railway ballast based on large-scale triaxial tests.* Journal of geotechnical and geoenvironmental Engineering, 1998. **124**(5): p. 439-449.

11. Sañudo, R., et al., *Track transitions in railways: A review.* Construction and Building Materials, 2016. **112**: p. 140-157.

12. *Geological Map of Qatar*. 2010, Environmental Information Center, The Ministry of Environment: Doha, Qatar.

13. EDEM, *EDEM version 4.2.0.* 2018, DEM Solutions: Edinburgh, United Kingdom.

14. Studio, M.V., *Microsoft Visual Studio version 15.7.4*. 2017, Microsoft Corporation.

15. MATLAB, *Matlab version 8.1.0.604*. 2013, The MathWorks Inc.: Natick, Massachusetts, USA.

16. Mahmoud, E., A.T. Papagiannakis, and D. Renteria. *Discrete Element Analysis of Railway Ballast under Cycling Loading*. in *Procedia Engineering*. 2016.

17. Ngo, N.T., B. Indraratna, and C. Rujikiatkamjorn, *Modelling geogrid-reinforced railway ballast using the discrete element method.* Transportation Geotechnics, 2016. **8**: p. 86-102.

18. Sadeghi, J., J.A. Zakeri, and M.E.M. Najar, *Developing Track Ballast Characteristic Guideline In Order To Evaluate Its Performance.* International Journal of Railway, 2016. **9**(2): p. 27-35.

19. Watters, B.R., M.J. Klassen, and A.W. Clifton, *Evaluation of ballast materials using petrographic criteria*. 1987.

20. Johansson, E., Š. Lukschová, and K. Miškovský, *Petrographic characteristics of granitoid and gabbroid intrusive rocks as a tool for evaluation of mechanical*

properties. E. Johansen (2011): Technological properties of rock aggregates. PhD Thesis, Luleå University of Technology, Luleå, Sweden, 2011.

21.   Raymond, G.P., *Research on railroad ballast specification and evaluation.* Transportation Research Record, 1985. **1006**: p. 1-8.

22.   Indraratna, B., *1st Ralph Proctor Lecture of ISSMGE. Railroad performance with special reference to ballast and substructure characteristics.* Transportation Geotechnics, 2016. **7**: p. 74-114.

23.   Indraratna, B. and W. Salim, *Mechanics of ballasted rail tracks: a geotechnical perspective.* 2005: CRC Press.

24.   Selig, E.T. and C.J. Roner, *Effects of particle characteristics on behavior of granular material.* Transportation Research Record, 1987(1131).

25.   Raymond, G.P. and V.A. Diyaljee, *Railroad ballast sizing and grading.* Journal of Geotechnical and Geoenvironmental Engineering, 1979. **105**(ASCE 14556 Proceeding).

26.   Selig, E.T., *Ballast for heavy duty track*, in *Track Technology*. 1985, Thomas Telford Publishing. p. 245-252.

27.   Vallerga, B.A., et al., *Effect of shape, size, and surface roughness of aggregate particles on the strength of granular materials*, in *Road and Paving Materials*. 1957, ASTM International.

28.   Roner, C.J., *Some effects of shape, gradation and size on the performance of railroad ballast.* M. Sc. Degree project report, Report No. AAR85-324P, Department of Civil Engineering, University of Massachusetts, Amherst, Massachusetts, 1985.

29.   Holtz, W.G. and H.J. Gibbs, *Triaxial shear tests on pervious gravelly soils.* Journal of the Soil Mechanics and Foundations Division, 1956. **82**(1): p. 1-22.

30. Leps, T.M., *Review of shearing strength of rockfill.* Journal of Soil Mechanics & Foundations Div, 1970.

31. Chrismer, S. and E.T. Selig. *Computer model for ballast maintenance planning.*

32. Aikawa, A., *Dynamic characterisation of a ballast layer subject to traffic impact loads using three-dimensional sensing stones and a special sensing sleeper.* Construction and Building Materials, 2015. **92**: p. 23-30.

33. Lackenby, J., *Triaxial behaviour of ballast and the role of confining pressure under cyclic loading.* 2006.

34. Gerald, P. and J.B. Richard, *Performance of large-scale model single tie-ballast systems.* Transportation Research Record, 1987. **1134**: p. 7-14.

35. Lim, W.L., *Mechanics of railway ballast behaviour.* 2004, University of Nottingham.

36. Han, X. and E.T. Selig, *Effects of fouling on ballast settlement*, in *6th International Heavy Haul Railway Conference.* 1997, Spoornet: Capetown; South Africa. p. 257-268.

37. Ionescu, D., *Ballast Degradation and Measurement of Ballast Fouling.* 2004.

38. Feldman, F. and D. Nissen, *Alternative testing method for the measurement of ballast fouling: percentage void contamination.* CORE 2002: Cost efficient railways through engineering, 2002: p. 101.

39. Indraratna, B., S.S. Nimbalkar, and N. Tennakoon, *The behaviour of ballasted track foundations: track drainage and geosynthetic reinforcement*, in *GeoFlorida 2010: Advances in analysis, modeling & design.* 2010. p. 2378-2387.

40. Remennikov, A.M. and S. Kaewunruen, *A review of loading conditions for railway track structures due to train and track vertical interaction.* Structural control and Health monitoring, 2008. **15**(2): p. 207-234.

41. Frýba, L., *Dynamics of railway bridges*. 1996, London Thomas Telford Publishing.

42. Sheng, X., C.J.C. Jones, and D.J. Thompson, *A comparison of a theoretical model for quasi-statically and dynamically induced environmental vibration from trains with measurements.* Journal of Sound and Vibration, 2003. **267**(3): p. 621-635.

43. Jones, C.J.C. and J.R. Block, *PREDICTION OF GROUND VIBRATION FROM FREIGHT TRAINS.* Journal of Sound and Vibration, 1996. **193**(1): p. 205-213.

44. Kaewunruen, S. and A. Remennikov, *Dynamic properties of railway track and its components: a state-of-the-art review.* 2008.

45. L. Lee, M., *A Numerical Study into the Reconstruction of Impact Forces on Railway Track-like Structures*. Vol. 4. 2005. 19-45.

46. Kumara, J.J. and K. Hayano, *Deformation characteristics of fresh and fouled ballasts subjected to tamping maintenance.* Soils and Foundations, 2016. **56**(4): p. 652-663.

47. Wright, S.E., *Damage caused to ballast by mechanical maintenance techniques.* British Rail Research Technical Memorandum, 1983.

48. Aursudkij, B., *A laboratory study of railway ballast behaviour under traffic loading and tamping maintenance.* 2007.

49. Nålsund, R., *Effect of grading on degradation of crushed-rock railway ballast and on permanent axial deformation.* Transportation Research Record: Journal of the Transportation Research Board, 2010(2154): p. 149-155.

50.   Wang, X.J., et al. *Study on the DEM Simulation of the Granular Railway Ballast Bed Tamping*. in *Advanced Materials Research*. 2012. Trans Tech Publ.

51.   Lekarp, F., U. Isacsson, and A. Dawson, *State of the art. I: Resilient response of unbound aggregates.* Journal of transportation engineering, 2000. **126**(1): p. 66-75.

52.   Lekarp, F., U. Isacsson, and A. Dawson, *State of the art. II: Permanent strain response of unbound aggregates.* Journal of transportation engineering, 2000. **126**(1): p. 76-83.

53.   Liao, C.-L., T.-P. Chang, and D.-H. Young, *Elasto-plastic constitutive modelling of granular assembly.* International journal of solids and structures, 1995. **32**(8-9): p. 1121-1133.

54.   Katzenbach, R. and G. Festag, *Material behaviour of dry sand under cyclic loading.* Cyclic Behaviour of Soils and Liquefaction Phenomena, 2004: p. 153-158.

55.   McDowell, G.R., M.D. Bolton, and D. Robertson, *The fractal crushing of granular materials.* Journal of the Mechanics and Physics of Solids, 1996. **44**(12): p. 2079-2101.

56.   Chan, F.W.K., *Permanent deformation resistance of granular layers in pavements.* 1990.

57.   Brecciaroli, F. and P. Kolisoja, *Deformation behaviour of railway embankment materials under repeated loading: literature review.* Publications of Finnish Rail Administration, 2006.

58.   Norman, G., *Ballast box experiments for evaluating ballast field performance.* FRA report, 1982: p. 82-291.

59.   GILLIAN, M., *Ballast performance evaluation with box tests.* AREA, 1983. **692**: p. 207-239.

60.   FRÝBA, L., *History of Winkler foundation.* Vehicle System Dynamics, 1995. **24**(sup1): p. 7-12.

61.   Madenci, E. and I. Guven, *The finite element method and applications in engineering using ANSYS®.* 2015: Springer.

62.   Zienkiewicz, O.C. and R.L. Taylor, *The finite element method for solid and structural mechanics*. 2005: Elsevier.

63.   Moaveni, S., *Finite element analysis theory and application with ANSYS, 3/e*. 2011: Pearson Education India.

64.   Ishikawa, T., et al. *Evaluation of roadbed stiffness on bearing capacity of railroad ballast with discontinuous analysis*. in *Bearing Capacity of Roads, Railways and Airfields. 8th International Conference (BCR2A'09) University of Illinois, Urbana-Champaign*. 2009.

65.   Shi, X., *Prediction of permanent deformation in railway track.* Rozprawa Doktorska, University of Nottingham, Nottingham, 2009.

66.   Bennett, K., C. Ho, and H. Nguyen, *Verification of Box Test Model and Calibration of Finite Element Model.* Transportation Research Record: Journal of the Transportation Research Board, 2011. **2261**: p. 171-177.

67.   Indraratna, B. and S. Nimbalkar, *Stress-strain degradation response of railway ballast stabilized with geosynthetics.* Journal of Geotechnical and Geoenvironmental Engineering, 2013. **139**(5): p. 684-700.

68.   Bharadwaj, R., et al. *A comparison of discrete element modeling, finite element analysis, and pHysical experiment of granular material systems in a direct shear cell*. in *AIP Conference Proceedings*. 2008. AIP.

69.   Winkler, E., *Die lehre von der elastizität und festigkeit (The Theory of Elasticity and Stiffness).* Dominicus, Prague, 1867.

70.   Cundall, P.A. and O.D.L. Strack, *A discrete numerical model for granular assemblies.* geotechnique, 1979. **29**(1): p. 47-65.

71.   Kerr, A.D., *Fundamentals of railway track engineering.* 2003, Omaha, NE: Simmons-Boardman Books, Inc.

72.   Zhu, H., et al., *Discrete particle simulation of particulate systems: theoretical developments.* Chemical Engineering Science, 2007. **62**(13): p. 3378-3396.

73.   Walton, O., J. Brandeis, and J. Cooper. *Modeling of inelastic, frictional, contact forces in flowing granular assemblies.* in *Proc. 21st Annual Meeting of The Society of Engineering Science, Blacksburg, VA.* 1984.

74.   O'Sullivan, C., *Particle-based discrete element modeling: geomechanics perspective.* International Journal of Geomechanics, 2011. **11**(6): p. 449-464.

75.   Cundall, P.A. and R.D. Hart, *Numerical modelling of discontinua.* Engineering computations, 1992. **9**(2): p. 101-113.

76.   Cundall, P.A. *A computer model for simulating progressive, large-scale movements in blocky rock system.*

77.   EDEM, *What is DEM? Theoretical background behind Discrete Element Method (DEM).* 2018. p. 22.

78.   Bian, X.C., et al., *"Critical particle size" and ballast gradation studied by Discrete Element Modeling.* Transportation Geotechnics, 2016. **6**(Supplement C): p. 38-44.

79.   Huang, H. and E. Tutumluer, *Image-aided element shape generation method in discrete-element modeling for railroad ballast.* Journal of Materials in Civil Engineering, 2014. **26**(3): p. 527-535.

80. Lim, W.L. and G.R. McDowell, *Discrete element modelling of railway ballast.* Granular Matter, 2005. **7**(1): p. 19-29.

81. Thornton, C., *Granular dynamics, contact mechanics and particle system simulations*. 2015: Springer.

82. Zhao, T., *Introduction to Discrete Element Method*, in *Coupled DEM-CFD Analyses of Landslide-Induced Debris Flows*. 2017, Springer Singapore: Singapore. p. 25-45.

83. Tsuji, Y., T. Kawaguchi, and T. Tanaka, *Discrete particle simulation of two-dimensional fluidized bed.* Powder Technology, 1993. **77**(1): p. 79-87.

84. Rougier, E., A. Munjiza, and N.W.M. John, *Numerical comparison of some explicit time integration schemes used in DEM, FEM/DEM and molecular dynamics.* International Journal for Numerical Methods in Engineering, 2004. **61**(6): p. 856-879.

85. Kruggel-Emden, H., et al., *Selection of an appropriate time integration scheme for the discrete element method (DEM).* Computers & Chemical Engineering, 2008. **32**(10): p. 2263-2279.

86. Mishra, B.K., *A review of computer simulation of tumbling mills by the discrete element method: Part I—contact mechanics.* International Journal of Mineral Processing, 2003. **71**(1): p. 73-93.

87. Pöschel, T. and T. Schwager, *Computational granular dynamics: models and algorithms*. 2005: Springer Science & Business Media.

88. Lazarević, D., J. Dvornik, and K. Fresl, *Contact detection algorithm for discrete element analysis.* KoG, 2003. **6**(6.): p. 29-40.

89.   Mio, H., et al., *Optimum cell size for contact detection in the algorithm of the discrete element method.* Journal of chemical engineering of Japan, 2005. **38**(12): p. 969-975.

90.   Nezami, E.G., et al., *A fast contact detection algorithm for 3-D discrete element method.* Computers and Geotechnics, 2004. **31**(7): p. 575-587.

91.   Williams, J.R. and R. O'Connor, *Discrete element simulation and the contact problem.* Archives of Computational Methods in Engineering, 1999. **6**(4): p. 279-304.

92.   Han, K., Y.T. Feng, and D.R.J. Owen, *Performance comparisons of tree-based and cell-based contact detection algorithms.* Engineering Computations, 2007. **24**(2): p. 165-181.

93.   Williams, J.R. and R. O'Connor, *A linear complexity intersection algorithm for discrete element simulation of arbitrary geometries.* Engineering computations, 1995. **12**(2): p. 185-201.

94.   Munjiza, A., N. Bicanic, and D. Owen. *BSD contact detection algorithm for discrete elements in 2D.* in *Proc., Second Int. Conf. on Discrete Element Methods (DEM).* 1993. IESL Publications, Massachusetts Institute of Technology Boston.

95.   Munjiza, A. and K. Andrews, *NBS contact detection algorithm for bodies of similar size.* International Journal for Numerical Methods in Engineering, 1998. **43**(1): p. 131-149.

96.   Perkins, E. and J.R. Williams, *A fast contact detection algorithm insensitive to object sizes.* Engineering Computations, 2001. **18**(1/2): p. 48-62.

97.   Perkins, E. and J.R. Williams, *Generalized spatial binning of bodies of different sizes*, in *Discrete element methods: Numerical modeling of discontinua*. 2002. p. 52-55.

98.   Hogue, C., *Shape representation and contact detection for discrete element simulations of arbitrary geometries.* Engineering Computations, 1998. **15**(3): p. 374-390.

99.   Williams, J.R., E. Perkins, and B. Cook, *A contact algorithm for partitioning N arbitrary sized objects.* Engineering Computations, 2004. **21**(2/3/4): p. 235-248.

100.   Munjiza, A. and K.R.F. Andrews, *NBS contact detection algorithm for bodies of similar size.* International Journal for Numerical Methods in Engineering, 1998. **43**(1): p. 131-149.

101.   Bonet, J. and J. Peraire, *An alternating digital tree (ADT) algorithm for 3D geometric searching and intersection problems.* International Journal for Numerical Methods in Engineering, 1991. **31**(1): p. 1-17.

102.   Feng, Y.T. and D.R.J. Owen, *An augmented spatial digital tree algorithm for contact detection in computational mechanics.* International Journal for Numerical Methods in Engineering, 2002. **55**(2): p. 159-176.

103.   Irazábal González, J., *Numerical analysis of railway ballast behaviour using the Discrete Element Method.* 2017.

104.   Sainsbury, D., et al. *Continuum and distinct element numerical modeling in geomechanics–2011.* in *Proc. 2nd Int. FLAC/DEM Symp*. 2011.

105.   Iwashita, K. and M. Oda, *Rolling resistance at contacts in simulation of shear band development by DEM.* Journal of engineering mechanics, 1998. **124**(3): p. 285-292.

106. Jiang, M., H.-S. Yu, and D. Harris, *A novel discrete model for granular material incorporating rolling resistance.* Computers and Geotechnics, 2005. **32**(5): p. 340-357.

107. Plassiard, J.-P., N. Belheine, and F.-V. Donzé, *A spherical discrete element model: calibration procedure and incremental response.* Granular Matter, 2009. **11**(5): p. 293-306.

108. Zhu, H. and A. Yu, *A theoretical analysis of the force models in discrete element method.* Powder Technology, 2006. **161**(2): p. 122-129.

109. Hertz, H., *Über die Berührung fester elastischer Körper.* Journal für die reine und angewandte Mathematik, 1882. **92**: p. 156-171.

110. Mindlin, R.D., *Elastic spheres in contact under varying oblique forces.* Trans. ASME, J. Appl. Mech., 1953. **20**: p. 327-344.

111. Di Renzo, A. and F.P. Di Maio, *Comparison of contact-force models for the simulation of collisions in DEM-based granular flow codes.* Chemical Engineering Science, 2004. **59**(3): p. 525-541.

112. Weatherley, D., V. Boros, and W. Hancock, *ESyS-particle tutorial and user's guide Version 2.1.* Earth Systems Science Computational Centre, The University of Queensland, 2011.

113. Cundall, P.A. *Formulation of a three-dimensional distinct element model—Part I. A scheme to detect and represent contacts in a system composed of many polyhedral blocks.* in *International Journal of Rock Mechanics and Mining Sciences & Geomechanics Abstracts.* 1988. Elsevier.

114. Hart, R., P. Cundall, and J. Lemos. *Formulation of a three-dimensional distinct element model—Part II. Mechanical calculations for motion and interaction of*

a system composed of many polyhedral blocks. in *International Journal of Rock Mechanics and Mining Sciences & Geomechanics Abstracts*. 1988. Elsevier.

115. G Nezami, E., et al., *Shortest link method for contact detection in discrete element method.* International Journal for Numerical and Analytical Methods in Geomechanics, 2006. **30**(8): p. 783-801.

116. Eliáš, J., *Simulation of railway ballast using crushable polyhedral particles.* Powder Technology, 2014. **264**(Supplement C): p. 458-465.

117. Ahmed, S., et al., *Numerical modelling of railway ballast at the particle scale.* International Journal for Numerical and Analytical Methods in Geomechanics, 2016. **40**(5): p. 713-737.

118. Lobo-Guerrero, S. and L.E. Vallejo, *Discrete element method analysis of railtrack ballast degradation during cyclic loading.* Granular Matter, 2006. **8**(3-4): p. 195-204.

119. Lu, M. and G.R. McDowell, *Discrete element modelling of ballast abrasion.* Geotechnique, 2006. **56**(9): p. 651-655.

120. Hossain, Z., et al., *DEM analysis of angular ballast breakage under cyclic loading.* Geomechanics and Geoengineering: An International Journal, 2007. **2**(3): p. 175-181.

121. Lu, M. and G.R. McDowell, *The importance of modelling ballast particle shape in the discrete element method.* Granular Matter, 2007. **9**(1-2): p. 69-80.

122. Lu, M. and G.R. McDowell, *Discrete element modelling of railway ballast under triaxial conditions.* Geomechanics and Geoengineering, 2008. **3**(4): p. 257-270.

123. Indraratna, B., P.K. Thakur, and J.S. Vinod, *Experimental and numerical study of railway ballast behavior under cyclic loading.* International Journal of Geomechanics, 2010. **10**(4): p. 136-144.

124. Indraratna, B., et al., *Behavior of fresh and fouled railway ballast subjected to direct shear testing: Discrete element simulation.* International Journal of Geomechanics, 2012. **14**(1): p. 34-44.

125. Tuan, N.Q. and H. Konietzky, *DEM simulation of mechanical lab tests for coarse-grained granular material*, in *Geotechnics for Sustainable Development*, Phung, Editor. 2013, Construction Publisher: Hanoi.

126. McDowell, G.R. and H. Li, *Discrete element modelling of scaled railway ballast under triaxial conditions.* Granular Matter, 2016. **18**(3).

127. Zhang, X., C. Zhao, and W. Zhai, *Dynamic behavior analysis of high-speed railway ballast under moving vehicle loads using discrete element method.* International Journal of Geomechanics, 2017. **17**(7).

128. Zhang, X., C. Zhao, and W. Zhai. *DEM analysis of ballast breakage under train loads and its effect on mechanical behaviour of railway track.* in *Springer Proceedings in Physics.* 2017.

129. Zhao, S., X. Zhou, and W. Liu, *Discrete element simulations of direct shear tests with particle angularity effect.* Granular Matter, 2015. **17**(6): p. 793-806.

130. Miao, C.X., et al., *DEM modeling of pullout behavior of geogrid reinforced ballast: The effect of particle shape.* Computers and Geotechnics, 2017. **81**: p. 249-261.

131. Wang, Z.J., G.Q. Jing, and G.X. Liu, *Analysis on railway ballast-glue micro-characteristics*, in *Applied Mechanics and Materials*. 2014. p. 535-538.

132. Ngo, N.T., B. Indraratna, and C. Rujikiatkamjorn, *Micromechanics-based investigation of fouled ballast using large-scale triaxial tests and discrete element modeling.* Journal of Geotechnical and Geoenvironmental Engineering, 2016. **143**(2): p. 04016089.

133. Khatibi, F., M. Esmaeili, and S. Mohammadzadeh, *DEM analysis of railway track lateral resistance.* Soils and Foundations, 2017. **57**(4): p. 587-602.

134. Jing, G., P. Aela, and H. Fu, *The contribution of ballast layer components to the lateral resistance of ladder sleeper track.* Construction and Building Materials, 2019. **202**: p. 796-805.

135. Wang, Z., et al., *Analysis of ballast direct shear tests by discrete element method under different normal stress.* Measurement: Journal of the International Measurement Confederation, 2015. **63**: p. 17-24.

136. Vizcarra, G.C., S. Nimbalkar, and M. Casagrande. *Modeling Behaviour of Railway Ballast in Prismoidal Apparatus Using Discrete Element Method*. in *Procedia Engineering*. 2016.

137. Harkness, J., et al., *Discrete element simulation of railway ballast: modelling cell pressure effects in triaxial tests.* Granular Matter, 2016. **18**(3).

138. Chung, Y.C., et al., *Mechanical behaviour of a granular solid and its contacting deformable structure under uni-axial compression - Part I: Joint DEM-FEM modelling and experimental validation.* Chemical Engineering Science, 2016. **144**: p. 404-420.

139. Ji, S., S. Sun, and Y. Yan, *Discrete element modeling of dynamic behaviors of railway ballast under cyclic loading with dilated polyhedra.* International Journal for Numerical and Analytical Methods in Geomechanics, 2017. **41**(2): p. 180-197.

140. Wang, X.J. and X.L. Geng. *Study on the Effects of Tamping Frequency to the Compaction Degree of Trackbeds*. in *Applied Mechanics and Materials*. 2012. Trans Tech Publ.

141. Suhr, B., S. Marschnig, and K. Six, *Comparison of two different types of railway ballast in compression and direct shear tests: experimental results and DEM model validation.* Granular Matter, 2018. **20**(4).

142. Li, H. and G.R. McDowell, *Discrete element modelling of under sleeper pads using a box test.* Granular Matter, 2018. **20**(2).

143. Saussine, G., et al., *Modelling ballast behaviour under dynamic loading. Part 1: A 2D polygonal discrete element method approach.* Computer methods in applied mechanics and engineering, 2006. **195**(19): p. 2841-2859.

144. Qian, Y., et al., *Characterization of geogrid reinforced ballast behavior at different levels of degradation through triaxial shear strength test and discrete element modeling.* Geotextiles and Geomembranes, 2015. **43**(5): p. 393-402.

145. Ouhbi, N., et al. *Railway Ballast: Grain Shape Characterization to Study its Influence on the Mechanical Behaviour*. in *Procedia Engineering*. 2016.

146. Irazábal, J., F. Salazar, and E. Oñate, *Numerical modelling of granular materials with spherical discrete particles and the bounded rolling friction model. Application to railway ballast.* Computers and Geotechnics, 2017. **85**: p. 220-229.

147. Qian, Y., et al. *Comparative evaluation of different aperture geogrids for ballast reinforcement through triaxial testing and discrete element modeling*. in *Proceedings of Geosynthetics*. 2013.

175

148. Qian, Y., et al. *Discrete element modeling of ballast reinforced with triangular aperture geogrid*. in *Proceedings of 9th International Conference on Bearing Capacity of Roads, Railways and Airfields*. 2013.

149. Qian, Y., et al., *Simulating ballast shear strength from large-scale triaxial tests: Discrete element method.* Transportation Research Record: Journal of the Transportation Research Board, 2013(2374): p. 126-135.

150. Qian, Y., et al., *Role of initial particle arrangement in ballast mechanical behavior.* International Journal of Geomechanics, 2018. **18**(3).

151. Feng, B., W. Hou, and E. Tutumluer, *Implications of Field Loading Patterns on Different Tie Support Conditions using Discrete Element Modeling: Dynamic Responses.* Transportation Research Record, 2019: p. 0361198118821936.

152. Coetzee, C., *Calibration of the discrete element method and the effect of particle shape.* Powder Technology, 2016. **297**: p. 50-70.

153. Kumara, J.J. and K. Hayano, *Importance of particle shape on stress-strain behaviour of crushed stone-sand mixtures.* Geomechanics and Engineering, 2016. **10**(4): p. 455-470.

154. Lane, J.E., P.T. Metzger, and R.A. Wilkinson, *A Review of Discrete Element Method (DEM) Particle Shapes and Size Distributions for Lunar Soil.* 2010.

155. Garcia, X., et al., *A clustered overlapping sphere algorithm to represent real particles in discrete element modelling.* Geotechnique, 2009. **59**(9): p. 779-784.

156. Harireche, O. and G. McDowell, *Discrete element modelling of cyclic loading of crushable aggreates.* Granular matter, 2003. **5**(3): p. 147-151.

157. McDowell, G. and O. Harireche, *Discrete element modelling of soil particle fracture.* GEOTECHNIQUE-LONDON-, 2002. **52**(2): p. 131-136.

158. Matsushima, T., et al., *3D shape characterization and image-based DEM simulation of the lunar soil simulant FJS-1.* Journal of Aerospace Engineering, 2009. **22**(1): p. 15-23.

159. Zhang, Z., et al., *Dynamic characteristics of track-ballast-silty clay with irregular vibration levels generated by high-speed train based on DEM.* Construction and Building Materials, 2016. **125**: p. 564-573.

160. Chen, C., et al., *Discrete element modelling of lateral displacement of a granular assembly under cyclic loading.* Computers and Geotechnics, 2015. **69**: p. 474-484.

161. Wensrich, C. and A. Katterfeld, *Rolling friction as a technique for modelling particle shape in DEM.* Powder Technology, 2012. **217**: p. 409-417.

162. Ai, J., et al., *Assessment of rolling resistance models in discrete element simulations.* Powder Technology, 2011. **206**(3): p. 269-282.

163. Alonso-Marroquín, F. and Y. Wang, *An efficient algorithm for granular dynamics simulations with complex-shaped objects.* Granular Matter, 2009. **11**(5): p. 317-329.

164. Wang, X., et al. *The research of the numerical simulation on the granular ballast bed tamping. Advanced Materials Research*. in *Proceeding (s) of the International Conference on Manufacturing Science and Engineering (ICMSE 2012), Vols*.

165. Chen, C., G.R. McDowell, and N.H. Thom, *Investigating geogrid-reinforced ballast: Experimental pull-out tests and discrete element modelling.* Soils and Foundations, 2014. **54**(1): p. 1-11.

166. Tutumluer, E., et al. *AREMA gradations affecting ballast performance using discrete element modeling (DEM) approach*. in *Proceedings of the AREMA 2009 Annual Conference, Chicago, Illinois, September*. 2009.

167. Huang, H. and E. Tutumluer, *Discrete Element Modeling for fouled railroad ballast.* Construction and Building Materials, 2011. **25**(8): p. 3306-3312.

168. Pakalavan, V., B. Nirvekala, and L.C. Kurukulasuriya, *SHEAR STRENGTH CHARACTERISTICS OF DIFFERENT GRADATIONS OF BALLAST USING PARALLEL GRADATION TECHNIQUE*. 2016.

169. ABNT, *Railway – Ballast – Requirements and test methods.* 2001, Brazilian Standard.

170. Indraratna, B., et al., *Ballast characteristics and the effect of geosynthetics on Rril track deformation.* 2004.

171. Australia, S., *Aggregates and rock for engineering purposes. 7: Railway ballast.* 1996: New South Wales, Australia.

172. Li, D., *Railway track granular layer thickness design based on subgrade performance under repeated loading*. 1994, University of Massachusetts Amherst: Ann Arbor. p. 317.

173. Zhai, W., K. Wang, and C. Cai, *Fundamentals of vehicle–track coupled dynamics.* Vehicle System Dynamics, 2009. **47**(11): p. 1349-1376.

174. Huang, H. and S. Chrismer, *Discrete element modeling of ballast settlement under trains moving at "Critical Speeds".* Construction and Building Materials, 2013. **38**(Supplement C): p. 994-1000.

175. Shen, S. and E. Tutumluer, *Moving load on track with Asphalt trackbed AU - Huang, Hai.* Vehicle System Dynamics, 2010. **48**(6): p. 737-749.

176. Selig, E. and D. Boucher, *Abrasion Tests for Railroad Ballast.* 1990.

177. Laryea, S., et al., *Comparison of performance of concrete and steel sleepers using experimental and discrete element methods.* Transportation Geotechnics, 2014. **1**(4): p. 225-240.

178. Ghaboussi, J. and R. Barbosa, *Three-dimensional discrete element method for granular materials.* International Journal for Numerical and Analytical Methods in Geomechanics, 1990. **14**(7): p. 451-472.

179. Dawei, Z., et al., *Three-dimensional discrete element simulation for granular materials.* Engineering Computations, 2006. **23**(7): p. 749-770.

180. Nezami, E.G., et al., *Simulation of front end loader bucket–soil interaction using discrete element method.* International Journal for Numerical and Analytical Methods in Geomechanics, 2007. **31**(9): p. 1147-1162.

181. Lobo-Guerrero, S., L.E. Vallejo, and L.F. Vesga, *Visualization of crushing evolution in granular materials under compression using DEM.* International Journal of Geomechanics, 2006. **6**(3): p. 195-200.

182. McDowell, G.R., et al., *Comparison of ballast index tests for railway trackbeds.* Proceedings of the Institution of Civil Engineers-Geotechnical Engineering, 2004. **157**(3): p. 151-161.

183. Qian, J., et al. *DEM Analysis of Railtrack Ballast Degradation under Monotonic and Cyclic Loading.* in *Procedia Engineering.* 2016.

184. Wang, B., U. Martin, and S. Rapp, *Discrete element modeling of the single-particle crushing test for ballast stones.* Computers and Geotechnics, 2017. **88**: p. 61-73.

185. Huang, H., et al. *Discrete element modeling of aggregate behavior in fouled railroad ballast.* in *Recent Advancement in Soil Behavior, in Situ Test Methods,*

Pile Foundations, and Tunneling: Selected Papers from the 2009 GeoHunan International Conference. 2009.

186. Gong, H., et al., *Direct shear properties of railway ballast mixed with tire derived aggregates: Experimental and numerical investigations.* Construction and Building Materials, 2019. **200**: p. 465-473.

187. Liu, S., et al., *Comparison of laboratory testing using smartrock and discrete element modeling of ballast particle movement.* Journal of Materials in Civil Engineering, 2017. **29**(3).

188. Thompson, D., *Railway noise and vibration: mechanisms, modelling and means of control*. 2008: Elsevier.

189. Timoshenko, S.P., *LXVI. On the correction for shear of the differential equation for transverse vibrations of prismatic bars.* The London, Edinburgh, and Dublin Philosophical Magazine and Journal of Science, 1921. **41**(245): p. 744-746.

190. Timoshenko, S.P., *X. On the transverse vibrations of bars of uniform cross-section.* The London, Edinburgh, and Dublin Philosophical Magazine and Journal of Science, 1922. **43**(253): p. 125-131.

191. Knothe, K.L. and S. Grassie, *Modelling of Railway Track and Vehicle/Track Interaction at High Frequencies*. Vol. 22. 1993. 209-262.

192. Ebnesajjad, S., *18 - Properties of Tetrafluoroethylene Homopolymers*, in *Fluoroplastics (Second Edition)*, S. Ebnesajjad, Editor. 2015, William Andrew Publishing: Oxford. p. 396-440.

193. Farmer, I.W., *Engineering Properties of Rock–Spon.* Google Scholar, 1968.

194. Melis Maynar, M., *Embankments and ballast in high speed rail.* Revista de Obras Publicas, 2006(153).

195. Blake, G.R. and K.H. Hartge, *Particle Density 1.* Methods of soil analysis: Part 1—Physical and mineralogical methods, 1986(methodsofsoilan1): p. 377-382.

196. Chen, C., G.R. McDowell, and N. Thom, *A study of geogrid-reinforced ballast using laboratory pull-out tests and discrete element modelling.* Geomechanics and Geoengineering, 2013. **8**(4): p. 244-253.

197. Coetzee, C.J., *Review: Calibration of the discrete element method.* Powder Technology, 2017. **310**: p. 104-142.

198. Taylor, D., *Fundamentals of soil mechanics*. 1948: Chapman And Hall, Limited.; New York.

199. Carrigy, M.A., *Experiments on the angles of repose of granular materials 1.* Sedimentology, 1970. **14**(3-4): p. 147-158.

200. Van Burkalow, A., *Angle of repose and angle of sliding friction: an experimental study.* Geological Society of America Bulletin, 1945. **56**(6): p. 669-707.

201. Parker, D.J., et al., *Positron emission particle tracking studies of spherical particle motion in rotating drums.* Chemical Engineering Science, 1997. **52**(13): p. 2011-2022.

202. Zhou, Y.C., et al., *Rolling friction in the dynamic simulation of sandpile formation.* Physica A: Statistical Mechanics and its Applications, 1999. **269**(2-4): p. 536-553.

203. Zhou, Y.C., et al., *An experimental and numerical study of the angle of repose of coarse spheres.* Powder technology, 2002. **125**(1): p. 45-54.

204. Grasselli, Y. and H.J. Herrmann, *On the angles of dry granular heaps.* Physica A: Statistical Mechanics and its Applications, 1997. **246**(3-4): p. 301-312.

205. Beakawi Al-Hashemi, H.M. and O.S. Baghabra Al-Amoudi, *A review on the angle of repose of granular materials.* Powder Technology, 2018. **330**: p. 397-417.

206. Van't Zand, J. and J. Moraal, *Ballast resistance under three dimensional loading.* TU Delft1996, 1997.

207. Kabo, E., *A numerical study of the lateral ballast resistance in railway tracks.* Proceedings of the Institution of Mechanical Engineers, Part F: Journal of Rail and Rapid Transit, 2006. **220**(4): p. 425-433.

208. Irazábal González, J., *Numerical modeling of railway ballast using the discrete element method*. 2015, Universitat Politècnica de Catalunya.

209. Solutions, D., *EDEM Manual*. 2018: Edinburgh, United Kingdom

210. Nijssen, R.P.L., *2 - Phenomenological fatigue analysis and life modeling*, in *Fatigue Life Prediction of Composites and Composite Structures*, A.P. Vassilopoulos, Editor. 2010, Woodhead Publishing. p. 47-78.

211. Navaratnarajah, S.K. and B. Indraratna, *Use of rubber mats to improve the deformation and degradation behavior of rail ballast under cyclic loading.* Journal of geotechnical and geoenvironmental engineering, 2017. **143**(6): p. 04017015.

212. Aursudkij, B., G. McDowell, and A. Collop, *Cyclic loading of railway ballast under triaxial conditions and in a railway test facility.* Granular Matter, 2009. **11**(6): p. 391.

213. McDowell, G. and P. Stickley, *Performance of geogrid-reinforced ballast.* Ground Engineering, 2006. **39**(1): p. 26-30.

214. Al-Saoudi, N.K. and K.H. Hassan, *Behaviour of track ballast under repeated loading.* Geotechnical and Geological Engineering, 2014. **32**(1): p. 167-178.

215.	Ferellec, J.-F., et al., *Analysis of compaction of railway ballast by different maintenance methods using DEM*. Vol. 140. 2017. 15032.

1- Constant Loading

```cpp
//QATAR UNIVERSITY
//COLLEGE OF ENGINEERING
//Masters of Science in Civil Engineering
//Title: DISCRETE ELEMENT MODELING OF RAILROAD BALLAST UNDER SIMULATED TRAIN
LOADING
// Copyright
// Yahia Alabbasi
// June 2019

//Validation-Constant Loading Type

//C++ essential libraries
#include <iostream>
#include <time.h>
#include <string>

//EDEM Coupling libraries
#include "IEDEMCoupling.h"
#include "vectorMaths.h"

using namespace std;
using namespace NApiEDEM;

//Defining the parameters
class CGeometry
{
public:

        // ID
        int         id;

        // Name
        string      name;

        // sleeper Properties
        double mass;

        // External forces
        C3dVector   force;
        C3dVector   torque;

        // Geometry accelerations & velocities
        C3dVector   acceleration;
        C3dVector   velocity;
        C3dVector   angularVelocity;

        // Geometry position
        C3x3Matrix  orientation;
        C3dVector   totalTranslation;
        bool        movePoA;
};
int main()
{
        // Simulation settings
        double simTime;
        double dt;
        unsigned int timeStepRatio = 10;
```

```cpp
        double endtime = 2;

        // Geometry Parameters
        CGeometry sleeper;
        C3dVector initialVelocity = { 0.0,0.0,-0.1 };//predefined velocity used
for displacement control mode
        sleeper.name = "sleeper";
        sleeper.mass = 0.06;
        bool applyForce = false;
        bool test = true;

        //Loading Parameters used only in the validation exercise
        C3dVector Fi; //Input load vector
        double p = -100;// value of input load-constant

        //Other Parameters
        double t0;

        //Coupling Initialisation
        IEDEMCoupling coupling;
        if (!coupling.initialiseCoupling())
        {
                cout << "Can't intialise the EDEM Coupling Client" << endl;
                exit(EXIT_FAILURE);
        }
        cout << "EDEM Coupling Client intialised" << endl << "Connecting to
EDEM..." << endl;
        // Connect to EDEM
        if (!coupling.connectCoupling())
        {
                cout << "Could not connect to EDEM" << endl;
                exit(EXIT_FAILURE);
        }
        cout << "Connection to EDEM successful" << endl;


        //Obtain Simulation Variables
        // Get current simulation time
        coupling.getEDEMTime(simTime);

        // Get simulation time step
        coupling.getEDEMTimeStep(dt);
        dt *= timeStepRatio;

        // Get the geometry ID
        if (coupling.getGeometryId(sleeper.name.c_str(), sleeper.id))
        {
                cout << "Found the geometry" << endl;
        }

        else
        {
                cout << "Could not find geometry" << endl;
                exit(EXIT_FAILURE);
        }

        sleeper.movePoA = true;

        //Main Simulation Loop
        while (simTime < endtime)
        {
                simTime += dt;
```

```cpp
                // Get current totaltranslation
                coupling.getGeometryTranslation(sleeper.id,
sleeper.totalTranslation);
                // Get current geometry forces (Fc)
                coupling.getGeometryForces(sleeper.id, sleeper.force,
sleeper.torque);

                // get the time when Fc close to Fi
                if (test)
                {
                        if (abs(sleeper.force.z()) > abs(0.98*p))
                        {
                                applyForce = true;
                                coupling.getEDEMTime(t0);
                                test = false;
                        }
                }

                if (applyForce)
                {
                        // Update force values
                        Fi = C3dVector(0, 0, p);
                        sleeper.force.setX(0); // Only 1 degree of freedom
                        sleeper.force.setY(0); // Only 1 degree of freedom
                        sleeper.force += Fi; // Fc-Fi

                        // Acceleration-equation 4.21
                        sleeper.acceleration = sleeper.force / sleeper.mass;

                        // Velocity-equation 4.22
                        sleeper.velocity += sleeper.acceleration*dt;

                        // Position-equation 4.24
                        sleeper.totalTranslation += sleeper.velocity*dt;
                }

                else // Initial compression using displacement control
                {
                        sleeper.velocity = initialVelocity;
                        sleeper.totalTranslation += sleeper.velocity*dt;
                }

                //Update geometry Motion
                coupling.setGeometryMotion(sleeper.id,
                        sleeper.totalTranslation,
                        sleeper.orientation,
                        sleeper.velocity,
                        sleeper.angularVelocity,
                        dt,
                        sleeper.movePoA);

                // Simulate geometry motion
                coupling.simulate(dt, endtime);

        }
        return 0;
}
```

2- Sinusoidal Loading

```cpp
//QATAR UNIVERSITY
//COLLEGE OF ENGINEERING
//Masters of Science in Civil Engineering
//Title: DISCRETE ELEMENT MODELING OF RAILROAD BALLAST UNDER SIMULATED TRAIN
LOADING
// Copyright
// Yahia Alabbasi
// June 2019

//Validation-Sinusoidal Loading Type

//C++ essential libraries
#include <iostream>
#include <time.h>
#include <string>
#include <cmath>

//EDEM Coupling libraries
#include "IEDEMCoupling.h"
#include "vectorMaths.h"

using namespace std;
using namespace NApiEDEM;

//Defining the parameters
class CGeometry
{
public:

        // ID
        int         id;

        // Name
        string      name;

        // sleeper Properties
        double mass;

        // External forces
        C3dVector   force;
        C3dVector   torque;

        // Geometry accelerations & velocities
        C3dVector   acceleration;
        C3dVector   velocity;
        C3dVector   angularVelocity;

        // Geometry position
        C3x3Matrix  orientation;
        C3dVector   totalTranslation;
        bool        movePoA;
};
int main()
{
        // Simulation settings
        double simTime;
        double dt;
        unsigned int timeStepRatio = 10;
        double endtime = 2;
```

```cpp
    // Geometry Parameters
    CGeometry sleeper;
    C3dVector initialVelocity = { 0.0,0.0,-0.1 };//predefined velocity used
for displacement control mode
    sleeper.name = "sleeper";
    sleeper.mass = 0.06;
    bool applyForce = false;
    bool test = true;

    //Loading Parameters used only in the validation exercise
    C3dVector Fi; //Input load vector
    double p=100; // value of input load
    double freq = 1;
    double a = 50;
    double pi = 3.141592653589793;

    //Other Parameters
    double t0;
    double t_1;

    //Coupling Initialisation
    IEDEMCoupling coupling;
    if (!coupling.initialiseCoupling())
    {
        cout << "Can't intialise the EDEM Coupling Client" << endl;
        exit(EXIT_FAILURE);
    }
    cout << "EDEM Coupling Client intialised" << endl << "Connecting to
EDEM..." << endl;
    // Connect to EDEM
    if (!coupling.connectCoupling())
    {
        cout << "Could not connect to EDEM" << endl;
        exit(EXIT_FAILURE);
    }
    cout << "Connection to EDEM successful" << endl;

    //Obtain Simulation Variables
    // Get current simulation time
    coupling.getEDEMTime(simTime);

    // Get simulation time step
    coupling.getEDEMTimeStep(dt);
    dt *= timeStepRatio;

    // Get the geometry ID
    if (coupling.getGeometryId(sleeper.name.c_str(), sleeper.id))
    {
        cout << "Found the geometry" << endl;
    }

    else
    {
        cout << "Could not find geometry" << endl;
        exit(EXIT_FAILURE);
    }

    sleeper.movePoA = true;

    //Main Simulation Loop
    while (simTime < endtime)
    {
```

```cpp
            simTime += dt;

            // Get current totaltranslation
            coupling.getGeometryTranslation(sleeper.id,
sleeper.totalTranslation);
            // Get current geometry forces (Fc)
            coupling.getGeometryForces(sleeper.id, sleeper.force,
sleeper.torque);

            // get the time when Fc close to first point of Fi
            if (test)
            {
                    if (abs(sleeper.force.z()) > abs(0.98*p))
                    {
                            applyForce = true;
                            coupling.getEDEMTime(t0);
                            test = false;
                    }
            }

            if (applyForce)
            {
                    // Update force values

                    t_1 = (simTime - t0) - dt;
                    p = -(a * sin((2 * pi*freq*t_1) + (0.5*pi)) + a);
                    Fi = C3dVector(0, 0, p);
                    sleeper.force.setX(0); // Only 1 degree of freedom
                    sleeper.force.setY(0); // Only 1 degree of freedom
                    sleeper.force = Fi + sleeper.force; // Fc-Fi

                      // Acceleration-equation 4.21
                    sleeper.acceleration = sleeper.force / sleeper.mass;

                    // Velocity-equation 4.22
                    sleeper.velocity += sleeper.acceleration*dt;

                    // Position-equation 4.24
                    sleeper.totalTranslation += sleeper.velocity*dt;
            }

            else // Initial compression using displacement control
            {
                    sleeper.velocity = initialVelocity;
                    sleeper.totalTranslation += sleeper.velocity*dt;
            }

            //Update geometry Motion
            coupling.setGeometryMotion(sleeper.id,
                    sleeper.totalTranslation,
                    sleeper.orientation,
                    sleeper.velocity,
                    sleeper.angularVelocity,
                    dt,
                    sleeper.movePoA);

            // Simulate geometry motion
            coupling.simulate(dt, endtime);
      }
      return 0;
}
```

3- Simulated Train Loading utilizing BOEF

```cpp
//QATAR UNIVERSITY
//COLLEGE OF ENGINEERING
//Masters of Science in Civil Engineering
//Title: DISCRETE ELEMENT MODELING OF RAILROAD BALLAST UNDER SIMULATED TRAIN
LOADING
// Copyright
// Yahia Alabbasi
// June 2019

//Validation-Simulated Train Loading utilizing BOEF

//C++ essential libraries
#include <iostream>
#include <time.h>
#include <string>
#include <cmath>

//EDEM Coupling libraries
#include "IEDEMCoupling.h"
#include "vectorMaths.h"

using namespace std;
using namespace NApiEDEM;

//Defining the parameters
class CGeometry
{
public:

        // ID
        int         id;

        // Name
        string      name;

        // sleeper Properties
        double mass;

        // External forces
        C3dVector    force;
        C3dVector    torque;

        // Geometry accelerations & velocities
        C3dVector   acceleration;
        C3dVector   velocity;
        C3dVector   angularVelocity;

        // Geometry position
        C3x3Matrix   orientation;
        C3dVector    totalTranslation;
        bool         movePoA;
};

//BOEF function
double beam(double Pa, double EI, double k, double z)
{

        double j = k / (EI*4.0);
        double d = 0.25;
        double lamda = pow(j, d);
```

```cpp
        double d1 = ((-Pa) / (8.0 * EI*pow(lamda, 3.0)));
        double d2 = exp(-lamda * abs(z));
        double d3 = cos(lamda*abs(z)) + sin(lamda*abs(z));
        double u = d1 * d2*d3;
        return u;
}

int main()
{
        // Simulation settings
        double simTime;
        double dt;
        unsigned int timeStepRatio = 10;
        double endtime = 2;

        // Geometry Parameters
        CGeometry sleeper;
        C3dVector initialVelocity = { 0.0,0.0,-0.1 };//predefined velocity used
for displacement control mode
        sleeper.name = "sleeper";
        sleeper.mass = 0.06;
        bool applyForce = false;
        bool test = true;

        //Loading Parameters used only in the validation exercise
        double EI = 10e6/2;
        double k = 40e6/2;
        double Pa = 140;
        double xm = 0;
        double v = 27.7778;
        double L1 = 2.5;
        double L2 = 15;
        double L3 = 1.25;
        double L = 2 * L1 + L2 + L3;
        double pi = 3.141592653589793;
        C3dVector Fi; //Input load vector
        double preload = -4;
        double p= -102;//first point of Fi

        //Other Parameters
        double t0;
        double t_1;

        //Coupling Initialisation
        IEDEMCoupling coupling;
        if (!coupling.initialiseCoupling())
        {
                cout << "Can't intialise the EDEM Coupling Client" << endl;
                exit(EXIT_FAILURE);
        }
        cout << "EDEM Coupling Client intialised" << endl << "Connecting to
EDEM..." << endl;
        // Connect to EDEM
        if (!coupling.connectCoupling())
        {
                cout << "Could not connect to EDEM" << endl;
                exit(EXIT_FAILURE);
        }
        cout << "Connection to EDEM successful" << endl;


        //Obtain Simulation Variables
```

```cpp
        // Get current simulation time
        coupling.getEDEMTime(simTime);

        // Get simulation time step
        coupling.getEDEMTimeStep(dt);
        dt *= timeStepRatio;

        // Get the geometry ID
        if (coupling.getGeometryId(sleeper.name.c_str(), sleeper.id))
        {
                cout << "Found the geometry" << endl;
        }

        else
        {
                cout << "Could not find geometry" << endl;
                exit(EXIT_FAILURE);
        }

        sleeper.movePoA = true;

        //Main Simulation Loop
        while (simTime < endtime)
        {
                simTime += dt;

                // Get current totaltranslation
                coupling.getGeometryTranslation(sleeper.id,
sleeper.totalTranslation);
                // Get current geometry forces (Fc)
                coupling.getGeometryForces(sleeper.id, sleeper.force,
sleeper.torque);

                // get the time when Fc close to Fi
                if (test)
                {
                        if (abs(sleeper.force.z()) > abs(0.98*p))
                        {
                                applyForce = true;
                                coupling.getEDEMTime(t0);
                                test = false;
                        }
                }

                        if (applyForce)
                        {

                                t_1 = (simTime - t0) - dt;

                                        double a1 = -0.625; // The initial distance
from the simulation box to the first axle from the left=x

                                        double m1 = round((-a1 - v * t_1) / L);
                                        double u1 = beam(Pa, EI, k, -a1 - v * t_1 - (m1)*L)
+ beam(Pa, EI, k, -a1 - v * t_1 - (m1 - 1)*L) + beam(Pa, EI, k, -a1 - v * t_1 -
(m1 + 1)*L);

                                        double a2 = a1 - L1;
                                        double m2 = round((-a2 - v * t_1) / L);
```

```cpp
                              double u2 = beam(Pa, EI, k, -a2 - v * t_1 - (m2)*L)
+ beam(Pa, EI, k, -a2 - v * t_1 - (m2 - 1)*L) + beam(Pa, EI, k, -a2 - v * t_1 -
(m2 + 1)*L);

                              double a3 = a1 - L1 - L2;
                              double m3 = round((-a3 - v * t_1) / L);
                              double u3 = beam(Pa, EI, k, -a3 - v * t_1 - (m3)*L)
+ beam(Pa, EI, k, -a3 - v * t_1 - (m3 - 1)*L) + beam(Pa, EI, k, -a3 - v * t_1 -
(m3 + 1)*L);

                              double a4 = a1 - L1 - L2 - L1;
                              double m4 = round((-a4 - v * t_1) / L);
                              double u4 = beam(Pa, EI, k, -a4 - v * t_1 - (m4)*L)
+ beam(Pa, EI, k, -a4 - v * t_1 - (m4 - 1)*L) + beam(Pa, EI, k, -a4 - v * t_1 -
(m4 + 1)*L);

                              double u = u1 + u2 + u3 + u4;

                              p = ((k*u) + preload);

                              Fi = C3dVector(0, 0, p);
                              sleeper.force.setX(0); // Only 1 degree of freedom
                              sleeper.force.setY(0); // Only 1 degree of freedom
                              sleeper.force = Fi + sleeper.force; // Fc-Fi
                              // Acceleration-equation 4.21
                              sleeper.acceleration = sleeper.force /
sleeper.mass;

                              // Velocity-equation 4.22
                              sleeper.velocity += sleeper.acceleration*dt;

                              // Position-equation 4.24
                              sleeper.totalTranslation += sleeper.velocity*dt;
                      }

                      else // Initial compression using displacement control
                      {
                              sleeper.velocity = initialVelocity;
                              sleeper.totalTranslation += sleeper.velocity*dt;
                      }

              //Update geometry Motion
              coupling.setGeometryMotion(sleeper.id,
                      sleeper.totalTranslation,
                      sleeper.orientation,
                      sleeper.velocity,
                      sleeper.angularVelocity,
                      dt,
                      sleeper.movePoA);

              // Simulate geometry motion
              coupling.simulate(dt, endtime);
      }
      return 0;
}
```